Z-wire – a micro-scaffold that supports guided tissue assembly and intramyocardium delivery for cardiac repair

Z-wire – a micro-scaffold that supports guided tissue assembly and intramyocardium delivery for cardiac repair

By: Luis Eduardo Portillo Esquivel, B.Eng.

A Thesis

Submitted to the School of Graduate Studies

In Partial Fulfilment of the Requirements

For the Degree Master of Applied Science

McMaster University

Master of Applied Science (2020) McMaster University
Chemical Engineering Hamilton, ON

Title: Z-wire – a micro-scaffold that supports guided tissue assembly and intramyocardium delivery for cardiac repair
Author: Luis Eduardo Portillo Esquivel, B.Eng. (ITESM)
Supervisor: Dr. Boyang Zhang
Number of pages: vi, 97

ABSTRACT

Cardiovascular diseases (CVD) are the leading cause of death around the world, being responsible for 31.8% of all deaths in 2017.[1] The leading cause of CVD is Ischemic heart disease (IHD), which caused 8.1 million deaths in 2013.[2] IHD occurs when coronary arteries in the heart are narrowed or blocked, preventing the flow of oxygen and blood into the cardiac muscle, which could provoke acute myocardial infarction (AMI) and ultimately lead to heart failure and death. Cardiac regenerative therapy aims to repair and refunctionalize damaged heart tissue through the application of (**1**) intramyocardial cell delivery, (**2**) epicardial cardiac patch, and (**3**) acellular biomaterials. These approaches have provided benefit of cell localization and tissue structure respectively. However, to improve cell retention and integration, there is a need for the intramyocardial delivery of functional tissues while preserving anisotropic muscle alignment. Here, we developed a biodegradable z-wire scaffold that supports the scalable gel-free production of an array of functional cardiac tissues in a 384-well plate format. The z-wire scaffold design supports cellular alignment, provides tunable mechanical support, and allows for hallmark tissue contraction. When the scaffold is imparted with magnetic properties, individual tissues can be assembled with macroscopic alignment under magnetic guidance. When used in combination with a customized surgical delivery tool, z-wire tissues can be injected directly into the myocardial wall, with controlled tissue orientation according to the injection path. This modular tissue engineering approach, in combination with the use of smart scaffolds, could expand opportunity in functional tissue delivery.

ACKNOWLEDGEMENTS

TABLE OF CONTENTS

LIST OF FIGURES

LIST OF TABLES

LIST OF ABBREVIATIONS AND SYMBOLS

AMI acute myocardial infarction
ASC adult stem cells
BMC bone marrow cells
BMMSCs human bone marrow MSCs
CDC cardiosphere-derived cells
CFDA 5-Carboxyfluorescein diacetate
Chi/Glyp chitosan/β-glycerophosphate
CM cardiomyocytes
CMPC cardiomyocyte progenitor cells
CSC Cardiac stem cells
CVD cardiovascular diseases
DFBS dermal fibroblasts
DMEM Dulbecco's modified Eagle's medium
DMSO Dimethyl Sulfoxide
EC endocardial
EC endothelial cells
ECM extracellular matrix
EMMPRIN extracellular matrix metalloproteinase inducer
EnMSCs human endometrium-derived mesenchymal stem cells
ESC embryonic stem cells
EV extracellular vehicles
FBS Fetal Bovine Serum
hBMMSC human Bone Marrow Mesenchymal Stem Cells
hFBS human Fibroblasts
HGF human growth factor
HUVEC human umbilical vein endothelial cells
IGF-1 insulin-like growth factor 1
IHD ischemic heart disease
IL1-iGF interleukin 1 inhibitor growth factor
IM intramyocardial
iPSCs induced pluripotent stem cells
IV intravenous
LV left ventricle
LVEDD left ventricle end diastolic dimension
LVEDP left ventricle end-diastolic pressure
LVEF left ventricle ejection fraction
LVESD left ventricle end systolic dimension
LVSP left ventricle systolic pressure
MEF mouse embryonic fibroblasts
MI myocardial infarction
MMP matrix metalloproteinase
MMPs matrix metalloproteinases
MSC mesenchymal stem cells
NMRs Nuclear Magnetic Resonance spectroscopy
NRCMS Neonatal rat CMS
PBS Phosphate-Buffered Saline
PCL poly a-caprolactone
PCLA poly a-caprolactone-co-L-lactide
PDGF-BB platelet-derived growth factor-BB
PDMS Polydimethylsiloxane
PEUU poly(ester urethane)urea
PGS Poly(glycerol sebacate)
PGS polyglycerol-sebacate
PGSA Poly(glycerol sebacate) acrylate
PI Photoinitiator
PI Photoinitiator
PIo Propidium Iodine
PLA poly-L-lactide
PLGA poly lactic-co-glycolic acid
POMaC poly octamethylene maleate (anhydride) citrate
PSC prosurvival cocktail
rFBS rat Fibroblasts
SM skeletal myoblasts
Tb4 thymosin b4
VEGF vascular endothelial growth factor
VSMC vascular smooth muscle cells

CHAPTER 1. INTRODUCTION

Ischemic heart disease (IHD) is the term given to the group of heart affections that are caused due to the narrowing of the heart arteries. This narrowing can lead to further and more deadly problems such as acute myocardial infarction (AMI) and ultimately heart failure. In 2013, 8.56 million cases of AMI in the world were recorded.[2] The pathophysiological process leading to AMI is called atherosclerosis, where the accumulation of lipids, cholesterol, calcium, cellular debris, scarring, and inflammation of the vascular walls intimal space occur.[3,4] All these factors thicken the vascular wall and diminish the lumen of the vessels until a point where oxygen and blood cannot perfuse into the heart muscle. The heart needs a constant supply of these two physiological inputs to maintain its high metabolic activity. Hence, when the myocardium stops receiving all the required metabolites, infarction occurs leading to tissue damage, necrosis, and apoptosis.[5] Myocardial damage occurs in two zones: the central or ischemic zone with no flow or very low flow of oxygen and nutrients, and the peri-infarct zone surrounding the central zone.[6] Severe myocardial infarction (MI) can wipe out up to one-fourth of the total amount of cells in the heart, approximately 1 billion of cardiomyocytes, after just a few hours.[7] Most of the cells die acutely within the ischemic area over the first 6 to 24 hours after infarction. [8,9] The rest die chronically in the peri-infarct zone over the following six months due to both the acute effects of ischemia and to cardiac structural and functional remodeling.[8,9] Adult cardiomyocytes have a low proliferation rate and are terminally differentiated, limiting the regenerating capabilities of the heart of replacing dead cardiac cells with new ones.[10]

To compensate for the loss of cardiac function, physiological remodeling will take place. Postinfarction cardiac physiological remodeling is divided into three stages: acute and

chronic inflammation; tissue repair; and structural and functional remodeling of the heart. [11] In the stage of tissue repair, fibroblasts proliferate and deposit extracellular matrices, mostly collagen, forming scar tissue. The scar tissue is nonfunctional due to the lack of mechanical and electrical conduction, causing a decrease in the ejection fraction and pumping capabilities in the heart. This limits the proper perfusion of blood and oxygen to peripheral organs and tissues. To atone this, the volume of blood ejection from each heart cycle needs to increase. Hence, structural, and functional remodeling occurs. Remaining cardiomyocytes become hypertrophied as they try to compensate the loss of ejection fraction by increasing the blood volume that enters to the heart ventricles in each cycle, heart rate increases to eject more blood in the same amount of time [11], and vasoconstriction occurs to increase blood pressure due to the activation of the renin-angiotensin system.[12] The chronic hypertrophy of cardiomyocytes narrows the heart ventricle walls over time, diminishing the contractile strength of the myocardium and can ultimately lead to heart failure and death. To slow down remodeling, reverse wall thinning, and lessen the risk of permanent heart failure, new treatments and approaches have been developed, especially in the field of regenerative medicine.

Although the structure of large organs can be extremely complex, many key components of an organ are often made of individual repeating functional units (e.g., cardiomyocytes in myocardium, nephrons in kidney, and lobules in liver). Therefore, assembling complex tissues with macroscopic structural organization from smaller tissue modules is an attractive tissue engineering technique. Current modular tissue assembly strategies are limited by 2-dimensional patterning[13], passive 3D aggregation[14], or manual manipulations[15]. Specifically, in the development of cardiac tissue engineering modules, design strategies fail to address the need for automatic anisotropic tissue assembly from

modular tissues. A hallmark of functional cardiac tissue *in vivo*, achieving 3D anisotropic tissue alignment and orientation in a scalable manner, is critical for the fabrication of large-scale cardiac tissue while maintaining proper contractile function.

Furthermore, to perform therapeutic repairs using lab-grown tissues that have organized tissue structures, strategies employing *in vivo* delivery often involve invasive implantation surgery. On the other hand, delivery of cells can be achieved in a minimally invasive manner, but the lack of tissue-level organization impedes the immediate functionality and the retention of the injected cells[16-22]. Shape-changing scaffolds have been used to implant engineered tissues through a keyhole surgery approach, but with limited regenerative impact given that delivery is localized to the organ surface, such as the myocardial surface of the heart[23]. Recent studies showed the functional improvement from the epicardial implantation of engineered cardiac patches is not necessarily owed to tissue engraftment, but to cell-independent effects (e.g., activation of immune cells or mechanical supports) and mechanical coupling[24]. To further improve cardiac functions and attain functional integration with host tissues, it might be necessary to bypass the cardiac epithelium with intramyocardial delivery of functional tissues directly to the infarcted regions to re-muscularize the infarcted tissues and achieve electro-mechanical integration. For this reason, there is a need for the intramyocardial delivery of functional cardiac tissues in a minimally invasive manner to overcome the challenges in both cell delivery and epicardial implantation of engineered tissue patch by facilitating cell retention/survival, re-muscularization, functional coupling, and reduced arrhythmias.

1.1 Thesis objective

To address challenges in tissue assembly and delivery, here we report a new strategy for guided tissue assembly *in vitro* and the intramuscular delivery of engineered tissues in a surgical setting. This thesis objective is the engineering of micro-cardiac tissues that can be delivered to the interior of the heart as a group and assemble preserving anisotropic muscle alignment. The overarching hypothesis is that this strategy will improve cell retention by delivering cardiomyocytes, not as single cells, but as a community; accelerate tissue integration by pre-maturing the tissue in vitro; improve functional coupling with the host muscle by bypassing the epithelium layer outside the heart; alleviate arrhythmia by providing tissue alignment with respect to host muscles; and alleviate surgical risk with minimal invasive surgery.

1.2 Thesis outline

This thesis has been divided into seven chapters. The introduction and outline are presented in Chapter 1. Chapter 2 is a literature review of the three regenerative medicine main approaches for treating post-MI effects: intramyocardial cell therapy, epicardial patches, and acellular therapy. Chapter 3 describes the materials and methods used in this research thesis. Chapter 4 presents the results and discussion of the research. Chapter 5 concludes the current results and establishes future work continuing the project. Chapter 6 presents references.

CHAPTER 2. LITERATURE REVIEW

Translational research efforts in medicine, tissue engineering, and biology have established a field denominated as regenerative medicine. Regenerative medicine's main objective is to replace damaged tissues and organs with new engineered cells or tissues with the purpose of re-establishing proper physiological function.[25] Up to date, research groups have tried to regenerate different organs and tissues, such as brain[26], vascular[27], cartilage[28], bone[29], kidney[30], liver[31], and cornea[32], etc. In the case of the heart, multiple approaches have been tried to regenerate its functionality, including acellular biomaterial application[33], growth factor[34] and gene therapy[35], extracellular vesicles delivery[36-38], intramyocardial delivery of cells[39-41], and cardiac patches[42,43]. All these treatment methods have shown some improvement in the diseased heart, but functional regeneration of the cardiac muscle, especially functional remuscularization, has proven a challenge. The three main current approaches in cardiac regenerative medicine that will be discussed here are intramyocardial cell therapy, epicardial cardiac patches and acellular therapy. A general overview of these approaches and their specific challenges for cardiac regenerative therapy (Figure 1) are presented.

2.1 Intramyocardial cell delivery

One of the first approaches for cardiac repair was the injection of cells into the MI heart with the purpose of replacing the dead tissues with healthy ones. Since then, extensive research exploring numerous cell types, culturing methodologies, delivery techniques, and optimization throughout more than 20 years has been done. Amongst the wide variety of cells explored for cardiac repairs, cells from fetal or newborn animals, cardiac muscle cell lines,

skeletal myoblasts , smooth muscle cells, and a variety of stem cells, either adult, embryonic (ESCs) or induced pluripotent stem cells (iPSCs) can be found.[44]

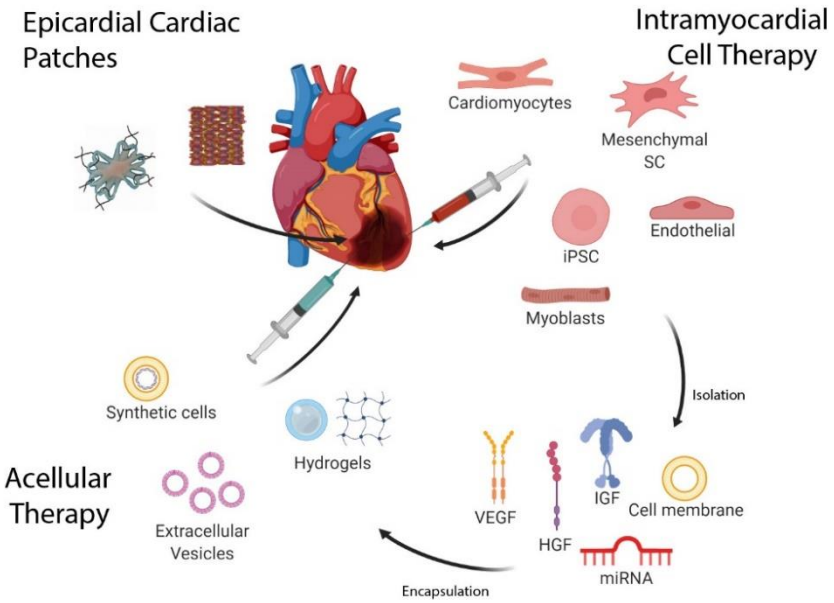

Figure 1: Current approaches in cardiac regenerative medicine. Cell therapy approach delivers individual cells intramyocardially. Cardiac patch approach delivers engineered tissues epicardially. Acellular therapy approach delivers biomaterials, growth factors, synthetic cells, or secretome.

2.1.1 Delivery of cardiac cells and skeletal myoblasts

Cardiac cells were some of the first choices for cardiac repair due to their functional properties. Müller-Ehmsen et al. explored the long-term effects of injection of neonatal rat cardiomyocytes into adult rats by testing the survival rate of the injected cells and their functional impact.[21,45] Around 1 million isolated cardiomyocytes were suspended in serum-free MEM and injected in the apical region of the left ventricle. Findings showed that up to 60% of the cells were lost almost immediately after injection, and only 15% of injected cells survived after 12 weeks. The surviving cells became elongated and developed sarcomeres, indicating that remuscularization was achieved to some extent. Nevertheless, grafted cells were smaller than the adult host muscles, suggesting a lack of maturation (**Figure 2A**).[21]

Even though the caspase inhibitor AcYVADcmk was administered, the survival rate was not improved, indicating that cell loss was caused externally to caspase-regulated mechanisms. A possible explanation for such rapid loss might be a combination of cell retention in the syringe's dead space, leakage into the chest cavity or lymphatic and blood vessel wash-out. Nevertheless, Murry et al. showed that persistent factors after the delivery process continue decreasing the viability of the grafted cells.[46] They performed terminal deoxynucleotidyl transferase dUTP nick end labeling (TUNEL) staining, an assay that detects the DNA breaks formed when DNA fragmentation occurs in the last phase of apoptosis. TUNEL results showed that almost all cells looked viable 30 minutes after implantation but only 1% of graft cells survived after seven days. Electron microscopy revealed evidence of ischemic injury and apoptosis. The delivery of cells to healthy vascularized myocardium reduced the TUNEL index by 83%, confirming ischemia as a key factor for cell death. Furthermore, adenoviral infection with the cytoprotective kinase Akt also reduced TUNEL index by 40%, suggesting that apoptosis can be limited by activating the Akt pathway.[46]

Similar observations were made by injecting skeletal myoblasts into mice. Suzuki et al. reported that 60% of the injected myoblasts into mice myocardium were lost in the first 10 min after delivery, and kept decreasing until reaching 92.4% of cell loss after 72 hours.[47] In addition , they also evaluated the contribution of oxidative stress into cell loss by comparing a nontreated myoblasts group with a myoblast group treated with superoxide dismutase (SOD), an enzyme known to provide strong cellular protection by scavenging hazardous superoxide such as myeloperoxidase (MPO).[47] A two-fold survival rate increase was observed in the SOD treated group at 24 and 72 hours in comparison to the non-treated group. These findings suggest that oxidative stress and inflammation contribute to cell death in the acute phase of implantation. Khan et al. also showed that the delivery of skeletal

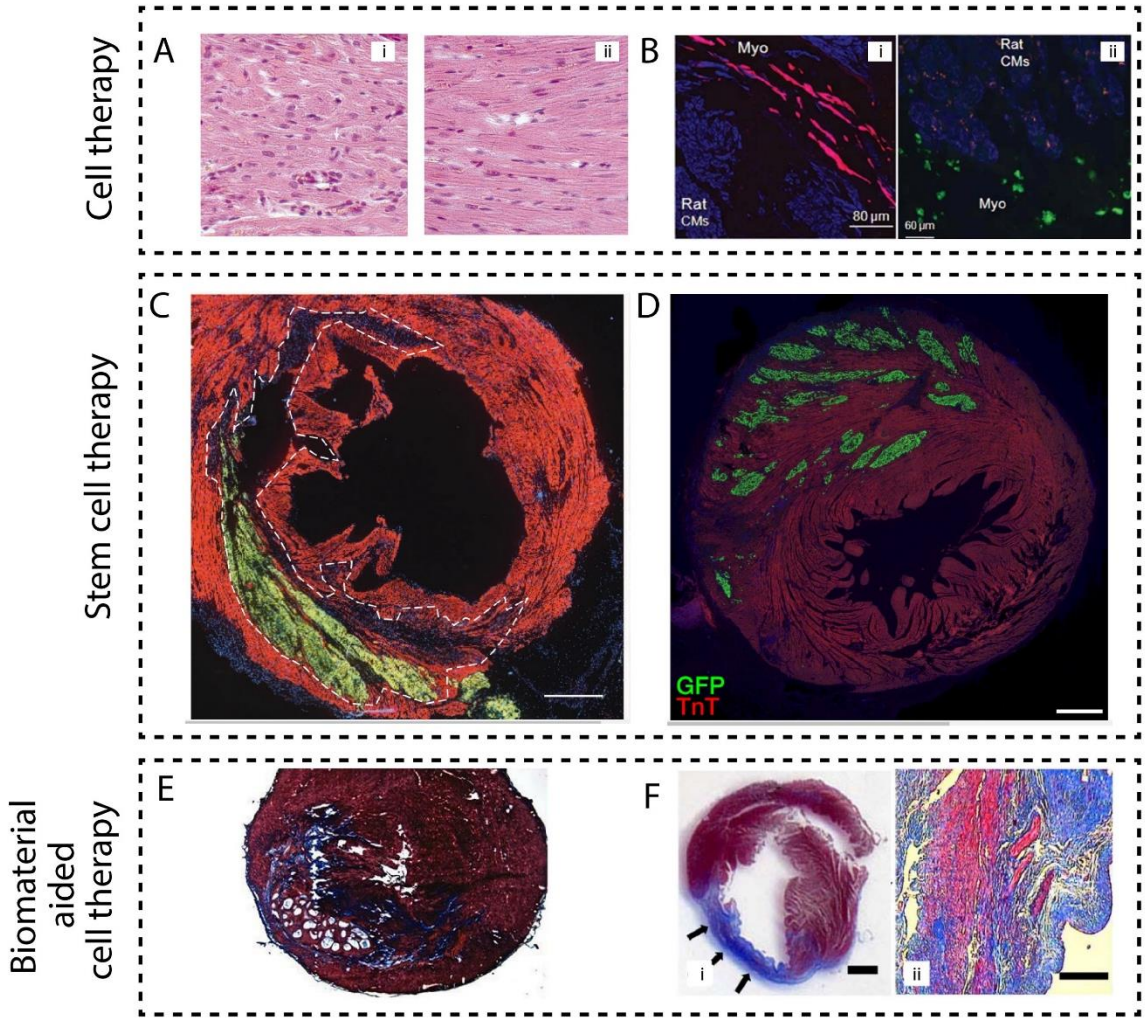

Figure 2: Examples of intramyocardial cell delivery approach for cardiac therapy. Traditional cell therapy had its origins by delivering primary cardiomyocytes (A) and skeletal myoblasts (B). (**A**) H&E-stained sections of (i) neonatal cells 12 weeks after implantation showing smaller cell size and nuclei than (ii) host tissues.[21] (**B**) (i) Fluorescent images show the transplanted skeletal myocytes stained for cardiac (TnI, blue) and skeletal muscle (MY32, green) markers, and (ii) the absence of gap junctions (Cx43,red) in between DiO-labeled (green)-grafted skeletal myocytes and host rat cardiomyocytes (TnI, blue).[48] (**C-D**) Fluorescent image of primate hearts subjected to myocardial infarction and transplantation of (C) hESC-CMs[49] and (D) iPSC-CMs[50] and showed remuscularization of a substantial portion of the infarct region. (**E-F**) Masson's trichrome stain of infarcted myocardium (E) after 10 weeks post injection of MSCs using alginate as vehicle[51] and (F) after 8 weeks post injection of BMMNC using fibrin matrix as vehicle.[52] Permission for reprints of all images shown has been acquired.

myoblasts enhances myocardial oxygenation through the promotion of neoangiogenesis, and improves cardiac function at four weeks after MI, by increasing in LV systolic pressure

(LVSP) and decreasing in LV end-diastolic pressure (LVEDP).[53] Despite the reported functional improvements, immunostaining studies targeting cardiac (troponin I), skeletal muscle (skeletal muscle myosin, MY32) and connexin 43 (Cx43) markers demonstrated that myoblasts do not form gap junctions with host cardiomyocytes (**Figure 1B**). [48] The lack of gap junctions resulted in significant electrical and mechanical conduction slowing and block. This caused arrhythmogenicity as 50% of the rat MI model group that received myoblast transplantation developed sustained monomorphic ventricular tachycardias.[48]

The therapeutic effects of skeletal myoblasts seem to come from external factors rather than direct contractility of the implanted cells. He et al. reported mild improvements in hemodynamics and LV function, and reduced LV remodeling in dog MI models even though no histologic evidence of engraftment was found in some of the animals.[54] These findings suggested that the active contraction of engrafted cells was not the primary mechanism that could explain the therapeutic effects of cell delivery. Later on, a theory called the paracrine effect was established, stating that cells produce several cytokines and growth factors that increase angiogenesis, reduce apoptosis, decrease fibrosis and induce cardiac regeneration.[55] The paracrine effect has been further proved and has become well accepted in the research community.[56] By delivering skeletal myoblast overexpressing vascular endothelial growth factor (VEGF) higher angiogenesis was achieved. [57]This resulted in better engraftment of the injected cells and further differentiation into multinucleated myotubes, reduction of the infarct size, improvement of LV contractility and reduction of intraventricular pressure. Murtuza et al. injected skeletal myoblasts overexpressing Interleukin-1 inhibitor growth factor and demonstrated the relevance of inflammation in cardiac cell therapy.[58] Through the addition of this growth factor, they were able to improve

myoblast survival after transplantation as well as the cardiac function by increasing the left ventricle ejection fraction (LVEF), , and attenuating the LV wall dilatation.

Due to their earlier promising results in animal studies, skeletal myoblasts have been subjected to several human clinical trials.[59-62] Phase 1 clinal trials proved feasibility in the treatment by discarding possible postoperative complications or deadly after-effects such as infection and showed promising results in the improvement of LVEF.[59-61] Also, even though myoblasts do not differentiate into endothelial cells, CD31 staining for endothelial cells in patient biopsies revealed an increase of arterioles reinforcing the paracrine effect theory observed in animal models.[61] Despite the initial positive results, the Myoblast Autologous Grafting in Ischemic Cardiomyopathy (MAGIC) trial, a multicenter, phase 2 study showed that 120 myoblast-treated patients did not show incremental improvement in regional or global LV function.[62] It was hypothesized that apoptosis due to cell detachment and ischemia of the cellular graft were the main causes of this lack of improvement. Interestingly, the group that received the highest dose of myoblasts (800 million) showed a reversal on LV remodeling in comparison to control group, similar to results found in the injection of myoblasts in sheep[63] and swine[64]. This suggests that higher doses of cells are required to have an observable therapeutic effect due to reduced survival rate. Finally, the MAGIC trial concluded that skeletal myoblasts might not be the optimal candidates for improving severe LV dysfunction in chronically infarcted hearts and that such cases would likely require the delivery of contractile and electromechanically integrated cells.[62]

2.1.2 Delivery of adult stem cells

Stem cells have become so attractive to the field of regenerative medicine as they have the potential to divide into specialized cell types present in the body. Stem cells are

usually classified as three main categories: adult stem cells (ASCs), embryonic stem cells (ESCs), and induced pluripotent stem cells (iPSCs).[36] Mesenchymal stem cells (MSCs) are multipotent adult stem cells that can be isolated from stromal sources (i.e., bone marrow, amniotic fluid, endometrium, umbilical cord, adipose tissue) in human and animals. They can differentiate into osteoblasts, chondrocytes, myocytes, and adipocytes.[65,66] Besides skeletal myoblasts, MSCs are also well-characterized and extensively studied in cardiac repair.[41] MSCs can be delivered as normal MSCs or as MSCs-derived cardiomyocytes.[67,68] Shake et al. injected 6 million Di-iridium–labeled bone marrow MSCs in swine two weeks after MI, to avoid the peak of the postinfarct inflammatory phase, and performed functional and immunohistochemistry evaluations to assess their effects.[69] After two weeks, results showed attenuation of contractile dysfunction and wall thinning and engraftment of MSCs into the host myocardium, which expressed muscle-specific proteins such as a-actinin, tropomyosin, troponin-T or myosin heavy chain. More cardiac-specific (desmin, cardiac troponin T and connexin-43) as well as vasculature-specific (von Willebrand factor and smooth muscle actin) makers were found in some rats injected with MSCs.[70] These MSCs-treated hearts also increased their capillary density, decreased the collagen volume fraction in the myocardium and the LVEDP, and increased the LV maximum contractility ratio dP/dt.[70]

The effects of incorporating other adult stem cells into the MSC injection cocktail have also been explored. Williams et al. showed that the injection of MSCs combined with c-kit+ cardiac stem cells (CSCs) reduced the infarct scar size by 2-fold in comparison to cell therapy alone, as well as improvement in LV compliance and contractility in Yorkshire swine MI models.[71] Katritis et al. delivered a combination of MSCs and endothelial progenitor cells into eleven MI human patients.[72] Cardiographic assessments showed a trend for improvement

in end-diastolic diameter, end-systolic diameter, fractional shortening (FS), ejection fraction (EF), end-diastolic volume, and end-systolic volume of the left ventricle, but the differences did not achieve statistical significance. Even though it has been stated that c-kit+ CSCs and other CSCs such as cardiosphere-derived stem cells do not produce new cardiomyocytes within the heart[73,74], the finding from Williams et al. illustrate the important biological interactions between CSCs and MSCs in enhancing cell-based therapeutic responses[71]

MSCs have shown promising therapeutic effects and the potential to remuscularize the MI heart to a certain degree. But similar to cardiac cells and myoblasts, low cell retention and survival rate remain as limitations.[75] As aforementioned, one of the suspected reasons for low engraftment is cell leakage right after delivery[21]. Therefore, optimizing delivery techniques is vital to improving cell engraftment. Freyman et al. carried out a study quantifying the survival and engraftment rates of MSCs after intravenous (IV), intracoronary (IC), or endocardial (EC) delivery in a porcine myocardial infarction (MI) model.[76] By internalizing iridium nanoparticles into the MSCs, they were able to measure ex-vivo the iridium concentration in the infarct. Results showed that IC and EC delivery had higher engraftment in comparison to IV infusion. Even though IC delivery is more efficient than EC delivery, IC delivery was also associated with decreased coronary flow. On the other hand, EC delivery was safer, well-tolerated, and had lower remote organ engraftment in comparison to IC and IV.

2.1.3 Delivery of embryonic stem cells

ESCs are pluripotent stem cells (capable of unlimited and undifferentiated proliferation) derived from totipotent cells from the inner cell mass of a blastocyst, an early mammalian embryo..[77] ESCs' pluripotency enables the possibility to engineer and

differentiate them into nodal, atrial, and ventricular cardiomyocytes, making them a promising treatment for cardiac repair.[78]

Caspi et al. injected undifferentiated human ESCs (uhESCs), hESCs-cardiomyocytes (hESCs-CMS), noncardiomyocyte hESCs derivatives into rat MI models.[79] Even though the injection of uhESCs resulted in the formation of teratoma-like structures, hESC-CMS didn't. Also, the engrafted hESC-CMS survived, proliferated, and functionally integrated with the host heart, resulting in attenuation of LV remodeling and improvement of myocardial performance. Furthermore, it was theorized that the improvements came directly from the contractility of the hESC-CMS as immunohistochemistry showed structural and functional cardiomyocyte phenotype of the grafted cells while the noncardiomyocyte hESCs group showed no significant functional improvement.[79] These findings are also supported as research has shown that hESCs-CMS form gap junctions with neighboring cardiomyocytes, and seem to electrically integrate with host cardiac tissue preventing any significant conduction disturbance.[48] Even though Caspi et al. didn't report teratoma formation in delivery of hESCs-CMS, Leor et al. did find teratoma formation in one healthy rat treated with hESCs-CMS.[79,80] However, this might be due to lack of proper cell differentiation and maturation. Leor et al. also reported similar findings in rat MI models as they found hESCs-CMS attenuate post-MI scar thinning and left ventricular dysfunction.[80] Results also showed that injected cells can survive transplantation better in healthy hearts and to a lesser extent in MI models, suggesting that the lack of blood and nutrient perfusion in the infarct area limits the survival rate of the delivered cells.[80]

To improve engraftment and survival, further research has been done to improve delivery techniques. Moon et al. showed that better engraftment and survival rate can be achieved by delivering aggregates of purified cardiomyocytes as a community instead of as

single cells.[81] By purifying hESCs-CMS other unwanted cell populations are removed through cell culturing in serum-free media, which decreases the risks of arrhythmia and teratoma formation. Also, the aggregates increased cell survival in hypoxia and induced high-level functional engraftment after transplantation into the infarcted myocardium.[81] Laflamme et al. showed that the addition of a prosurvival cocktail (PSC) which included Matrigel, cell-permeant peptide, cyclosporine A, pinacidil, IGF-1 and caspase inhibitors, made the graft size fourfold larger in comparison to control.[22] Results showed that the effective engraftment of hESCs-CMS in rat MI models generated 2.5-fold greater LV wall thickening, decreased both the LV end diastolic dimension (LVEDD) and the LV end systolic dimension (LVESD), and increased the fraction shortening. In addition, they found that non-cardiomyocyte grafts were non-existent after four weeks and suggested that cardiomyocytes might be the correct option for cell delivery. Van Laake et al. evaluated as well the effects of the delivery of hESCs-CMS and non-cardiomyocyte cells with PSC to mice. [82] Even though the significant improvements in cardiac function were similar to the ones reported by Laflamme et al.[22] for the first four weeks, after three months the difference in between the CMS and non-CMS groups was no longer significant, which suggest a need for more extended period of evaluations.

Even though the aforementioned rodent studies didn't report arrhythmia, the rapid heart rates of rats and mice might conceal possible arrhythmogenic effects form the delivery of hESCs-CMS.[83] Therefore, Shiba et al. worked with a novel guinea pig (230 beats/min in comparison to 600 beats/min in mice and 400 beats/min in rats) MI model to further assess possible arrhythmogenic effects of hESCs+PSC.[83] By using GCaMP3 signal, genetically encoded calcium indicator, they were able to assess graft activation and propagation in vivo in both viable and scarred muscle. Results showed that hESCs-CMS grafts in viable muscle

activated uniformly suggesting synchronous activation through multiple contact points with host muscle. In contrast, graft activation in scarred tissue was spatially and temporally heterogeneous with lower spread activation. This difference is probably due to limited contact in between the graft and the host and lack of graft maturation. Nevertheless, these intravital imaging studies could demonstrate that hESCs-CMS can integrate and contract synchronously with the host myocardium supporting the hypothesis that these cells can improve mechanical function by creating new force-generating units.[83]

Significant cardiac function enhancement has been found when scaling up to higher mammalian models. Nevertheless, ventricular tachyarrhythmias have been reported as well. Romagnuolo et al. implanted 1 billion hESC-CMS into pig MI models and reported the maturation of the implant over time, the formation of vascular networks connecting to the host tissues, and minimal cellular rejection.[84] The grafts occupied 15% of the infarct scar. However, treated pigs presented frequent monomorphic ventricular tachycardia. Murry's research group transplanted 1 billion GCaMP3 hESC-CMS+PSC into macaque MI models.[49] Confocal immunofluorescence confirmed extensive remuscularization and engraftment of the hESC-CMs co-expressing GFP (**Figure 1C**), as well as time-dependent graft maturation in the macaques.[49] Also, tomography showed that blood vessels extend from the host coronary network into the graft. Furthermore, ECG and imaging showed that 100% of the hESCs-CMS grafts retained 1:1 electrically coupling to host myocardium during atrial pacing at rates of up to 240 beats per minute in comparison to only 60% in a guinea pig model.[49,83] Later on, this research group reported a long term cardiac function enhancement by improving LVEF in macaque monkeys with large myocardial infarctions by >20% in comparison to controls.[85] Despite these highly promising results, all macaques that received hESCs-CMS showed arrhythmias including premature ventricular contractions and runs of

ventricular tachycardia. [49] These symptoms were more frequent within the first two weeks after transplantation suggesting immaturity of the implanted cells.

2.1.4 Delivery of induced pluripotent stem cells

In 2006 Takahashi and Yamanaka made the breakthrough discovery of reprogramming mouse fibroblasts by ectopically expressing four key pluripotency factors (Oct-3/4, Sox2, c-Myc, and Klf4). [86] Reprogrammed cells exhibited morphology, growth properties and expressed cell marking genes of ESCs. These cells were named as induced pluripotent stem cells (iPSCs). Nelson et al. delivered fibroblast-derived human iPSCs into immunocompromised rats.[87] Results showed that iPSCs improved cardiac contractility by achieving 50% ejection fraction by four weeks, and increased FS from 20% on day 1 after infarction up to 31% after four weeks. Furthermore, iPSCs increased the LV septal wall thickness and attenuated the global LVEDD. Singla et al. were able to generate iPSCs from H9c2 embryonic cardiac ventricular cells and implanted them into mice MI models.[88] Immunolabel staining with sarcomeric a-actin and connexin-43 showed that transplanted iPSCs differentiated into cardiomyocytes and that gap junctions were generated and connected to the host tissue. In addition to this, TUNEL analysis showed that iPSCs treatment inhibits apoptosis. Also, similar to the findings by Nelson et al.[87] FS was increased, LV interior systolic diameter (LVIDs) was decreased, and fibrosis remodeling was attenuated.[87,88] Templin et al. were also able to confirm the long-term survival and differentiation of human cord blood-derived iPSCs in a preclinical pig MI model by using sodium iodide symporter (NIS) transgene and SPECT/CT imaging.[89]

Although the aforementioned studies didn't report teratoma formation[87,88], Ahmed et al. observed that 40% of mice treated with mice skeletal myoblast-derived iPSCs formed

cardiac tumors.[90] Results showed that the tumors contained structures from all three embryonic germ layers generating an intense inflammatory response. Zhang et al. also reported tumorigenesis in which incidence was independent of cell dose, transplant duration, and the presence or absence of myocardial infarction.[91] The exact mechanism for the tumorigenic potential of undifferentiated iPSC was not elucidated. But these findings showed the intrinsic risk of delivering undifferentiated iPSCs which may not always adopt cardiac phenotypes and lead to tumor propagation.[90,91]

The tumorogenic properties of undifferentiated iPSCs showed the need of differentiation before moving forward to other bigger MI models. Therefore, protocols for differentiating iPSCs into cardiomyocytes were established.[92,93] Shiba et al. generated fibroblast-derived iPSCs from major histocompatibility complex haplotype homozygous animals, differentiated them into cardiomyocytes (iPSC-CMS), and made allogeneic transplantation into macaque MI models.[50] Fluorescent microscopy analysis 84 days after transplantation of 400 million iPSCS-CMS demonstrated a substantial remuscularization of the infarcted hearts (**Figure 1D**). CD31 staining showed that engrafted CMS were well vascularized by host-derived endothelial cells. Cadherin and Cx43 staining confirmed cell adhesion and gap junction formation in between the graft and the host muscle. Electrical 1:1 coupling with host cardiomyocytes was further confirmed using intravital fluorescence imaging. CT scans showed an improved contractile function as ejection fraction and FS were increased. Nevertheless, echocardiography and Holter monitoring showed episodes of sustained ventricular tachycardia, which peaked at day 14 after transplantation and gradually decreased throughout the rest of the study period with non-apparent ventricular tachycardias on days 56 and 84. These results suggest low iPSCs-CMS maturation at transplantation but further maturation *in-vivo*.[50]

2.1.5 Cell therapy through injectable biomaterial vehicles

A major limitation with cell therapy is low engraftment and cell survival after delivery. As mentioned before, oxidative stress, inflammation, and cell leakage and wash-out are amongst the identified causatives for cell loss and death.[44] In addition, anoikis, the programmed cell death induced by inadequate cell-matrix interactions, , has also been identified as a factor to consider.[94] Besides Matrigel[22], the delivery of cells with other ECM-like biomaterial vehicles such alginate, or fibrin, etc., can help increase engraftment by reducing the risk of anoikis.

Alginate is a polysaccharide obtained from brown seaweed that has ease of gelation. Alginate derivatives containing cell-adhesive peptides enable its use as a supporting lattice and anchoring point for cell attachment.[95] Yu et al. encapsulated MSCs in RGD alginate microspheres and delivered them to rat MI models (**Figure 1E)**.[51] Delivery of MSCSs encapsulated in alginate increased cell survival significantly. A possible explanation might be that RDG alginate reduces anoikis as MSCs attached better to RGD alginate *in-vitro.* In addition, cell survival might have been enhanced by the increment in vascularization generated by a higher Fibroblast growth factor-2 (FGF2)gene expression on RGD modified surface.[51] Roche et al. also confirmed that both alginate hydrogel and chitosan/β-glycerophosphate hydrogel have five-fold more DiD labeled MSCs retention immediately after transplantation in comparison to delivery through saline control.[96] Alginate hydrogel and chitosan/β-glycerophosphate hydrogel also showed 8-fold and 14-fold more fluorescence, an indicator of higher engraftment, in comparison to saline delivery 48 hours after transplantation.

Fibrin hydrogels are formed by a polymerization mechanism in between fibrinogen and thrombin, key proteins involved in blood clotting, which allows control of gelation and

network structure.[97] Christman et al. delivered skeletal myoblasts through fibrin hydrogel in rat MI models and compared its results with skeletal myoblasts alone.[98] Five weeks after transplantation, fibrin glue-delivered myoblasts increased arteriole density and decreased the infarct size in comparison to myoblasts alone and control. Ryu et al. also reported that the implantation of bone marrow mononuclear cells in a fibrin matrix enhanced neoangiogenesis, produced a larger amount of viable tissues, and a smaller amount of fibrous tissues in comparison to single cell delivery (**Figure 1F**).[52] The overall properties of fibrin hydrogel can be further toned. Seliktar et al. developed an injectable biosynthetic material made by conjugating polyethylene glycol (PEG) with fibrinogen through radical chain polymerization reaction of acrylate end groups induced by a photoinitiator and UV light enabling control over the degradation rate through photo-polymerization.[99]Later on, delivery of neonatal rat cardiomyocytes or hESCs-CMS through the PEGylated fibrinogen hydrogel was performed.[100] Results showed that cell survival was increased and echocardiography showed 26% improvement in FS change.

Besides alginate and fibrin, other biomaterials have been implemented to improve cell survival in cell therapy. Kraehenbuehl et al. developed a synthetic and injectable matrix metalloproteinase (MMP) as a carrier for thymosin b4 (Tb4), a pro-angiogenic and pro-survival factor, along with hESC-derived endothelial cells and delivered it into rat MI models.[101] Previous work by this group showed that MMP mimicked key biochemical characteristics of collagen matrices, which stimulates HUVEC adhesion, survival, migration, and organization.[102] When delivered into rat MI hearts, significant angiogenesis was generated and cardiomyocytes appeared to be better preserved and aligned.[101] Tang et al. encapsulated CSCs inside poly(N-isopropylacrylamineco-acrylic acid) (P(NIPAM-AA)) nanogel and delivered them into mice and swine MI models.[103] Masson trichrome staining

showed that encapsulated CSCs conferred the best therapeutic effects by increasing the % of ejection fraction, reducing the scar size and thickening the LV wall over four weeks in comparison to the non-existent therapeutic effects observed in CSCs delivered through saline.

Ideally, transplanted cells in cell therapy should replace fibrotic scar tissue with viable healthy cardiac muscle tissue while improving cardiac output and function accordingly.[104] Limitations in this approach include significant cell loss and low engraftment due to both delivery techniques and persistent proapoptosis environment.[10,21,46] Intramyocardial injection might be the best delivery approach in comparison to intracoronary and endocardial delivery.[76] Ischemia, inflammation and anoikis are major sources of injury and cell death, therefore to improve cell survival and engraftment, correct vascularization, cell-ECM interactions and prosurvival cocktails that include growth factors and antiapoptotic peptides are needed.[20,22,46,94] The low percentage of engraftment requires the delivery of higher amounts of cells to see observable improvements.[62] The delivery of cell therapy mediated through biomaterial vehicles might reduce the amount of cells needed as the engraftment rate is improved. [22,96,98] However, cells in the order or billions are still needed to have a significant therapeutic effect after MI.[7] The use of primary CMS might be insufficient to satisfy this demand. However, the use of ESCs and iPSCs have opened up the possibility to meet this high demand for cells needed in cell therapy.[79] Nevertheless, the use of ESCs has ethical and immunogenic limitations, and both ESCs and iPSCs may lead to severe events such as major arrhythmias and/or teratoma formations if unwanted cell types are delivered into the myocardium.[49,50,79,90] Therefore, efficient cell source selection, differentiation into CMS, maturation and purification of CMS are clinical requirements.[39]

2.2 Epicardial delivery of tissue engineered cardiac patches

The other classical approach in cardiac regenerative medicine is the use of engineered cardiac tissue patches. The goal is to implant functional and living heart muscle tissue into diseased hearts in order to restore its functions.[105] These engineered cardiac tissues usually come in the form of patches and are produced by seeding cell types found in the heart , into synthetic scaffolds, extracellular matrix materials such as fibrin, collagen and gelatin or decellularized hearts.[106] Other approaches for engineered cardiac patches include the fabrication of cell sheets.[107,108]

2.2.1 Natural hydrogel-based approach

Dr. Zimmerman, Dr. Eschenhagen, and colleagues are pioneers in developing engineered heart tissues[109-112] and implanting them into MI animal models to evaluate their therapeutic effects.[113-115] The first approaches by this group consisted of seeding cardiomyocytes from neonatal Fischer 344 rats into circular liquid collagen type I and Matrigel constructs and let them mature for 28 days.[113] These cardiac patches were then implanted on the exterior layer of the heart of syngeneic rats. Nevertheless, immunogenic factors could not be eliminated completely during the production of the cardiac patches mainly attributed to allogenic nonsoluble matrix components, alterations of the expression of self-antigens or impregnation of implanted cells with soluble components of culture media. This resulted in total degradation of the cardiac patches, therefore, the study was performed under immunosuppression. Results showed that the patches attached to post-MI hearts retained their contractile functions and developed thicker and more mature cardiac muscle structures.

Zimmermann's group further modified the cardiac patch by stacking five circular patches and generating a multiloop cardiac patch in order to provide more mechanical support in comparison to the previous one.[114] They optimized the twitch tension of the cardiac patch by culturing them under elevated ambient oxygen, auxotonic load, and culture media with insulin. Four weeks after implantation, H&E staining showed a compact and well differentiated heart muscle attached to the epicardium (**Figure 3A)**.[114] The grafted hearts were smaller, had lower left ventricular end-diastolic pressure (LVEDP) and tau, as well as better fractional area shortening (FAS) and anterior wall thickening fraction (AWThF). Electrical integration was reported by performing point stimulation of an implanted patch and recording the propagated potential in both the patch and the host myocardium, measuring the total activation time and the QRS amplitude. Nevertheless, in posterior cardiac patch models, the research group found evidence against extensive cardiac patch/host myocardium electrical coupling.[115] They developed a cardiac patch in the shape of a spherical pouch-like structure that could be slipped over and cover most of the ventricular heart surface. Similar to their previous fabrication methods, they seeded neonatal rat cardiomyocytes into the collagen and Matrigel matrix and guided the formation of a pouch-like cardiac construct as it contracted by introducing spherical casting molds. Results showed that the cardiac pouch was vascularized and contained thick muscle aggregates in vivo. However, they observed a 50-200 μm gap free of cells in between the cardiac pouch and the host muscle in some areas. In addition, preservation of the nonmyocytes surface lining of the cardiac pouches in vivo was also reported. These results suggested that patch integration might not be electrical but mechanically coupled.[115] Their most recent model consists of a hexagonal clinical-sized

cardiac patch with the capacity of 40×10^6 cells/8 mL and is currently on its way to clinical trials.[116]

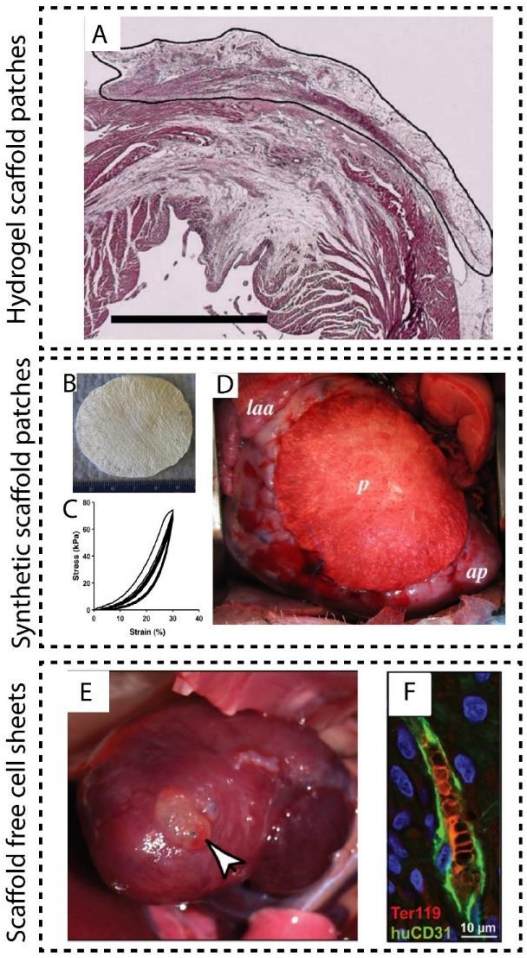

Figure 3: Examples of epicardial delivery of tissue engineered patches for cardiac therapy. (**A**) H&E stained image of an engineered heart tissue made from collagen type 1 matrix mixed with neonatal rat cardiomyocytes engrafted on the surface of an infarcted heart.[114] (**B-C**) Macroscopic view of a porous circular PEUU patch fabricated by thermally induced phase separation that presented a (C) typical cyclic tensile response curves with a maximum 30% strain. (**D**) A macroscopic image of the PEUU patch implanted 2 weeks after I-R injury (laa, left atrial appendage; ap, apex of heart).[117] (**E**) An imager of a scaffold-free cardiac tissue patches grafted on the surface of a rodent heart. (**F**) Immunostained image shows Ter-119-positive blood cells (red) inside a engrafted vessels indicating connection with host vasculature.[118] Permission for reprints of all images shown has been acquired.

Other research groups have also engineered collagen-based cardiac patches. Miyagi et al. worked with ultrafoam collagen sponge scaffolds embedded with high or low quantities of recombinant VEGF-165 seeded with H5V endothelial cells and bone marrow cells

(BMC).[119] Patches with higher quantities of VEGF showed higher regenerative responses by promoting more cell proliferation within the graft, increasing blood vessel density and cellular engraftment, all characteristics needed for higher perfusion and retention of cells in thicker grafts. Roche et al. also reported a 47 fold increase of cell retention by using collagen patches seeded with hMSCs in comparison to saline control cell delivery, retaining in between 50% to 60% of cells present immediately after transplantation.[96] Due to its tunable mechanical properties, alginate has also been investigated as a scaffold for cardiac patches. Leor et al. seeded fetal cardiac cells into 3D porous alginate scaffolds and implanted them into rat MI models.[19] Little to no trace of the alginate scaffolds was found after nine weeks of implantation. Also, host hearts showed significant neovascularization and attenuated LV dilatation and failure. Later, this research group improved the alginate scaffold by mixing in IGF-1, stromal-cell derived factor 1 (SDF-1), and VEGF, and prevascularized the cardiac patch on rat omentum before cardiac implantation into MI models.[120] Once implanted, the heart with omentum-generated cardiac patches showed lower fractional area change, FS, LVEDD and LVESD in comparison to MI hearts. Furthermore, the group reported electrical integration of the cardiac patch into the host myocardium as they detected higher signal amplitude and lower capture threshold in Langerdorff heart preparations treated with omentum-generated patches. The addition of growth and angiogenic factors increased the survival of host tissue and vascularization and tissue maturation of the cardiac patch. Nevertheless, alginate is not a good conductive material and could limit the ability of the patches to contract strongly as a unit.[121] However, Dvir et al. showed that alginate conductivity can be improved by embedding gold nanowires, which resulted in tissues that were thicker, better aligned and contracted synchronously when electrically stimulated. [122]

Fibrin has also been explored as a scaffold for cardiac patches. Liu et al. developed a patch by mixing fibrinogen and thrombin and entrapping MSCs inside the matrix.[123] By applying the cardiac patch into swine MI models, a significant increase of the LV systolic wall thickening fraction and neovascularization was reported. A fibrin patch embedded with vascular cells derived from human iPSCs was also used by Xiong et al., with the purpose of testing the functional consequences of this type of cells.[124] Immunosuppressed Yorkshire swine subjected to this cardiac patch application also showed a reduced LV remodeling and improvement of vascular density, as well as improvements in the contractile function and ATP utilization rate of the heart.

Besides collagen, alginate, and fibrin, a wide variety of natural scaffolds have been implemented in cardiac regenerative medicine. Some examples include chitosan, silk fibroin, and hyaluronic acid[125,126], gelatin[127] and decellularized matrixes[128,129]. Chi et al. fabricated a patch with chitosan, silk fibroin, and hyaluronic acid and tested the therapeutic effects both with MSCs[125] and without any cells[126]. Both the patches with and without MSCs implanted in rat MI models stimulated the secretions of various paracrine factors such as VEGF, bFGF and HGF with a significant increase of the released paracrine factors in the cell patch group. Also, both groups reduced the dilation of LVs, increased the thickness of their walls, and improved their FS and angiogenesis. The MSC patch group also reduced the apoptosis of cardiac cells in the infarct zone. Li et al. inoculated fetal rat ventricular cells into a gelatin mesh and stitched it to scar tissue in adult rat hearts.[127] Cardiac-like tissue within the grafts and a partly absorbed gelatin mesh was observed five weeks after implantation. The ventricular function and morphology were not statistically different between the gelatin patch group and the non-treated group. Fleischer et al. electrospun albumin nanofibers and formed a patterned patch with cage-like structures that held PLGA (poly lactic-co-glycolic acid)

microparticulate systems that controlled the release of VEGF and dexamethasone.[130] By seeding cardiac cells and endothelial cells in the patterns and grooves of the individual scaffolds, they were able to stack up multiple layers, achieving a modular assembly of a vascularized thick cardiac patch. The addition of VEGF further enhanced vascularization, while dexamethasone promoted anti-inflammatory effects at the infarct site.

Ott et al. was the first group to completely decellularize an entire heart and use the obtained natural extracellular matrix (ECM) as a scaffold for cellular reperfusion.[131] Taking advantage of the preservation of the heart´s original architecture and protein contents through this technique, Wang et al. developed a patch from decellularized heart ECM.[128] They inoculated the ECM patch with iPSC-derived cardiac cells and implanted it into rat MI models. The natural heart ECM promoted the maturation of hIPSC-derived cardiac cells as cTnT, MYH6, atrial natriuretic factor (ANF), and B-type natriuretic peptide (BNP) and other genes required for contractile function and indicators of maturation were increased in the engineered ECM patches in comparison to cell aggregates. Results also showed that the LVEF and LVFS were increased and both the left ventricular systolic inner diameter (LVIDs) and left ventricular diastolic inner diameter (LVIDd) were decreased when the cardiac patches were applied. Besides natural heart ECM, other sources of ECM, such as the mucosal side of a decellularized porcine jejunal submucosa ECM, can been used as a scaffold for cardiac patches. Frederick et al. showed that ventricular remodeling was attenuated and profound neovasculogenic response was generated by implanting a jejunal submucosa ECM patch seeded with bone marrow mononuclear cells into rat MI model. [129]

2.2.2 Synthetic scaffold-based approach

Ideally, the scaffolds should recreate the characteristics of the native ECM without triggering an immune response that could lead to fibrous encapsulation or destruction of the material.[132] As mentioned in the previous section, the advantage of using natural scaffolds such as ECM or hydrogels is that the architecture of the constructs and protein contents are preserved. In addition to bringing structural support, natural scaffolds also promote cell migration, proliferation, differentiation, and maturation.[133] Nevertheless, a limitation of using natural scaffolds is that current decellularization techniques cannot eliminate DNA contents completely. Research has shown that most commercially available ECM scaffold materials contained measurable amounts of DNA, which could generate inflammatory or immune response affecting the graft.[134] In addition, batch-to-batch variation is a common denominator of natural biomaterials when applied as ECM scaffolds, reducing the effectiveness of the treatments and their reliability as research tools significantly.[135,136] A possible alternative to these limitations is the incorporation of synthetic polymeric biomaterials as a replacement to natural scaffolds.

A wide variety of synthesizable polymers have been explored as scaffolds in cardiac regenerative medicine. Matsubayashi et al. seeded vascular smooth muscle cells into a biodegradable PCLA (poly a-caprolactone-co-L-lactide) reinforced with knitted poly-L-lactide sponge fabric.[137] PCLA enhanced cell colonization while PLA maintained patch structure and dimension while cells developed their own ECM. Both seeded and unseeded patches limited LV dilatation and preserved systolic function meaning that the stiffness of the PCLA-PLA scaffold was responsible for mechanical support. Similar to this, Kai et al. electrospun PCL (poly a-caprolactone) and gelatin nanofibrous scaffolds and seeded them with MSCs.[138] Some of the properties given by these nanofibrous scaffolds are high porosity

to permit nutrient and waste diffusion, high surface area to volume ratio favoring cell adhesion, migration and proliferation, and controllable fiber size and mechanical properties. Nevertheless, PCL has been used as toughening material and PLA has inherent brittleness limiting their practical applications when modulation of toughness is needed.[139,140]

Cyclic mechanical strain enhances the development and function of tissues such as smooth and cardiac muscles.[141,142] Thus, the ideal material for cardiac patches should be sufficiently strong to withstand the force of repeated contraction in the myocardium.[143] The speculated advantage of using elastomeric polymers instead of stiffer materials is that cardiac muscle fibers in both the risk zone and border zone can stretch during diastole and contract during systole, mimicking in a more optimal way the native characteristics of the heart. Wagner et al. developed a porous elastic PEUU (poly(ester urethane)urea) and placed it on MI rodent[144] and Yorkshire swine[117] models (**Figure 3B, D**). Adverse LV remodeling was prevented through the reduction of wall stress and thinning, and cardiac function was preserved. Most importantly, by using an elastic scaffold, they were able to obtain more compliant LVs which approximated better passive mechanical properties of healthy cardiac tissue in comparison to other elastic yet stiffer materials, resulting in thicker heart walls (**Figure 3C)**.[117,145]

Two elastomers with desirable characteristics for scaffolds in cardiac regenerative therapy were developed in the last decade. Langer et al. developed PGS (polyglycerol-sebacate) by polycondensation of glycerol and sebacic acid.[146] In vitro and in vivo studies confirmed low immune response and biodegradability as implants were totally absorbed within 60 days. The tensile Young's modulus of the polymer was reported as 0.282 ± 0.0250 MPa and ultimate tensile strength of >0.5 MPa, therefore considered a soft polymer. Marsano et al. further explored the effects of incorporating PGS scaffolds into a cardiac patch and how

the scaffold stiffness affects cardiac contractility.[147,148] By testing three different PGS (polyglycerol-sebacate) scaffolds stiffnesses, they were able to determine that the lowest (2.35 ± 0.03 kPa) compressive stiffness of the scaffold generates the greatest contraction amplitude, ECM deposition, and compressive modulus after eight days.[148] Further improvements in the viability, vascularization, and functionality of these cardiac patches were obtained by providing intrinsic vascularization stimuli through VEGF release.[147]

Tranet al.l synthesized POMaC (poly octamethylene maleate (anhydride) citrate), a soft biodegradable and biocompatible elastomeric material that can mimic mechanical properties of a wide range of tissues.[149] POMaC mechanical properties can be controlled through its dual UV radiation and/or polycondensation crosslinking mechanisms, and by regulating the monomer ratios of its precursors. POMaC displays an elastic modulus range in between 0.03 and 1.54 MPa, and elongation at break between 48% and 534% strain. By toning POMaC mechanical characteristics and microfabricating a lattice-shaped construct, Montgomery et al. were able to develop a flexible and shape-memory scaffold.[23] This flexibility and shape-memory characteristics enabled the possibility of minimally invasive delivery as the cardiac patch could be folded and delivered through 1mm orifices such as endoscopy surgical instruments. In addition, the tunable elasticity values of POMaC approach those of the native human myocardium (10-20 kPa at the beginning of diastole).[150] The POMaC patch seeded with cardiac cells resulted in functional cardiac improvement following MI in rat and swine models as total wall thickness was increased and collagen levels in the border zone were decreased. Nevertheless, the application of fibrin glue or stitches was needed to secure the correct placement of the cardiac patches.

2.2.3 Scaffold free cell sheets

Not all cardiac patches require the use of a scaffold. In the 1990s, Okano et al. developed a novel technique to culture and harvest cells called cell sheet technology.[151] By coating normal polystyrene dishes with the temperature-responsive poly(N-isopropyl acrylamide) (PIPAAm), it is possible to change the hydrophilicity-hydrophobicity of the surface. This enables cells to attach into the plate over 32°C, and to detach completely below this temperature. Because no enzymatic digestion is needed, detached cells form a cell sheet with cell-to-cell connections through adhesion proteins. Miyaharaet al.al used this technology in order to develop monolayered MSCs and dermal fibroblasts sheets with the purpose of repairing the heart after MI.[107] They were able to implant these cell sheets into rat MI models without the need for sutures or additives, which may be due to cell-to-cell connections and ECM deposits. After implantation, MSCs sheets thickened gradually up to 600μm, which served both as mechanical support preventing wall thinning and stress, and functional support decreasing the LVEDP and increasing the left ventricle maximum contractility dP/dt. In addition to this, significant neovascularization was observed in the MSCs sheets. More importantly, a small amount of cardiomyocyte markers such as cardiac troponin T and desmin were found inside the graft, suggesting the differentiation of some MSCs into cardiomyocytes. Nevertheless, because the number of cardiomyocytes found in the MSCs sheet was low, both the functional improvements and the neovascularization may be attributed to the paracrine effects of the high levels of angiogenic and antiapoptotic cytokines excreted by the cells.

Both hESCs and hIPSCs derived cardiomyocytes have been used as a cell source in cell sheet implantation. Stevens et al. first tried to develop cell sheets made of pure hESCs

derived cardiomyocytes, but no substantial engraftment and poor survival were found in vivo.[118] The research group attributed this issue to ischemia due to slow vascularization, so in order to improve engraftment HUVEC and mouse embryonic fibroblasts (MEF) were incorporated into the culture. Cardiac cell sheets containing supporting vascular and stromal cells presented a 20-fold more vessel structures in comparison to pure cardiomyocyte sheets as well as a better active contraction and a more myocardial-like passive mechanical stiffness. These sheets also resulted in >10-fold larger MHC-positive and CD31-positive grafts than cardio-only sheets. This showed that the inclusion of vascular and stromal elements into cardiac sheets increases both performance and viability after transplantation as well as engraftment and integration of human microvessels into the host myocardium (**Figure 3F**). Nevertheless, sutures were needed in order to keep the cell sheets in place, as simple attachment was not effective (**Figure 3E**).[118] Zhang et al. showed that the addition of fibrin gel during cardiac sheet delivery can increase the engraftment rate by 31%.[152] Even though the group used a >92% pure hIPSCs derived cardiomyocyte sheet, they reported significant vascularization in the graft and improvement in the LVEF and LVFS of the MI heart in rats. A possible explanation for the observed differences could be the implementation of fibrin glue or the epigenetic memory of the iPSCs used by Zhang. Since cardiac fibroblasts were used as a source for the iPSCs in comparison to hESC, better therapeutic effects may result from using cardiac cells instead of noncardiac-lineage cells as a source for iPSCs.[153,154]

Cardiac patches have been developed and further improved and optimized since the 2000s. Extensive research has been done on their regenerative capabilities for post-MI hearts. Functional improvements have been reported including reduction of wall thinning and FS and improvement in LV dimensions, volumes and ejection fraction. The scaffolds within the patch provide mechanical and structural support and suitable elasticity for cells preventing

LV remodeling.[155] Other important therapeutic effects such as angiogenesis and cardioprotection might be attributed to the paracrine factors excreted by the cells within the patch. The improvement of cell survival, viability and engraftment after delivery in comparison to cell therapy might be due to the application of more mature and well-developed tissues instead of individual cells. A major requisite for successful cardiac repair is the correct electrical and mechanical integration of the graft with the host tissue.[60] Even though some cases of electrical integration have been reported, there is evidence suggesting otherwise. For example arrhythmogenicity wasn't found despite spontaneous electrical activity in their cardiac graft[114] and gaps in between the patch and the host heart were observed.[115]. A possible explanation for the lack of electrical integration is the endocardium layer that exists in between the cardiac path and the heart muscle. Therefore, cardiac patches functional integration might be mechanically based instead of electrical. Another important limitation is the highly invasive approach, as the delivery of most types of cardiac patches requires open-chest surgery. The development of foldable scaffolds that enable minimally invasive surgeries such as endoscopy might be the way to overcome this limitation.[23]

2.3 Acellular-based approach to cardiac repair

2.3.1 Biomaterials as a mechanical support and delivery vehicle for growth factors

The complications presented in cell therapy and cardiac tissue patches have led research groups to explore acellular methods. Injectable biomaterials, such as alginate or fibrin, have had promising results in preclinical trials serving as a bulking agent that maintains the LV geometry, thickness and mechanically supports the heart wall.[156] Furthermore, biomaterials can serve as carriers of bioactive molecules such as growth factors, cytokines and other peptides in order to enhance the therapeutic effects.[157]

Alginate has been the most widely used injectable hydrogel for post-MI treatment. Some of the ideal characteristics that injectable biomaterials for cardiac repair should have are: controllable gelation, no detrimental effects on myocardial function or remote organs, enough tissue-bulking properties, biodegradable, nonimmunogenic, and nonthrombogenic.[158] The adjustable gelation, mechanical properties and degradation rate of alginate make it a good candidate for preventing further ventricular remodeling post-MI. Landa et al. developed a low viscosity, bioresorbable, calcium-crosslinked alginate solution that undergoes phase transition after injection.[159] MI rat models were intracoronary injected with this biomaterial, resulting in the increment of scar thickness as well as diastolic and systolic anterior wall thicknesses, and prevented LV systolic and diastolic dilatation and dysfunction compared with control. Leor et al further explored the effectiveness of this treatment on swine MI models.[158] Results showed that alginate prevented LV enlargement and increased scar and anterior wall thickness compared with saline control by filling the scar with myofibroblasts and collagen (**Figure 4A**).

To enhance its therapeutic effect, alginate can be further embedded with bioactive molecules or mixed with other polymers. Mihardja et al injected a blend of 0.025% polypyrrole with alginate into the infarct zone of rats, and observed a higher arteriole density in comparison to pure alginate.[160] Yu et al. also reported a higher angiogenic response by modifying alginate with arginine-glycine-asparagine (RGD) peptides, which improved human umbilical vein endothelial cells (HUVEC) proliferation and adhesion in comparison to pure alginate and saline (**Figure 4B-D**).[161] Ruvinov et al. developed an injectable IGF-1/HGF affinity-binding alginate system and tested it on rat MI models.[162] They observed that the treatment preserved scar thickness, attenuated infarct expansion, reduced scar fibrosis and increased angiogenesis. In addition, mature blood vessel formation at the infarct

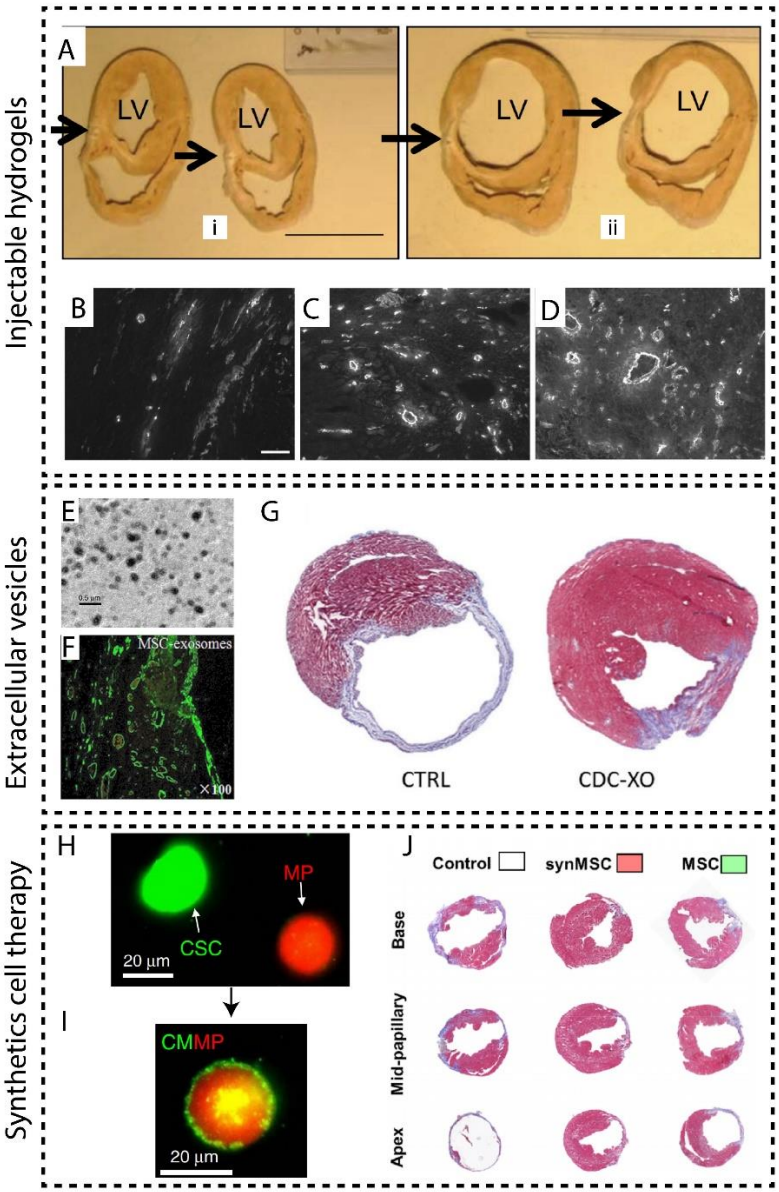

Figure 4: Examples of acellular based approach for cardiac therapy. (**A**) Sections of heart treated with (i) alginate or (ii) saline showing an increase in scar thickness (arrows).[158] (**B-D**) Fluorescent images of vessels (white) in the infarct area treated with (B) PBS, (C) LVM, and (D) LVM-PPy, showing an increased angiogenesis and myofibroblast infiltration.[160] (**E**) Transmission electron microscopic image of conditioned medium showing the presence of EV.[163] (**F**) Fluorescent image of (alpha-smooth muscle actin staining, green) neoangiogenesis in the infarcted zone four weeks after MSC-EVs treatment.[164] (**G**) Masson's trichrome-stained sections of media (control) or CDC exosomes treated post-MI hearts.[165] (**H, I**) Texas red succinimidyl ester-labelled MPs (H, red) were cloaked with the membrane fragments of green fluorescent DiO-labelled CSCs (H, green) to form CMMP (I, red particle with green coat).[166] (**J**) Masson trichrome stained images of infarcted heart treated with PBA (control), synMSC-, and MSC, showing the protective effects of synMSC and MSC treatment on heart morphology.[167] Permission for reprints of all images shown has been acquired.

prevented cell apoptosis and induced cardiomyocyte cell cycle re-entry. Alginate protected the growth factors from degradation, retaining bioactivity, and therapeutic effect for a longer period in comparison to alginate without further supplementation.[162] Hao et al. also developed an alginate system with sustained delivery of vascular endothelial growth factor-A165 (VEGF-A165) and platelet-derived growth factor-BB (PDGF-BB).[168] The immersion of the growth factors in the alginate enabled a precise sustained delivery, which resulted in a greater formation of mature vessels and improved cardiac function compared to delivery of single factors.

Fibrin glue has also been used as an injectable biomaterial for cardiac repair. Similar to alginate, studies have shown that fibrin glue preserves LV geometry and cardiac function following myocardial infarction[169] and increases the arteriole density in the infarct scar[98]. Even though the molecular properties of fibrin such as binding domains for various growth factors and RGD sequence make it more bioactive in comparison to alginate, studies have shown that no significant difference was found in the degree of angiogenesis of both polymers.[170,171] Mukherjee et al. tested a combination of both approaches and injected a mixture of fibrin-alginate hydrogel and concluded that the infarct expansion was diminished by altering the collagen composition within the MI and border regions.[172]

Besides alginate and fibrin, other hydrogels have been used as injectable biomaterials for cardiac repair. Dorsey et al. evaluated the effects of an injectable hyaluronic acid-based hydrogel with a degradation profile greater than eight weeks and an initial compressive modulus greater than ten times that of the normal myocardium in swine MI models.[173] MRI analysis showed that the hydrogel injection improved LV structure and function, preserved infarct thickness, and limited infarct dilation. Wu et al. synthesized a temperature-sensitive, aliphatic polyester hydrogel conjugated with VEGF and evaluated its therapeutic effects on

rats post-MI. [174] Results showed that even though the polyester hydrogel alone increased scar thickness, ejection fraction, and blood vessel density, when conjugated with VEGF, a significant increment in these cardiac indicators was detected.

Biomaterial injection into the MI heart has been taking relevance in the scientific community as it is an acellular approach, reducing the limitations observed with cell therapy. Also, this approach has yielded some good results in preventing LV remodeling and certain improvement of cardiac function. The therapeutic effects of biomaterial injection are mainly due to the mechanical support they bring as bulking agents inside the myocardium and the angiogenic capability of biomaterials by promoting cell migration. Further anti-apoptotic and pro-survival effects can be achieved by embedding biomaterials with cytokines and growth factors. Nevertheless, no real cardiac muscle regeneration has been achieved yet through this approach.

2.3.2 Extracellular vesicles

The trophic and paracrine effects of cell therapy and cardiac tissue patches are not mediated by soluble molecules alone. Exosomes, large lipid extracellular vesicles (EV) with a diameter of 50–100 nm, containing miRNAs, growth factors, cytokines and other functional proteins have shown to have a cardioprotective effect as demonstrated by Lai et al. [163] This group prepared a MSCs conditioned medium concentrated by using a tangential flow filtration system, and injected it into MI injured mice (**Figure 4E**). Arsnal et al. further explored this approach and quantified that the infarct sizes as a percentage of the area at risk (ISAAR%) were reduced to 45% in comparison to saline control.[175] They concluded that MSCs exosomes increase the ATP and NADH, reduce oxidative stress, activate pro-survival signaling, and prevent remodeling in ischemic/reperfused hearts. Protein contents inside

MSCs EVs increase significantly during hypoxia and serum-free incubation which promote the proliferation, migration, and tube formation of HUVECs and blood vessels, hence a higher blood flow recovery in rat myocardial infarction model (**Figure 4F**).[164,176] MSCs EVs also have shown to reduce the inflammatory response in the infarct site by inhibiting cell proliferation and impairing T-cell function.[164] EV extracted from Akt-modified human umbilical cord MSCs also improve cardiac function and enhance blood vessel formation in vivo by activating platelet-derived growth factor D.[177]

Gene therapy aims to deliver plasmids in the form of microRNAs or DNA with the purpose of correcting genetic defects or to express gene products that are therapeutically useful.[35] MicroRNAs, which are involved in cell proliferation, differentiation and development, have shown to have a cardioprotective role after MI. Feng et al. were able to capture the release of miR-22 enriched exosomes from MSCs through time-lapse confocal imaging and showed that the delivery of these exosomes reduced apoptosis in ischemic cardiomyocytes, ameliorated fibrosis and improved cardiac function post-MI via downregulation of Mecp2.[178] Similar to this, Yu et al, also showed that both miR-221 and miR-19a extracted from MSCs are important cardioprotective factors as they prevent apoptosis by reducing the expression of p53 upregulated modulator of apoptosis (PUMA), and activating the Akt and ERK signaling pathways.[179,180] Wang et al compared the cardioprotective effects of conditioned media from human endometrium-derived (EnMSCs), human bone marrow (BMMSCs), and adipose-derived (AdMSCs) MSCs, and determined that EnMSCs EV offer superior cardioprotection as they expressed higher miR-21 content, which also enhances cell survival through PTEN/Akt pathway.[181] MiR-210 enriched MSCs EV also has shown to improve cardiac function through angiogenesis enhancement. [182]

Cardiosphere-derived cells (CDC) are a cardiomyocyte progenitor cell (CMPC) type obtained through the primary culture of endogenous adult heart tissue. This type of cells have shown to reduce scarring after myocardial infarction, increase viable myocardium, and boost cardiac function in preclinical models.[183-185] CMPC have been explored as possible EV sources. Ibrahim et al. explored the therapeutic effect of CDC EV and showed that exosomes reproduce CDC-induced therapeutic regeneration and that inhibition of exosome production undermines the benefits of CDCs.[165] This group detected that CDC EV are enriched with miR-146a, miR-22 and miR-24, which seem to increase the viable heart mass, to increase adaptability to cardiac stress, and to decrease myocardial scar formation through modulation of TGF-b signaling pathway **(Figure 4G)**. Vandergriff et al. increased the retention of CDC EV by using cardiac homing peptide (CHP) as a targeting agent of exosomes delivered intravenously to the infarcted heart.[186] Vrijsen et al. showed that human fetal CMPC EV contain matrix metalloproteinases (MMPs) and extracellular matrix metalloproteinase inducer (EMMPRIN) which might suggest that EV can break down and remodel the extracellular matrix, key processes for endothelial cell migration and angiogenesis.[187]

Other cell sources such as ESCs and iPSCs have been explored as EV sources. Khan et al. showed that ESCs EV are enriched with miR290-295, particularly miR-294, which was tied to the enhanced neovascularization, cardiomyocyte and CPC proliferation and survival in mice after MI.[188] Liu et al developed a EV delivery system through a cardiac patch in order to improve EV retention and prolongate therapeutic effects.[189] In addition, the group compared which cell source between differentiated iPSCs-CMS and undifferentiated iPSCs showed better results as EV source. Genomic analysis of both iPSCs-CMS and iPSCs showed a marked difference in the miRNA contents of their EV. This difference in more cardiac-specific miRNAs in the iPSCS-CMS patch resulted in lower infarct size area, lower LVDD

and LVSD, and higher LVEF in comparison to the iPSCS patch. Furthermore, this research showed that EV treatment didn't induce arrhythmias as observed in cell-related therapies.[189]

2.3.3 Synthetic cell therapy

Recently, Tang et al. were able to fabricate cell-mimicking microparticles (CMMP) by coating poly(lactic-coglycolic acid) (PLGA) microparticles with CSCs[166] or MSCs[167] membranes and loading them with their respective secretomes, including both soluble factors and exosomes (**Figure 4H,I**). The hypothesis behind this technique is that both cell-to-cell contact and EV delivery trigger intracellular protective/regenerative pathways in the host cells; therefore, by mimicking this mechanism, similar therapeutic effects can be observed. CSCs-CMMP delivery reduced the scar size, and improved the LVEF four weeks after delivery.[166] Similar to this, MSCs-CMMP (synMSCs) intramyocardial injection into mice MI models reduced significantly the infarction area and undistinguishable changes on the LV volume in between synMSCs and MSCs were found (**Figure 4J**).[167]

Despite the positive results, the research group found that the delivery strategy generated accumulation of synMSCs in the lungs, distant from the site of injection. This was likely due to heart vessel damage by needle injection which led to posterior venous drainage of the particles into the lungs.[166] More recently, the research group developed a new delivery approach by embedding the CMMP into a cardiac patch made from decellularized myocardial ECM and fixing it to the epicardium with sutures.[190] This method showed better retention of the CMMP on the heart and reduced the off-target biodistribution to other organs while improving % LVEF and % LVFS, reducing the infarct size and increasing the viable myocardial tissue. Most importantly, immunostaining with Ki67, vWF and pH3 suggested a promotion in angiomyogenesis, one of the key limitations of acellular approach so far. In addition, both the CMMP and CMMP-cardiac patch approaches showed that the limitation

of cryopreservation stability of cells might have been overcome as rapid thawing did not alter the structure and lyophilization did not alter the traits of synthetic cells while maintaining a similar secretome and surface antigen profiles as stem cells.[166,167,190]

Even though the therapeutic effects of acellular approach seem to be promising, there are some underlying limitations. Biomaterial injection has shown good results by preventing LV remodeling through mechanical support and by promoting angiogenesis through cell migration which can be further enhanced with the addition of growth factors. Single delivery of various growth factors and genes have been explored as therapeutic agents yielding several therapeutic effects such as cardioprotection, enhanced angiogenesis, and reduced inflammation and apoptosis.[191,192] Nevertheless, these therapeutic effects have a limited propagation due to low diffusion and short half-life as protein degradation occurs.[34,193] Hence, in order to be beneficial, the cargos need to be delivered specifically to the damaged heart tissue. Previous work has shown that most of the EV or synthetic cells delivered intravenously are absorbed within the liver[194] or the lung[166] far away from the desired target. This limitation could be overcome by injecting them intramyocardially, but since continuous delivery is needed, periodically injections would be needed, making the treatment more invasive and less feasible. Other methods such as incorporating cardiac homing peptide have potential to improve targeted delivery, but further studies need to be made.[186] Furthermore, no reports were found on remuscularization of the myocardium through the implementation of EV, meaning that the functional improvements are due to cardioprotection and the anti-inflammatory, anti-apoptotic and pro-survival signals delivered through the contents of the EVs. Better results in comparison to simple growth factor and gene therapy may be due to the protein protection against degradation increasing their half-life and range of action. Novel approaches such as the incorporation of synthetic cells into a cardiac patch have shown to

help overcome both limitations by having a more specific delivery of the desired therapeutic factors into the heart as well as certain degree of angiomyogenesis but further functional characterization is needed.[190]

2.4 Summary

Despite the great advances made in cardiac regenerative medicine, each of the three major categories have key limitations that need to be overcome to successfully heal the MI heart. Intramyocardial cell delivery has had very low cell survival and engraftment rate from its beginnings. The addition of biomaterials as carriers and prosurvival cocktails have improved these rates, nevertheless, a high number of cells in the order of billions is still needed to achieve significant remuscularization. The use of iPSCs could satisfy this high demand for cells. Although earlier studies reported teratoma formation with the use of iPSCs, significant advances have been made in differentiating cardiomyocytes with high efficiency and purity, greatly diminishing this risk. This approach has also shown the most remuscularization of the three major categories of cardiac therapy, however, the lack of proper maturation of the delivered cells can lead to arrhythmias and tachycardia.

Cardiac patches have shown better tissue survival, viability, and engraftment after application in comparison to cell therapy likely because they are delivered as more mature and better structured tissues instead of individual cells. Furthermore, cardiac patches give mechanical support to the heart wall preventing LV geometry distortion. However, little to no evidence has been found on the remuscularization properties of this approach. There is also contradicting evidence on proper electrical integration of the cardiac patches with the host muscle, which could be mainly due to the endocardium layer in between the myocardium and the patch. Even though the mechanical integration of the cardiac patch with myocardium

has shown functional improvements, electrical integration might be needed to further enhance the therapeutic effects. Another drawback is that cardiac patches usually require a highly invasive open chested surgery. But the implementation of synthetic flexible scaffolds with shape-memory has enabled much less invasive keyhole surgeries.

Acellular cardiac therapy has emerged as the latest approach in cardiac therapy. It is based on the assumptions that most of the therapeutic effects found in both intramyocardial cell delivery and cardiac patches come mainly from the paracrine effect of growth factors, cytokines and miRNAs, and the mechanical support brought by biomaterials. Studies have shown that this approach promotes recovery of contractile function and cardioprotection without the arrhythmic burden of cell related therapies. The most pressing limitation with this approach is the need for a highly specific and constant delivery of the treatment to the damaged heart tissue as more general delivery systems, for example intravenous delivery, have shown to be ineffective. Incorporation of a low invasive sustained delivery system such as EV or synthetic cell cardiac patches could help overcome this limitation. However, a drawback of this approach is the lack of evidence of remuscularization in most studies of this approach. More recent studies have reported some level of remuscularization but more functional assessments are required to further confirm this claim.[190]

Then, which of the current approaches has the best therapeutic result? A detailed summary of the current treatment methods (**Table 1**) is presented. There are multiple parameters that measure the therapeutic effect of cardiac repairs including infarct area, heart wall thickness, LV contractility, amount of blood vessels, LV pressure and LV dimensions. However, the most common functional parameters for cardiac output are % EF and % FS. We performed a meta-analysis of 65 studies and compared these two parameters after treatment in rodent MI models. No statistically significant difference was found between the

three categories of cardiac repair strategies (**Figure 5**). However, these comparisons and results should be carefully evaluated as there is extensive variation in the protocols between studies, such as the timepoint at which the treatment was applied and the duration of the study. Application of the therapy immediately after the MI was generated could lead to higher final EF and FS in comparison to application of the therapy a few hours or even days after the MI. Nonetheless, the similarity of results in EF and FS between each approach is likely due to the respective unique pros and cons of each method.

Table 1: Selected works representing current approaches in cardiac regenerative therapy.

Approach		Cell Sources	Biomaterials	Bioactive factors	References
Intramyocardial cell delivery	Cell therapy	NRCMS	-	-	21,45,46
		SM	-	-	47,48,53,54,59,60,63,64,98
			-	VEGF	57
			-	IL1-iGF	58
		MSCs	-	-	69-72,75,76
		ESCs	-	-	79-81
		iPSCs	-	-	87-91
		iPSCs-CMS	-	-	50
	Biomaterial vehicle delivery	ESCs	PSC	PSC	22,49,82,83
		HUVEC	alginate	RGD	161
		MSCs		RGD, FGF2	51
		MSCs	alginate/Chi/ Glyp	-	96
		SM	fibrin	-	98
		BMC		-	52
		NRCMS/hESCs-CMS	PEG/fibrinogen	-	100
		ESCs	MMP	Tb4	101
		CSCs	P(NIPAM-AA)	-	103
Epicardial delivery of tissue engineered cardiac patches	Hydrogel/ natural patches	NRCMS	collagen/ Matrigel	-	113-115
		H5V EC & BMC	collagen	VEGF	119
		MSCs		-	96
		fetal CMS	alginate	-	19
				IGF-1, SDF-1, VEGF	120
			Alginate w/ Au nanowires	-	122
		MSCs	Fibrin	-	123
		iPSCs		-	124

		MSCs	chitosan, silk fibroin and hyaluronic acid	-	[125,126]
		fetal CMS	gelatin	-	[127]
		CMS & EC	Albumin/PLGA	VEGF	[130]
		iPSCs-CMS	ECM	-	[128]
		BMC		-	[129]
Epicardial delivery of tissue engineered cardiac patches	Synthetic scaffold-based approach	VSMC	PCLA/ PLA	-	[137]
		MSCs	PCL/gelatin	-	[138]
		-	PEUU	-	[117,144,145]
		CMS	PGS	-	[148]
		CMS, SM		VEGF	[147]
		RNCMS	POMaC	-	[23]
	Scaffold free cell sheets	MSCs/DFBS	-	-	[107]
		ESCs-CMS/ HUVEC/ MEF	-	-	[118]
		iPSCs	fibrin glue	-	[152]
Acellular based cardiac repair	Injectable hydrogels	-	alginate	-	[158,159,170,171]
				RGD	[161]
				IGF-1/ HGF	[162]
				VEGF/ PDGF-BB	[168]
			Alginate/ polypyrrole	-	[160]
			Fibrin glue	RGD	[98,169-171]
			fibrin/alginate	-	[172]
			hyaluronic acid	-	[173]
			polyester	VEGF	[174]
	Extracellular Vesicles	MSCs EV	-	miR-22, 221, 19a, 21, 210	[163,175,177-182]
		CDC EV		miR-146a, 22, 24	[165,186]
		CMPC EV		MMPs, EMMPRIN	[187]
		ESCs EV		miR290-295	[188]
	Synthetic cell therapy	CSCs CMMP	PLGA	secretomes	[166]
		MSCs CMMP			[167]

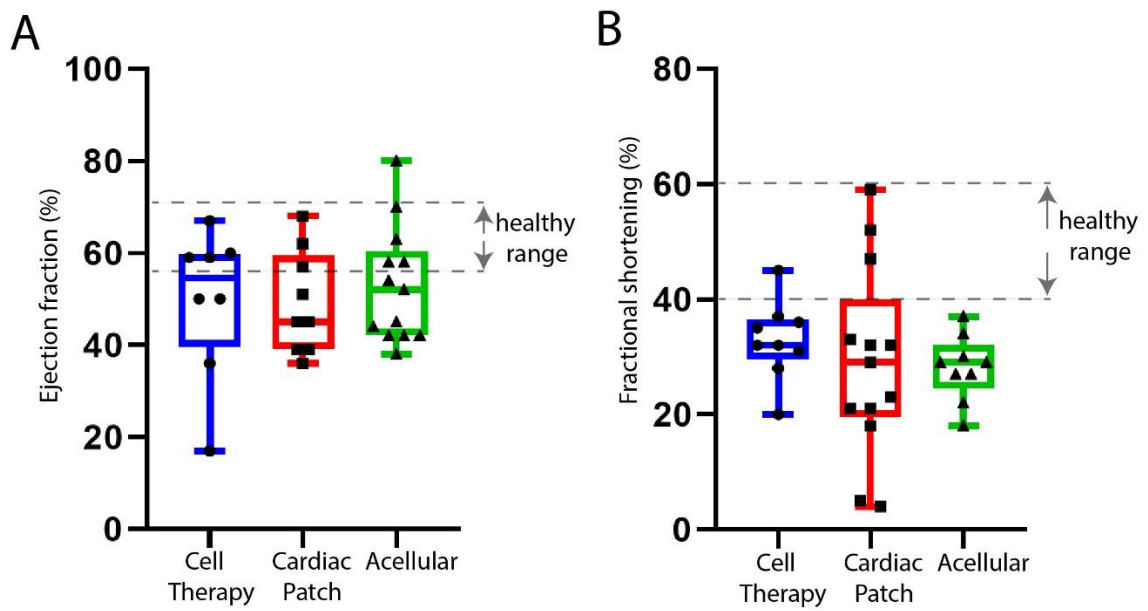

Figure 5: Comparison of cardiac functional outputs resulted from treatments with cell therapy, cardiac patches, or acellular therapy from 65 different studies. (**A-B**) Quantification of (A) ejection fraction and (B) fractional shortening after treatment with cell therapy, cardiac patches or acellular therapy in MI rodent models. One-way ANOVA showed no significant statistical difference between the treatment groups. Gray dotted lines show the normal range of the cardiac functional output in healthy rodent models.

Cardiac regenerative medicine is an extensive field that has rapidly evolved and improved in the past two decades. The ideal cardiac therapy approach should be applied in a low invasive manner, have a high delivery efficiency and efficacy, generate substantial remuscularization that is properly electromechanically integrated to the host muscle, and bring enough mechanical support to the heart. Cardiac therapy will need satisfy these key requirements to effectively heal the post-MI heart. Functional comparison of current cardiac therapy approaches highlighted the potential need to implement combinatory approaches to enhance the therapeutic advantages. A potential future direction in this field could be to explore novel ideas that integrate specific aspects and benefits from intramyocardial cell therapy, cardiac patches, and acellular approach. Therefore, here we present biodegradable, magnetically responsive scaffolds (here referred to as **z-wire** scaffolds), that support the high-throughput gel-free formation of cardiac tissues with subsequent macroscopic tissue

assembly behavior *in vitro*. In application, z-wire scaffolds support the intramuscular delivery of cardiac tissues with minimally invasive injection using a customized surgical delivery tool. To reproduce the anisotropic properties of the native myocardium[195-199], z-wire scaffolds support microscopic cellular alignment through topographical guidance and scaffold-mediated tensile forces. Macroscopic tissue alignment can be controlled through either magnetic guidance *in vitro* or by controlling the angle of tissue injection during *in vivo* delivery. Collectively, we demonstrate that z-wire scaffolds can guide biological growth in stepwise fashion at multiple length and time scales from *in vitro* tissue assembly to surgical delivery.

CHAPTER 3. MATERIALS AND METHODS

3.1 Polymer synthesis

Poly(glycerol sebacate) acrylate (PGSA) was synthesized according to protocol used previously[200]. Briefly, the prepolymer was first synthesized with polycondensation reaction between equimolar of glycerol (Sigma, G5516-1L) and sebacic acid (Sigma, 283258-250G). The two reagents were combined and allowed to react at 120°C under nitrogen purge for 1h and then under vacuum for 24h. The resulted prepolymer (20g) was then dissolved in 200mL of anhydrous dichloromethane with 20mg of 4-(dimethylamino) pyridine (Sigma, 107700-25G). The reaction flask was cooled to 0°C under a nitrogen purge. 3.05mL Acryloyl Chloride was slowly added to the reaction flask parallel to an equimolar amount of trimethylamine. The reaction was allowed to reach room temperature and was stirred for an additional 24h. The resulting mixture was dissolved in ethyl acetate, filtered, and dried at 45°C and 5Pa. Finally, 5% (w/w) photoinitiator (PI) 2-hydroxy-1-[4(hydroxyethoxy)phenyl]-2- methyl-1 propanone (Irgacure 2959) was added and thoroughly mixed with the polymer solution. The resulted PGSA polymer mixture was stored at 4°C and protected from light. The polymer structures were verified using ^{1}H NMR spectroscopy as shown in **Figure 6**.

3.2 Z-wire scaffold fabrication and characterization

A SU-8 master mold containing an array of 384 z-wire structures matching the standard 384-well plate was designed in AutoCAD and fabricated according to standard photolithography. A PDMS mold was then replicated from the SU-8 master mold. PGSA, a heat and photo cross-linkable polymer was spread onto the PDMS mold with a glass slide to

fill the structural features on the PDMS mold. Excessive PGSA polymer was scraped off. The PDMS mold filled with PGSA polymer was then place inside a transparent bag filled with nitrogen and placed under a UV lamp. To crosslink the PGSA polymer a UV energy output of 15mW/cm^2 was applied for a duration of 30 to 120 min. All experiments used an exposure time of 60min unless the contrary is stated. The crosslinked PGSA z-wires were immersed in 70% ethanol to sterilize as well as to release the z-wires from the PDMS mold. To impart the z-wires with magnetic properties, magnetic Iron (III) oxide nanoparticles (Sigma, 544884-5G) were randomly mixed with the polymer solution at 0.2% (m/m) prior to casting and UV-crosslinking. To characterize the degradation of the z-wire scaffolds, the scaffolds were placed in 200µL of 0.1M NaOH solution at room temperature for 6h to accelerate the hydrolytic degradation process. A brightfield image was acquired every 2h until the z-wire scaffolds visible disappeared, confirming complete degradation. Five to six z-wire scaffolds were used. For the mechanical testing of the PGSA material, PGSA discs with a thickness of 0.5mm and a radius of 1mm were fabricated at 30, 60, 90 and 120 min of UV exposure. Discs were washed with 70% ethanol to remove the non-crosslinked polymer. Compression tests were performed on CELLSCALE® UniVert™ mechanical tester with a 3mm cylindrical compression probe at room temperature. Young's modulus was calculated from the stress and strain curve.

3.3 Fabrication of customized 384-well plate and assembly

A customized 384-well plate containing funnel-shaped wells was first designed in AutoCAD, and the design was inverted to create the design for a mold. The mold design for the customized 384-well plate was 3D printed with a Stratasys 3D printer using Tangoblack plus ink. The printed mold was washed in NaOH solution for two days, dried and then baked

at 80°C for one day. The mold was then coated with Trichloroperfluorooctyl silane (Sigma, 448931-10g). A PDMS plate was replicated from the 3D printed mold. The PDMS plate was hard-baked at 300°C for 15min before it is glued onto a CELLSTAR® OneWell™ polystyrene plate (VWR, 30617-592) with additional PDMS glues. To assemble the z-wire scaffolds onto the plate, the PDMS plate was first filled with 70% ethanol. Then the PDMS mold containing the UV-crosslinked PGSA z-wires was capped onto the plate so that each z-wire scaffold was placed onto of each well. Then the PDMS mold was pressed against the plate to release the z-wires scaffolds in 70% ethanol and dropping each z-wire into its corresponding well. The plate was then centrifuged for 30sec at 1000RPM to push the z-wires to the bottom of each well. The plate was left in 70% ethanol to sterilize for 2h. Lastly, the ethanol in the plate was slowly switched to culture media after 2-3 media changes and ready for cell seeding.

3.4 Cardiac tissue production and in vitro assembly

Fresh cardiomyocytes were isolated from 2-day-old neonatal Long Evans rat pups as we previously reported with minor modifications[201]. Briefly, rat pups were euthanized by decapitation and their hearts were collected and placed in ice-cold PBS. The hearts were then quartered into small pieces and digested overnight in a 0.5% (w/v) solution of porcine trypsin (Sigma, T4799) in PBS at 4°C overnight. After, the hearts were further digested in a 50% (w/v) solution of Collagenase II (Worthington, LS004176) in PBS at 37°C in a series of five 8min digestions. The collected cells were pre-plated in T75 flasks for 60min at 37°C and 5% CO_2. The supernatant was collected, and the nonadherent cells were classified as the enriched CM population and the adherent cells were classified as the enriched fibroblast population. Primary human cardiac fibroblasts or a mixture of 50% iPSC-derived human cardiomyocytes

(hiPSC-CMs) and 50% primary human cardiac fibroblasts were used for seeding. HiPSC-CMs were purchased from Cell Dynamics or differenitated from a healthy hiPSC line in our lab using a using a 2-D monolayer protocol in a chemically defined medium[202]. Human cardiomyocytes were used wherever possible. But due to the limited supplies of human cardiomyocytes, rat cardiomyocytes were used to demonstrate high-throughput tissue production and tissue assembly where large quantities of cells are needed. Rat cardiomyocytes were also used for the ex vivo tissue injection into rat hearts and for in vivo implantation in immuno-competent rats. Rat cardiac cells were cultured in cardiac culture media that is composed of Dulbecco's modified Eagle's medium (Gibco) containing glucose (4.5g/liter), 10% (v/v) fetal bovine serum (FBS; Gibco), 1% (v/v) Hepes (100U/ml; Gibco), and 1% (v/v) penicillin-streptomycin (100mg/ml; Gibco). Human cardiac cells were culture in plating media purchased from Cellular Dynamics (R1132). Cells were suspended in culture media at 40 million cells per mL. Next, 7.5µL of cell suspension were pipetted into each well which is equivalent to 0.3 million cells per well. The plate was then centrifuged for 1min at 150G to aggregate the cells to the bottom of the well and completely embeds the z-wire with cells. The plate was placed in an incubator, and media was changed once every day for one week. The cells self-aggregated and compacted around the z-wires over four days. The length of the tissue was measured in Adobe Photoshop from the brightfield images. For tissue delivery or implantation, tissues were removed and collected from the plate with a 1mL pipette where the pipette was cut to create a larger opening or sterile tweezers.

A mixture of 50% primary rat cardiomyocytes, 20% primary rat cardiac fibroblasts, and 30% green fluorescent protein HUVEC were used for the fabrication of vascularized microtissues. Cells were cultured in endothelial cell growth medium 2 (Cedarlane labs, C-

22011) containing 10% (v/v) fetal bovine serum (FBS; Gibco). Cells were suspended in culture media at 100 million cells per mL. Next 10µL of cell suspension was pipetted into each well which is equivalent to 1 million cells per well. The plate was then centrifuged for 1min at 150G to aggregate the cells to the bottom of the well and completely embeds the z-wire with cells. Tissues were cultured for nine days prior to analysis. The GFP-endothelial cells in the Z-wire tissues were images with confocal microscope (Nikon A1 confocal with ECLIPSE Ti microscope), as well as a Cytation™ 5 Cell Imaging Multi-Mode Reader (BioTek Instruments, Inc. Montreal, Canada). For the tissue assembly experiment, z-wire tissues were extracted and assembled with magnetic guidance from the neodymium magnet with a magnetic induction of 434 mT and cultured for an additional three days under the magnetic field to allow tissue integration. Magnetic induction was measured at multiple distance points from the magnet using a teslameter (Weite Magnetic Technology Co. WT10A) as shown in **Figure 14b**.

3.5 Skeletal muscle tissue fabrication and in vitro assembly

In collaboration with Dr. Raha Sandeep, a cell bank of C2C12 mice skeletal muscle cells (ATCC, CRL-1772) was established. Posterior to this, a mixture of 80% C2C12 cells, 15% green fluorescent protein HUVEC, and 5% rat fibroblasts were used for the fabrication of vascularized skeletal microtissues. Cells were cultured for the first four days in endothelial cell growth medium 2 (Cedarlane labs, C-22011) containing 10% (v/v) horse serum (FBS; Gibco). From day four until day eight cells were cultured in calcium enriched (200 mg/mL) endothelial cell growth medium 2 (Cedarlane labs, C-22011) containing 2% (v/v) horse serum (Dr. Raha Sandeep). Cells were suspended in culture media at 100 million cells per mL. Next 5µL of cell suspension was pipetted into each well which is equivalent to 0.5

million cells per well. The plate was then centrifuged for 1min at 150G to aggregate the cells to the bottom of the well and completely embeds the z-wire with cells. Tissues were cultured for eight days. The GFP-endothelial cells in the Z-wire skeletal tissues were imaged with a Cytation™ 5 Cell Imaging Multi-Mode Reader (BioTek Instruments, Inc. Montreal, Canada).

3.6 Immunofluorescent staining and imaging

To assess the morphology of the engineered cardiac tissues, the tissues were first fixed in 4% (w/v) paraformaldehyde in PBS for 15min at room temperature, then permeated and blocked in 5% FBS and 0.25% Triton X-100 in PBS for 1hr. Next, the tissues were incubated in primary antibody against sarcomeric a-actinin (mouse, 1:200, Abcam, ab9465), overnight at 4°C, followed by incubation with a secondary antibody, Alexa 488 conjugated anti-mouse immunoglobulin G (IgG) (1:200, Life Technologies, A21202) and a phalloidin 594–conjugated anti–F-actin (1:300, Life Technologies, A22285). Tissues were then washed and imaged with a confocal microscope (Nikon A1 confocal with ECLIPSE Ti microscope). DAPI was used to visualize cell nuclei. In order to determine the difference of cell alignment between the scaffold and no scaffold groups, tissues coherency analysis was made using ImageJ plugin OrientationJ as previous shown.[38] Coherency is a measurement of coherent directionality that is calculated to indicate whether local image features are oriented or not. [38] Higher coherency values indicate a strongly coherent orientation of the local fibers whereas low values indicate no preferential orientation. This parameter has been used to measure elastin and collagen architecture and orientation in arterial and scar tissue[38, 39]. In order to assess the viability of the tissues after the injection process, an assay to detect living and dead tissue was performed before and after injection. The z-wire tissue was first loaded

into the delivery tool and then injected into a six well plate. The tissues were then stained with 5-Carboxyfluorescein diacetate 95% (CFDA) (Sigma, C4916-25MG) at a working concentration of 0.0025mg/mL, as well as propidium iodine (PI) (Sigma, P4864) at a working concentration of 0.001 mg/mL in PBS. Live and dead images were captured with the Cytation™ 5 Cell Imaging Multi-Mode Reader (BioTek Instruments, Inc. Montreal, Canada).

3.7 Tissue contraction analysis

Video analysis of contracting tissues was made using ImageJ plugin MuscleMotion following previous published procedures[40]. Frequency was calculated dividing the number of recorded beats by the length of video sample multiplied by 60 to obtain beats per minute. Contraction time was calculated by subtracting the time point at which the contraction amplitude peak was highest minus the timepoint at which the contraction curve started rising from baseline. Relaxation time was calculated by subtracting the time point at which the contraction curve returned to baseline minus the timepoint at which the contraction amplitude peak was highest. Amplitude of contraction was calculated by measuring the tissue contraction (relaxed tissue length minus contracted tissue length). Rising slope of contraction curve was calculated by subtracting the highest amplitude of contraction minus the baseline amplitude of contraction before that peak and then divided by the contraction time.

3.8 Finite Element Analysis

The 2D AutoCad design of the z-wire was cut in half and a 3D rendering model was made using Autodesk Inventor (**Figure 12d**). Finite Element Analysis (FEA) was made with the purpose of correlating scaffold compression with the z-wire tissues' force of contraction using Autodesk Inventor. Different elastic moduli (0.77 MPa, 0.89 MPa, and 1.01 MPa),

corresponding to the ones measured experimentally at different crosslinking settings (30 min, 60 min, and 60 min + 10 min heat) were assigned to the material properties. To simulate mechanical compression tests, forces ranging from 0.04 to 2.6 μN were applied to the outer side of the 3D model while leaving the inner side static (**Figure 12e**). The resulting simulated displacements were recorded and plotted. (**Figure 12f**)

3.9 Drug testing

Two vascularized cardiac z-wire tissues fabricated as aforementioned were released from the 384 well-plate platform into a six well-plate (VWR) filled with cardiac culture media that is composed of Dulbecco's modified Eagle's medium (Gibco) containing glucose (4.5g/liter), 10% (v/v) fetal bovine serum (FBS; Gibco), 1% (v/v) Hepes (100U/ml; Gibco), and 1% (v/v) penicillin-streptomycin (100mg/ml; Gibco). Baseline contraction videos were recorded immediately after release. Epinephrine hydrochloride (Sigma Aldrich, E4642-5G) was diluted with PBS and applied into the well with one cardiac z-wire tissue to a working concentration of 100 nM. Isoprotenerol hydrochloride (Sigma Aldrich, I6504-100MG) was diluted with PBS and applied into the well with one cardiac z-wire tissue to a working concentration of 10 nM. One minute after drug administration, contraction videos were recorded. Tissue contraction analysis was made as aforehand mentioned using MuscleMotion software.

3.10 Tissue delivery and injection

For the fabrication of the delivery tool, a 22G needle was glued with epoxy to the piston of a 1mL syringe and was left to dry overnight. The barrel of the 1mL syringe was assembled with a 19G needle. The piston with the 22G needle was placed into the syringe's barrel with

the 19G needle. The 22G needle was trimmed to the length of the 19G needle so that they both aligned as shown in **Figure 16**. The collected z-wire tissues were then loaded into the delivery system from the needle side using a fine tweezers. A transparent heart model was made by heating a mixture of 7% (w/v) gelatin from bovine skin (Sigma, G9391-100G) in distilled water at 90°C for 15min and then cooling it on a plastic heart model at room temperature for 1hr as shown in **Figure 17c**. Collected micro-tissues were injected into the gelatin heart with either multiple injections of single tissue or a single injection of multiple tissues as shown in **Figure 17d and 17f** respectively. Z-wire tissues were injected into a cadaveric heart using the same procedure. After injection, the heart was sliced into 1mm thickness, and individual tissue slices were cleared in 70% (v/v) T 2,2'-Thiodiethanol (TDE, Sigma, 166782-500G) solution for 7 days prior to imaging.

3.11 Subcutaneous implantation

All procedures below were performed at the core Animal Facility of McMaster University under a protocol (AUP# 181246) approved by the Committee on Animal Care. For in vivo implantation, we delivered rat z-wire cardiac tissue into the subcutaneous space located on the dorsal region of adult Long Evans rats. The animal was first anesthetized with 3% isoflurane at a flow rate of 1 L/min. 5 mg/kg Carprofen analgesic was administered subcutaneously, and the dorsal pouch was prepared for surgery. A 1cm incision was made on the dorsal region and the z-wire micro-tissues (n=5) were delivered into the subcutaneous space. The incision was sutured using absorbable 4-0 vicryl sutures. For post-operative pain management, carprofen was administered subcutaneously for two days. The animals were monitored for four weeks, followed by euthanization with CO_2 inhalation. The site of injection was later isolated and processed for histological studies. Briefly, tissue explants

from the site of injection were fixed in 10% formalin, processed and sectioned. Tissue sections (4μm thick) were stained with Masson's trichrome and Hematoxylin and Eosin.

3.12 Sample size and statistical analysis

Normality and equality of variance were tested using SigmaPlot, as we have previously reported[203]. One-way ANOVA in conjunction with Tukey's test at $p < 0.05$ and a power greater than 0.90 will be used to determine the statistical significance. Means and standard deviation were plotted in all graphs. * denotes significant differences with $p < 0.05$.

CHAPTER 4. RESULTS AND DISCUSSION

4.1 Micro-scaffold fabrication

Guided assembly of complex biological tissues from individual tissue modules requires smart scaffolds with advanced functionalities in addition to basic structural support. We developed smart magnetically responsive micro-scaffolds from a biodegradable polymer, poly(glycerol sebacate) acrylate (**PGSA**) (**Figure 6a**). PGSA is a biocompatible and bioresorbable elastomer that has received market approval in Europe for clinical use as a surgical sealant[204,205]. Other U.S. Food and Drug Administration (**FDA)** approved synthetic polymers, including polylactones, poly(L-lactide), poly(glycolide) and their copolymers, are too stiff and therefore noncompliant when used in to elastic tissues such as the heart[206]. PGSA[205] has been extensively tested in animal models including vascular grafts[207], tissue scaffolds[195] and adhesives[204], etc. It has a double cross-linking mechanism by both UV light and heat. The UV crosslinking mechanism is necessary to enable rapid patterning. By controlling UV exposure time, photo initiator concentration, and post-molding heat-crosslinking, the Young's Modulus of PGSA was fine-toned to the range of 0.5-1MPa, which is close to the young's modulus of the native myocardium (**Figure 6b-d**). Complete hydrologic degradation of PGSA was confirmed under accelerated conditions (alkaline, 0.1M NaOH), where the microfabricated z-wire scaffolds presented complete material degradation within six hours (**Figure 6e**).

Using standard microfabrication techniques[208], a poly(dimethylsiloxane) (**PDMS**) sheet containing an array of 384 z-wire scaffold molds was fabricated. PGSA prepolymer solution was cast into the mold and photo-patterned into an array of 384 z-wire scaffolds. The scaffolds were subsequently released from the PDMS mold by immersing in an ethanol

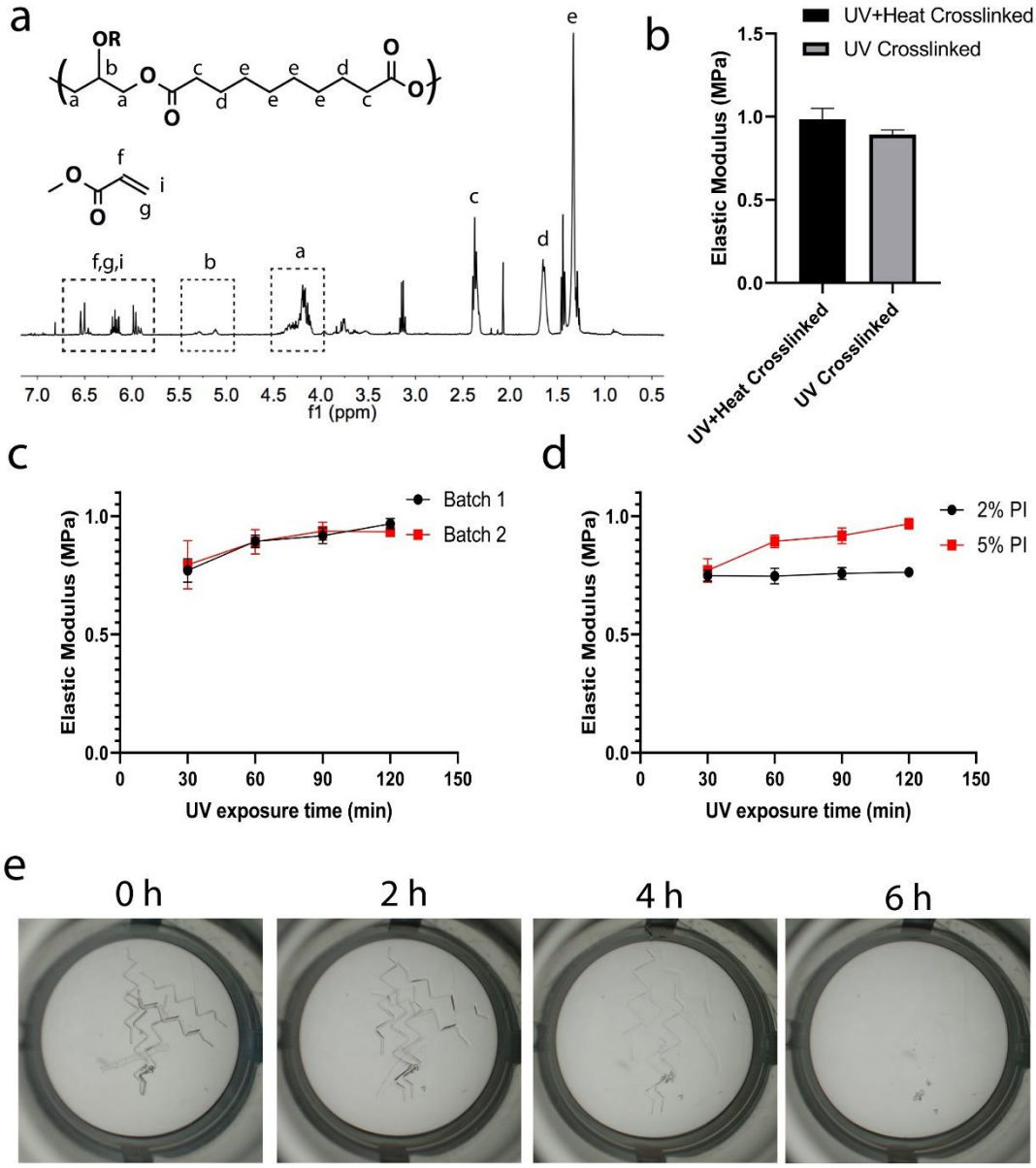

Figure 6. Chemical composition and degradation of PGSA micro-scaffolds. a, NMR of PGSA prepolymer shows the chemical structure and composition of the synthetic polymer. Molecular structure of the R group is shown in the dotted box. **b**, E elastic modulus of UV+Heat crosslinked PGSA (n=8) and UV crosslinked PGSA (n=7). *$p<0.05$. data displayed as mean ± SD and statistically assessed with one-way ANOVA. **c**, Repeatability of elastic modulus quantification in between different batches of PGSA at different UV exposure times. **d**, comparison of elastic modulus of PGSA with 2% and 5% (m/m) photoinitiator (PI). **e**, Brightfield images of the degradation process of PGSA z-wire scaffolds with 2% PI in 0.1 M NaOH solution. Z-wire scaffolds degraded to completion within 6h.

solution. Z-wire scaffolds have a zig-zag shape with a strut diameter of 100μm, which functions like a spring to facilitate scaffold compression (**Figure 7a**). This design is critical to functional tissue contraction; the bulk structures of synthetic elastomers are nearly incompressible, but such spring-like design can harness structural elasticity to support cyclic scaffold compression in cardiac tissue contraction. Moreover, the z-wire functions as a structural support to facilitate tissue compaction and remodeling, but also provides tension to induce alignment and elongation of the assembled cardiomyocytes along the scaffold.

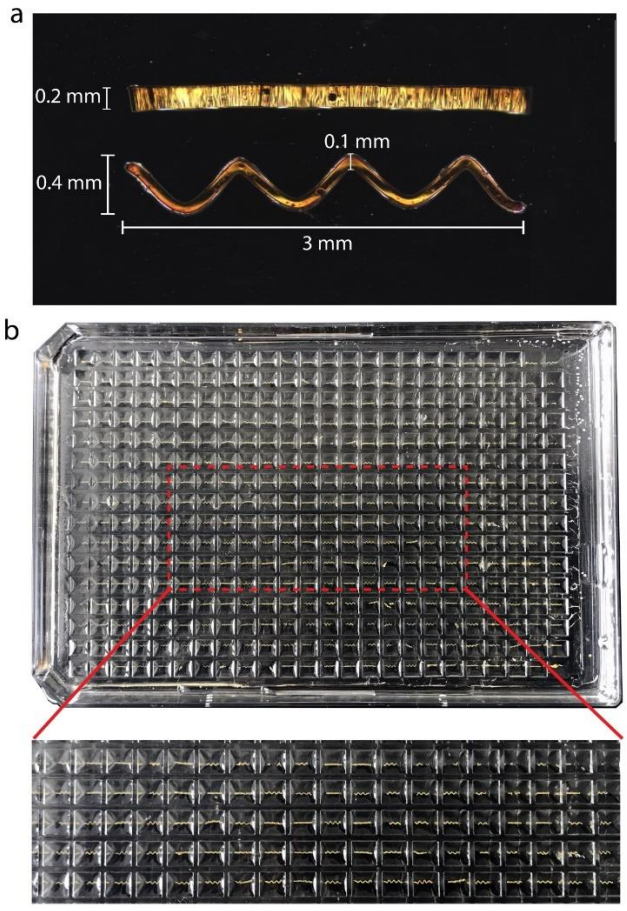

Figure 7. PGSA z-wire scaffold in customized 384-well plate. a, Image of the z-wire scaffold from side view and top view. Dimensions of the z-wire scaffold are labeled. **b**, Image of an entire customized 384-well plate loaded with micro-scaffolds and a zoomed-in image of the plate. The z-wire scaffolds appear in a yellow color.

4.2 Scalable gel-free tissue production

To facilitate high-throughput cell seeding and tissue assembly, we 3D printed a customized 384-well plate with funnel-shaped wells and rounded rectangular bottoms (0.5x3.5 mm) (**Figure 8a, Figure 7b**). Designed to match the layout of the 384-well plate, this array of micro-scaffolds was dropped into the customized 384-well plate in one step (**Figure 7b**). The funnel-shaped well design inherently directed and positioned the micro-scaffolds to the bottom of the wells (**Figure 8b**). To assemble the z-wire tissues, a cardiac cell mixture of iPSC-derived cardiomyocytes and primary human cardiac fibroblasts was pipetted into the wells with a repeater pipette at a concentration of 0.3 million cells per well (**Figure 8b**). The plate was then centrifuged at 150G for 1min to pack the cells at the bottom of the wells and encapsulate the micro-scaffolds (**Figure 8c-e**). The cardiac cells quickly self-assembled and started to contract around the scaffolds in 24h; the compaction process reached completion in 3-4 days (**Figure 9a-b**). The entire cell seeding process was carried out with standard tissue culture equipment (e.g., pipettes and centrifuge), which can be readily scaled up (e.g., with multi-channel pipettes). Most importantly, our cell seeding process does not require the use of any natural hydrogels (e.g., Collagen I, Fibrin, or Matrigel™, etc.), which can be expensive and introduce animal-derived growth factors not yet approved for clinical use and prone to batch-to-batch variation (e.g., Matrigel™). With the support of the z-wire scaffold, we found that the cells can naturally assemble on their own without a hydrogel matrix.

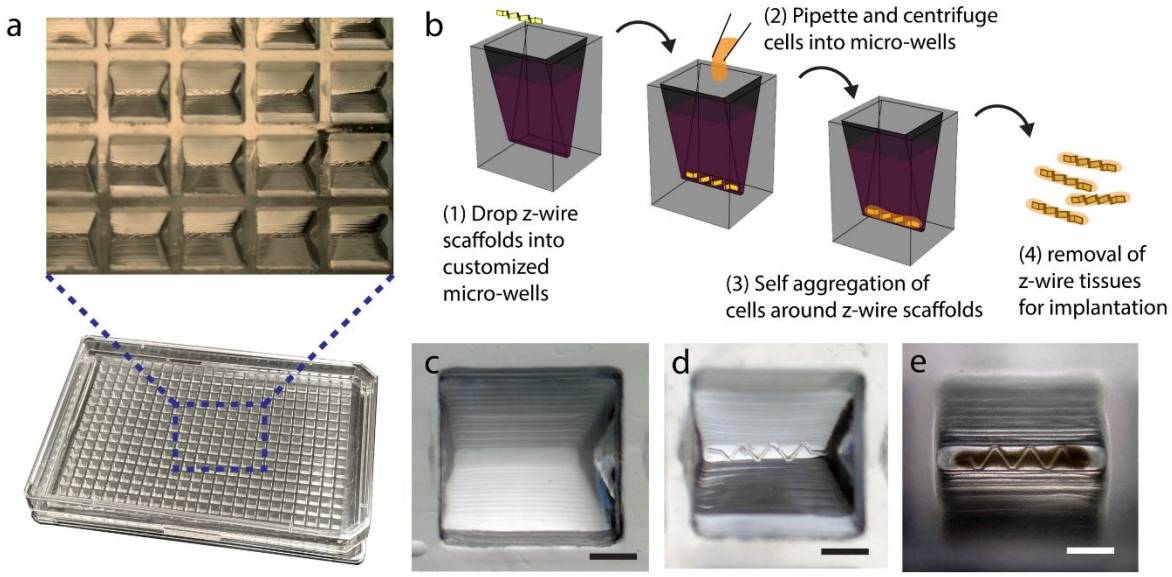

Figure 8. Design and operation of z-wire 384-well plate. **a,** A customized 3D printed 384-well plate with funnel-shaped wells to facilitate tissue assembly. **b,** A schematic outlining the process of (1) scaffold loading, (2) cell seeding, (3) tissue formation, and (4) tissue release. **c-e**, Brightfield images of (c) an empty funnel-shaped well, (d) a well loaded with a micro-scaffold, and (e) a well seeded with a cardiac tissue. Scale bar, 1mm.

The micro-scaffolds provided sufficient structural support for the formation of an elongated tissue, without hindering contraction, by allowing for structural compression (**Video S1**). As seeded cells connect with each other and aggregate around the z-wire scaffold, the cells collectively exert a force onto the z-wire scaffold, attempting to compress the scaffold. However, the relatively rigid z-wire scaffold, instead of being compressed, exerted a counter force onto the tissue, forcing the tissue to elongate along the scaffold. This scaffold-induced tension within the tissue readily aligned the cardiac cells, hence leading to the formation of a muscle fiber (**Figure 9a,e,f**). Without structural support from the scaffold, the tissue quickly formed a spheroid, inhibiting cardiac muscle alignment (**Figure 9a,c,d)**. F-actin staining highlighted uniform cellular alignment along the scaffold, while cell orientation appears to be random in the scaffold-free cell aggregates (**Figure 9c-f, Figure**

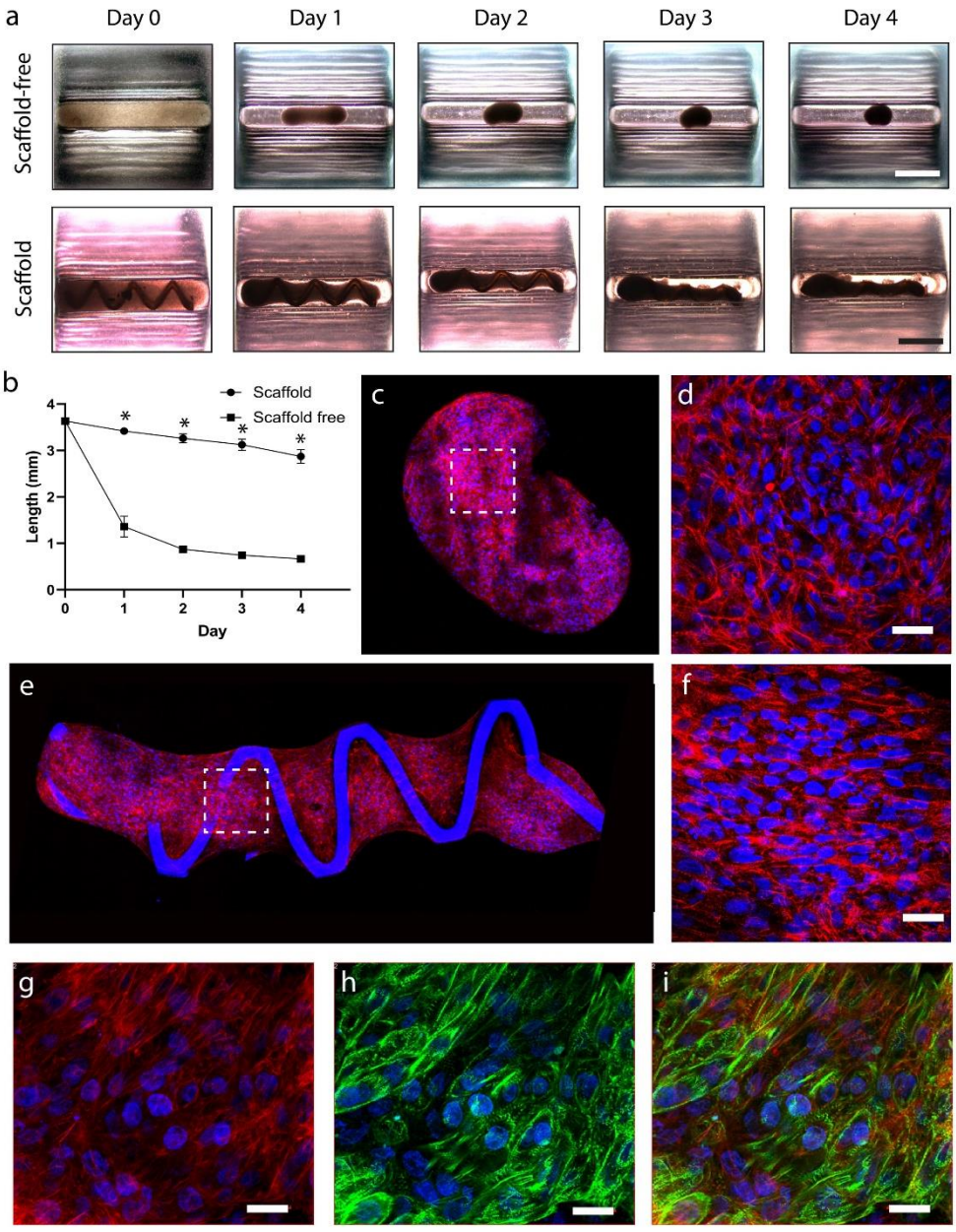

Figure 9. Scalable production of cardiac z-wire tissues. a, Brightfield image of micro-tissues assembled with or without micro-scaffolds. Scale bar, 1mm. **b**, Quantification of the tissue length of micro-tissues assembled with (n=5) or without micro-scaffolds (n=3) over time. * $p<0.05$. **c-d**, Fluorescent images of a micro-tissue assembled without a micro-scaffold and stained for F-actin (red) and DAPI (blue). **e-f**, Fluorescent images of a micro-tissue assembled with a micro-scaffold and stained for F-actin (red) and DAPI (blue). F-actin staining shows the collective alignment of the cellular structure. Z-wire scaffold autofluorescence in blue color. Final image is stitched from multiple images (e). Scale bar: 30μm. **g-i**, High magnification fluorescent images of a human cardiac micro-tissue assembled with a micro-scaffold and stained for F-actin (red), sarcomeric α-actinin (green), and DAPI (blue). The staining shows the presence and alignment of human cardiomyocytes within the micro-tissue. Scale, 20μm.

10). Sarcomeric-α-actinin staining revealed the presence of elongated cardiomyocytes with visible cross-striation intertwined with cardiac fibroblasts (**Figure 9g-i**). Scaffold-induced tensile force also presented a synergistic improvement of endothelial cell assembly and alignment along the scaffold struts. (**Figure 11a-b**). The presence of the scaffold was further highlighted in the context of achieving sufficient tissue stiffness for endothelial cell assembly; in just 3 days, a rudimentary vasculature network was visible throughout the entire tissue. Network integrity was highlighted by vessel interconnectivity and high density, with maximum vessel separation of 100-200μm. The assembled tissues can contract macroscopically. With this approach, a large array of tissue can be seeded and cultivated at a time (**Figure 11c**). The assembled tissues can also be easily released and collected from the plate for further manipulation or transplantation, as they were not anchored in the plate for cultivation (**Figure 11d**). The presence of a pre-assembled vasculature *in vitro* could accelerate vascular growth and integration *in vivo*.

4.3 Contraction force analysis

The contraction displacement of the z-wire tissue can be traced using video analysis software (**Figure 12a-b**). The amplitude and frequency along with other contraction parameters were calculated (**Figure 12c**). The amplitude of tissue contraction was translated into force of contraction by simulating the correlation between contraction force and the mechanical compression of the z-wire scaffolds through FEA (**Figure 12d-e**). By assigning different elastic moduli to the 3D z-wire render we were able to develop a model for estimating the contraction force at different displacement lengths (**Figure 12e**). Comparing the displacement observed on the video analysis to the simulation plot, we estimate that the peak force of contraction of vascularized cardiac z-wire tissues ranges between 0.6 to 1.2 μN.

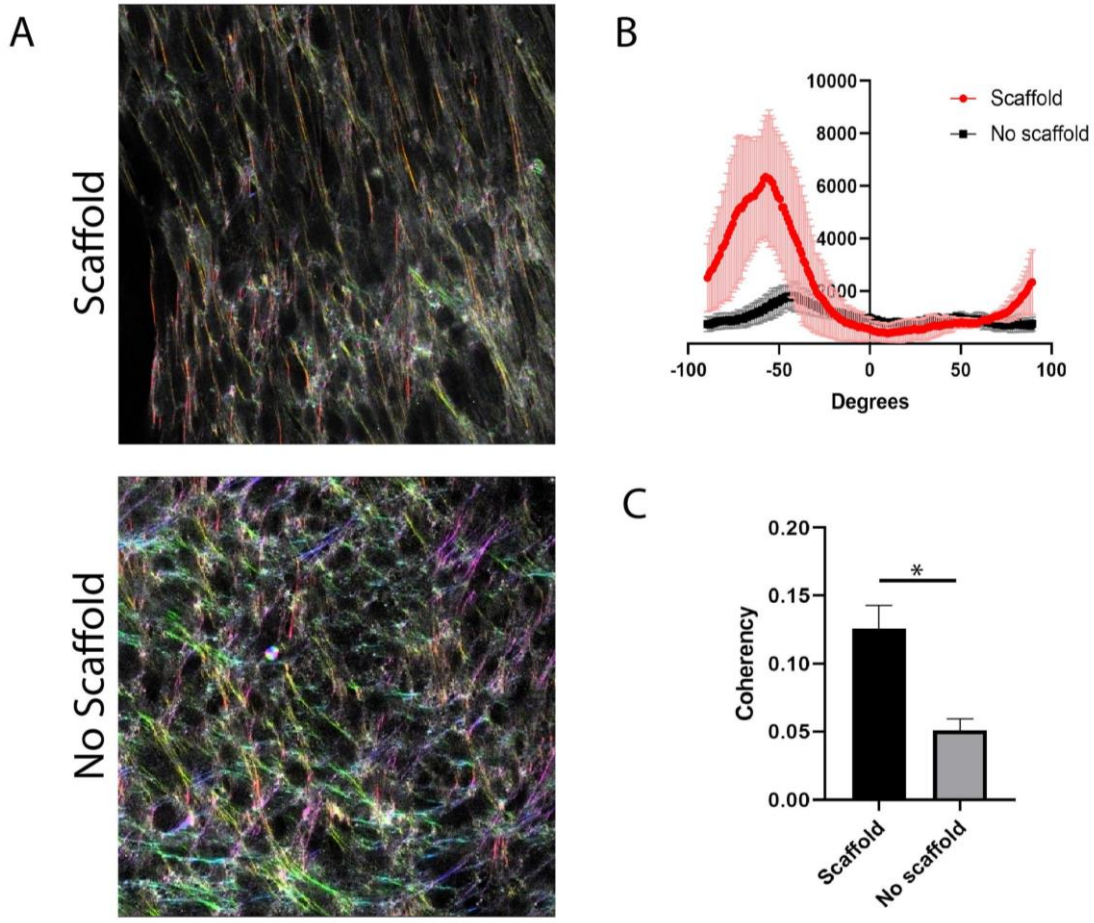

Figure 10. Quantification of tissue alignment. a, Visual directional analysis of cardiac tissue stained for F-actin with or without z-wire scaffolds. The features are gathered in a color map in HSB mode where hue indicates orientation, saturation indicates coherency. **b**, Histogram of orientation distribution of F-actin staining for cardiac tissue with or without z-wire scaffolds. The presence of a peak shows that the scaffold group had a higher alignment in comparison to the no scaffold group. **c**, Coherency analysis shows a higher orientation consistency in the scaffold group. n=3, * $p<0.05$, data displayed as mean ± SD and statistically assessed with a one-way ANOVA.

4.4 Drug testing

As a proof of concept, two commonly used cardiac drugs, epinephrine and isoprotenerol were applied to two different z-wire tissues. Baseline beating plots were captured using video analysis software and posteriorly compared to the beating plots after the drugs were administered (**Figure 13**). In both cases, the amplitude of contraction was increased after the drugs were administered in comparison to baseline. In the case of epinephrine, baseline

recordings presented background noise which generated fake contraction peaks making the heart rate analysis not reliable. Nevertheless, when comparing post-epinephrine z-wire tissue with the baseline isoprotenerol tissue an increase in heart rate can be observed. In the case of post-isoprotenerol beating plot, the heart rate was maintained while increasing the amplitude of contraction. Background noise can be reduced in the future by performing the experiments inside the 384 well plate and maintaining microscope brightness and focus throughout the video recording.

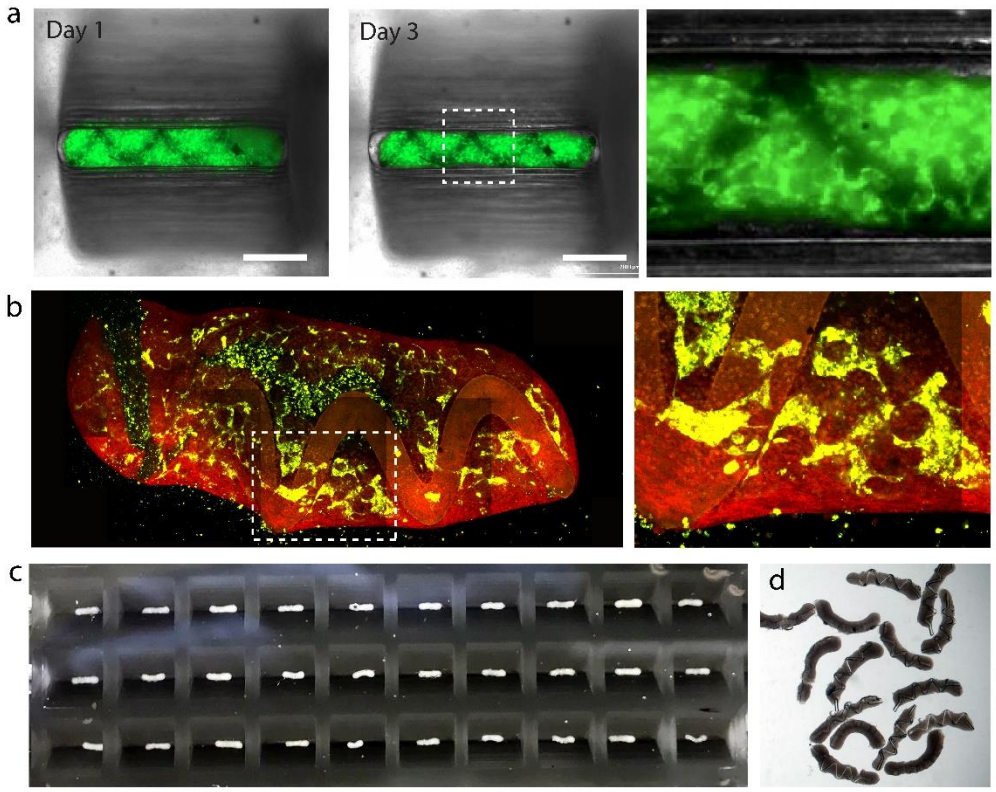

Figure 11. Scalable production of vascularized neonatal rat cardiac z-wire tissues. a, brightfield image overlaid with fluorescent images of a z-wire tissue assembled with 30% GFP-endothelial cells (green), 50% rat cardiomyocytes, and 20% rat fibroblasts over time. Scale bar, 1mm. **b**, confocal fluorescent image of vascularized cardiac tissue stained for F-actin (red) and GFP-endothelial cells (green). Final image is stitched from multiple images (b). High magnification images show regions of the tissue labeled by white dotted boxes. **c**, A brightfield image showing an array of cardiac z-wire tissues. **d**, A brightfield image showing a cluster of cardiac z-wire tissues released from the plate.

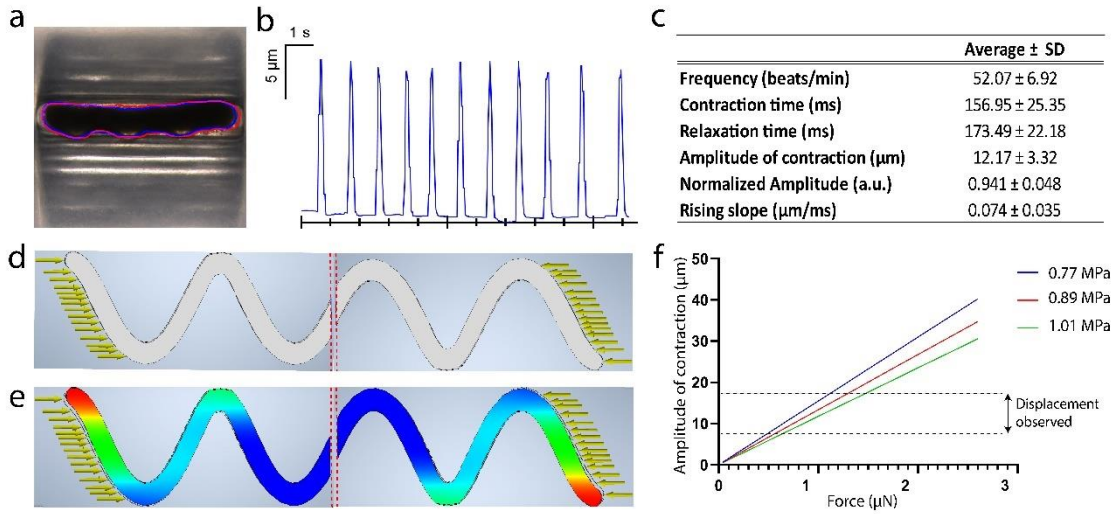

	Average ± SD
Frequency (beats/min)	52.07 ± 6.92
Contraction time (ms)	156.95 ± 25.35
Relaxation time (ms)	173.49 ± 22.18
Amplitude of contraction (µm)	12.17 ± 3.32
Normalized Amplitude (a.u.)	0.941 ± 0.048
Rising slope (µm/ms)	0.074 ± 0.035

Figure 12: Tissue contraction analysis. a, Brightfield image of z-wire tissue overlay with outlines of the tissue in relaxation (red) and contraction (blue) state. **b**, Representative tissue contraction traces. Scale bar shows the amplitude of contraction and time. **c**, Summary of functional parameters from tissue contraction (n=3). Data displayed as mean ± SD. **d**, Mirrored 3D rendering model of half z-wire design. **e,** Mechanical compression simulation of **d**. **f**, Force and displacement simulation plot at different elastic moduli.

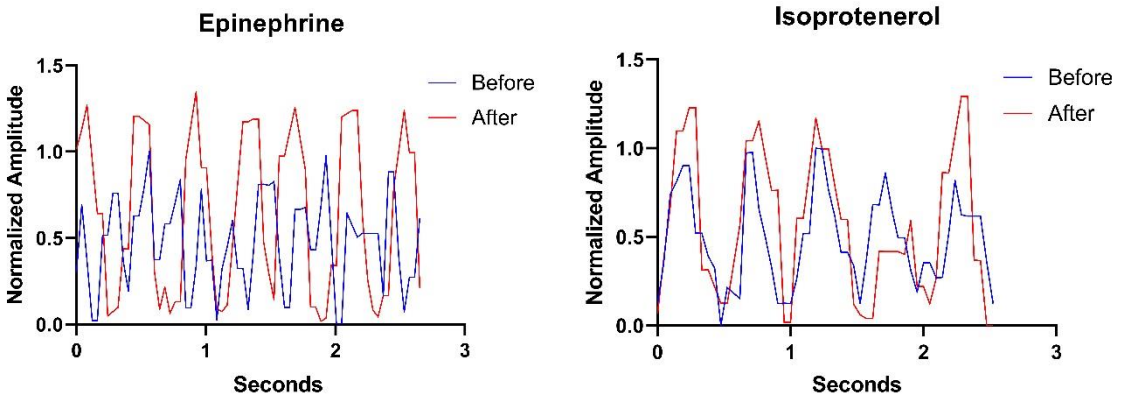

Figure 13: Drug testing on z-wire platform. Normalized amplitude of contraction plots of baseline (blue) and after epinephrine (left red) or after isoprotenerol (right red) stimulation of cardiac z-wire tissues.

4.5 Magnetic guided tissue self-assembly *in vitro*

To impart magnetic capability to the z-wire scaffolds, magnetic iron oxide (II, III) nanoparticles (<10nm in diameter) were dispersed in the PGSA prepolymer solution at concentrations of 0.2% (m/m) with sonication. The polymer nanocomposite was then cast onto the PDMS mold and crosslinked under UV light (15mW/cm^2 for 60min). The additional crosslinking time was required to achieve the desirable mechanical properties as the dispersed magnetic nanoparticles deflect light and reduce UV penetration efficiency. After photopolymerization, the nanoparticles were permanently trapped inside the polymer until polymer degradation. Magnetic fields offer an attractive opportunity to externally guide the assembly of individual functional tissues as: (**1**) magnetic fields are easy to generate and can penetrate thick materials and biological tissues to provide guidance in a remote fashion[209], (**2**) commercially available magnetic nanoparticles are widely used in bioimaging, and have been shown to be nontoxic and can be excreted from the body over time[210,211], and (**3**) magnetic fields can be easily directed with magnets into various patterns, with potential to guide organ-specific tissue organization. We chose to use <10nm nanoparticles because it has been shown that nanoparticles under 10nm can be readily excreted from the body[210]. Nanoparticle inclusion did not interfere with the degradation of the scaffolds (**Figure 6e**). To guide the organization of z-wire scaffolds and assembled micro-tissues, commercially available Neodymium magnets were used to generate a magnetic field with a local strength up to 0.5T (**Figure 14a-b**). We observed that the orientation of a cluster of micro-scaffolds embedded with magnetic nanoparticles was easily controlled on demand with a magnetic field strength above 0.13T using a hand-held magnet (**Figure 14a-b, Figure 15, Video S2**). Using the same procedure, a cluster of micro-tissues was readily assembled. The micro-

tissues quickly aligned in the direction of the magnetic field and assembled in a dense cluster with localization of the magnet (**Figure 14c**). Culture of the clustered micro-tissues for three days in the presence of the magnetic field presented the formation of intercellular junctions at tissue contact points, suggesting the formation of an integrated tissue (**Figure 14d**).

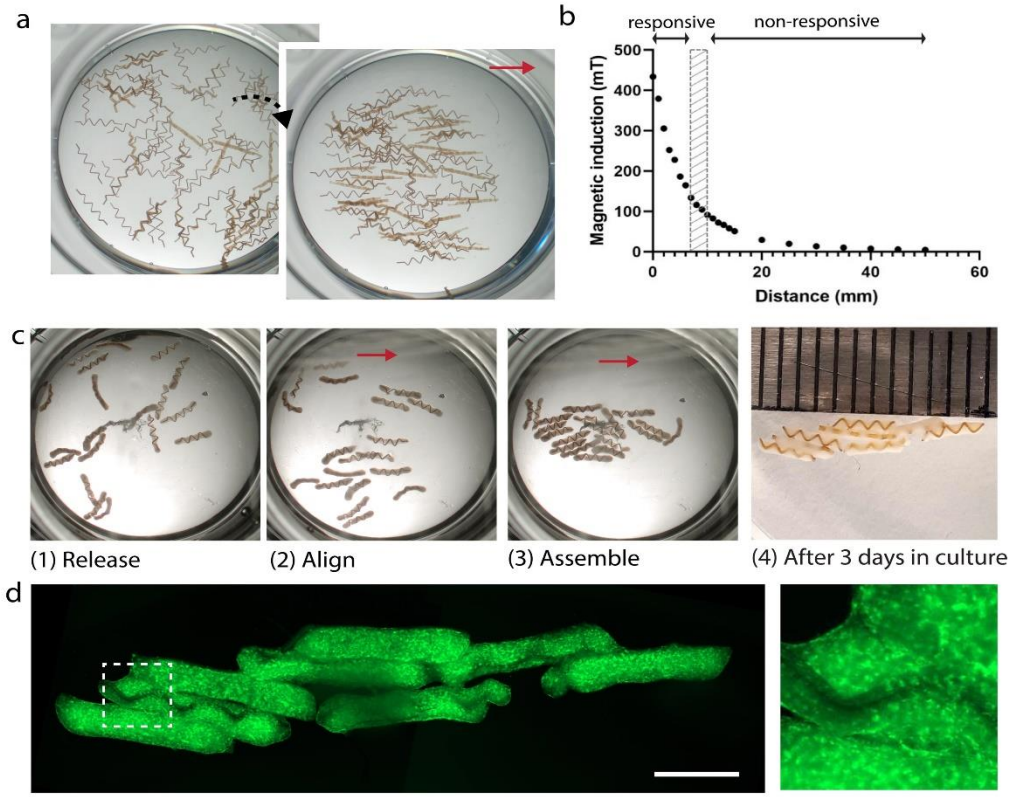

Figure 14. Magnetic guided anisotropic tissue assembly in vitro. a, Magnetic alignment of z-wire scaffolds. **b**, Correlation of magnetic field strength to distance from the magnet. The grey region is the cut off distance within which the z-wire scaffolds can respond to the magnet. **c**, Brightfield images show the self-alignment and physical integration of a cluster of z-wire tissues in response to an external magnetic field and after 3 days in culture post assembly. The ruler shown is in mm scale. **d**, fluorescent image of assembled z-wire tissues containing GPF-endothelial cells (green) 3 days post assembly. The final image is stitched from multiple images. Scale bar, 2mm. High magnification images show regions of the tissue labeled by white dotted boxes and highlights the integration between tissues.

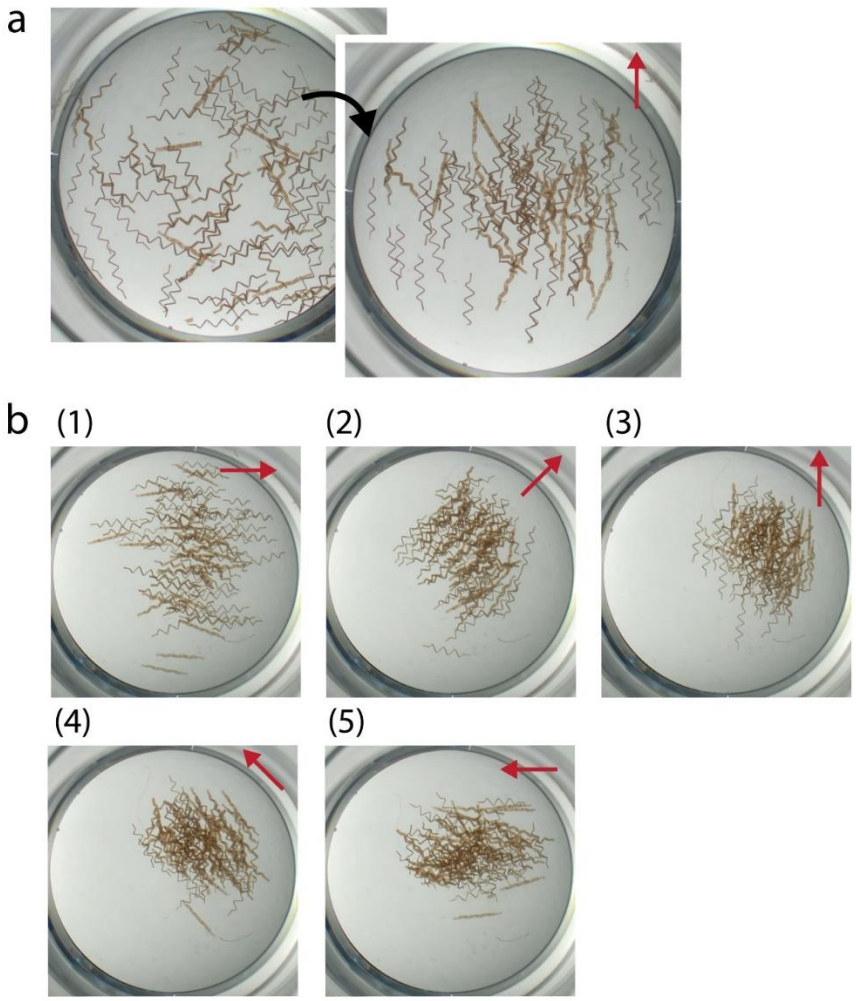

Figure 15. Magnetic alignment of z-wire scaffolds *in vitro*. a-b, Magnetic alignment of z-wire scaffolds in response to magnetic field of various direction. Red arrows indicate the direct of the magnetic alignment.

4.6 Ex vivo surgical tissue delivery and assembly

Given the small size of z-wire supported micro-tissues (300µm in diameter and ~3mm in length), they were easily loaded to, and injected with, a syringe without disrupting organized tissue structure. To demonstrate the feasibility of delivering the micro-tissues surgically with syringe injection, we developed a customized syringe with inserted plunger to optimize tissue loading and injection (**Figure 16**). After loading, tissues were stored inside the needle prior to injection to ensure a smooth delivery by the plunger. This plunger

mechanism is better than a normal syringe injection as it reduces the dead volume produced by the liquid injected alongside the tissues, which could produce tissue wash and affect the orientation of the injected tissues. Scaffold presence provides important structural stability to the delivery process; elongated tissues without scaffolds fold and crumble with handling, and cannot be easily manipulated, loaded, or injected while maintaining any predictable structural orientation (**Figure 17a**). With the z-wire scaffold, the injection process was quick and gentle; injected tissues showed comparable viability to tissues pre-injection (**Figure 17b**).

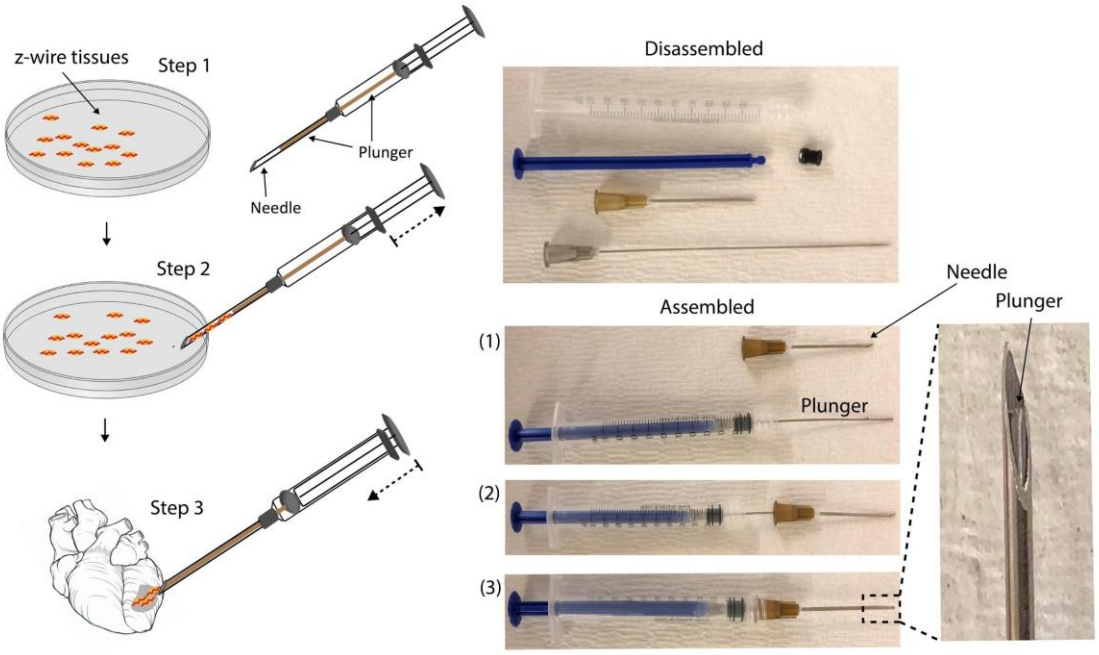

Figure 16. Customized surgical delivery tool from modified syringe for tissue injection. A 22-gauge needle that serves as a plunger is fitted inside a 19-gauge needle to push out the loaded tissues during injection. The z-wire tissues are loaded to the needle section of the syringe. The luminal space inside the needle is used as a reservoir for the z-wire tissues.

To visually demonstrate and understand the mechanistic intramuscular delivery of the micro-tissues in real time, we used a transparent gelatin hydrogel matrix that mimicked the

extracellular matrix properties of cardiac tissue for the purpose of demonstrating intra-organ delivery (**Figure 17c**). In this model, the syringe needle carrying the z-wire tissues precisely delivered the tissues with ease at the site of injection (**Figure 17d**). We found that injected tissues consistently self-aligned in the direction of injection without the need of magnetic guidance (**Video S3-6**). This is likely because the orientation of the delivered tissues is constrained by the open space created along the injection path, presenting an opportunity for localized tissue organization without the need of magnetic alignment. The same injection can be repeated multiple times, delivering an array of micro-tissues with uniform alignment without the use of magnets (**Figure 17e**). Alternatively, multiple z-wire tissues can be injected at the same location with one injection (**Figure 17f, Video S7**).

Translation of this process was demonstrated with the delivery of z-wire tissue to the myocardium of a heart cadaver (**Video S8)**. Although the injection process could not be seen directly as it is taking place, visualization was achieved with a tissue clearing technique (**Figure 18a**) which allowed us to visualize the injected tissue in its entirety, completely embedded inside the myocardium wall and oriented in the general direction along the myocardium wall (**Figure 18b-c**). The boundary of the GFP labelled z-wire tissue following injection was visible, confirming maintenance of *in vivo* tissue micro environmental structure. (**Figure 18d**). To understand implantation behavior of environments surrounding z-wire cardiac tissue over time, we implanted tissue subcutaneously to the dorsal region of an adult Long Evans rat (**Figure 18e**). One month after implantation, the z-wire tissue began to integrate with the host tissue when infiltration of host cells to the implant, including fibroblasts and blood vessels, was clearly visible (**Figure 18f-h**). Future studies are needed to examine the rate of vascularization and the extend of cardiomyocytes retention and

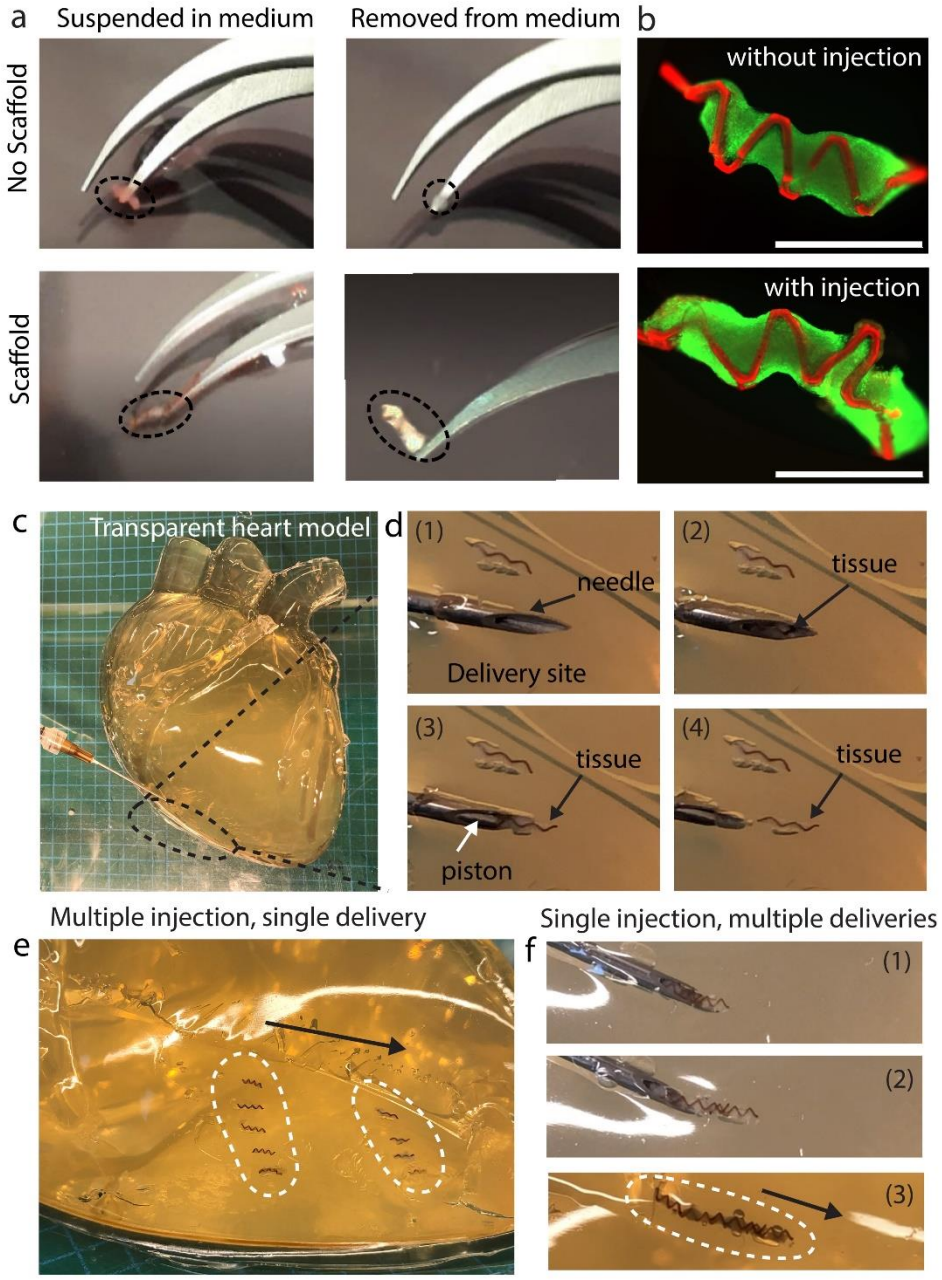

Figure 17. Tissue injection and delivery. a, manipulation of cardiac tissue with or without z-wire shows scaffold-free tissue lack mechanical strength to support tissue's own weight for surgical manipulation and injection. Black dotted circles indicate the tissue located at the tip of a tweezer. **b**, Live and dead staining with CFDA (green) and PI (red) on cardiac tissues with or without surgical injection in vitro. Z-wire scaffold autofluorescence in red color. Scale bar: 1mm. **c**, Surgical injection of functional cardiac tissues into a gelatin-based transparent heart model. **d**, high magnification images show the release and alignment of a z-wire issue in the orientation of the needle. Released z-wire tissue is embedded and immobilized inside the gelatin-based transparent heart model. **e**, Image of a cluster of tissues all oriented in the same direction after multiple injections. **f**, Image of multiple tissues delivered and aligned in a single injection. Dotted white circle outline the injected tissues. Black arrow indicates the orientation of alignment.

survival in the tissue implant, especially in the myocardial environment. Furthermore, to validate the therapeutic benefit of z-wire tissue delivery for cardiac repairs, we are currently developing ultrasound guided minimally invasive intramyocardial tissue delivery in rat myocardial infarction models. Our outcomes with z-wire scaffolds without magnetic particles simplified the material delivery strategy, further reducing barriers alignment of delivered micro-tissues will be pre-determined by the injection path during surgery. Building on this success with the technology, we envision functional cardiac tissues could feasibly be delivered with intramyocardial injection, bypassing the epicardium while maintaining a high-level tissue organization with respect to the host tissues.

4.7 Alternative applications: skeletal muscle

Similar to MI, there are certain neuromuscular diseases such as Duchene muscular dystrophy, multiple sclerosis or myasthenia gravis that progressively degenerate the skeletal muscle contractility hindering the patient's mobility and muscle force generation.[212] This loss of muscle mass and functionality can also occur by traumatic events such as major injury or tumor removals.[213,214] In the past, tissue engineering approaches have been used with the purpose of creation and regeneration of skeletal muscle.[215] Due to their contractility and force generation, both skeletal and cardiac muscle require a scaffold or material that allows contraction while maintaining its structure. Therefore, skeletal muscle cells were seeded into the z-wire platform as a first proof of concept. Results show that the z-wires can support the tension of skeletal muscle tissues maintaining an elongated shape in comparison to scaffold free tissues (**Figure 19a-b**). However, a z-wire scaffold with higher elastic modulus (1.01 MPa) in comparison to cardiac tissues was needed to prevent tissue collapsing. This suggests that skeletal muscle tissues generate more passive tension than cardiac tissues.

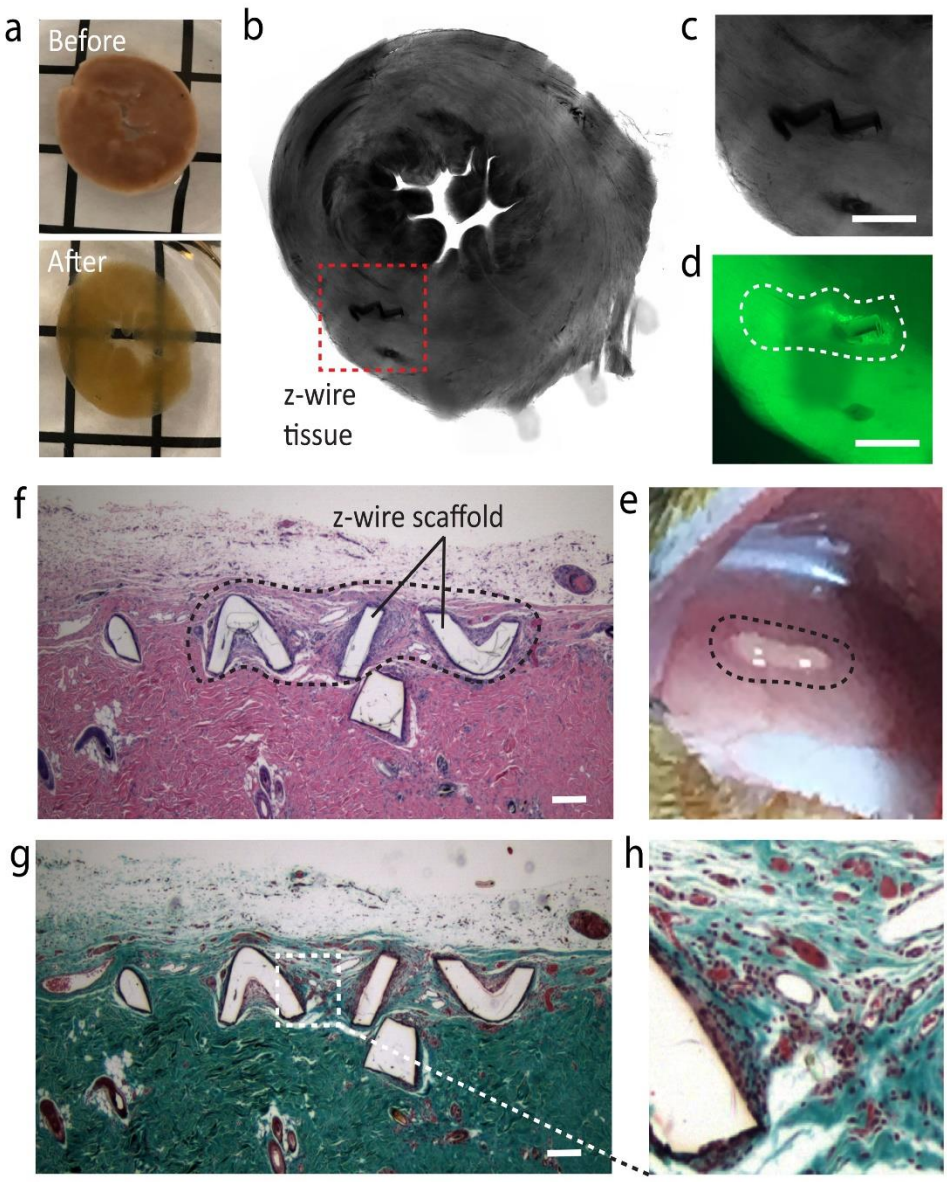

Figure 18. Ex vivo Intra-muscular tissue delivery and *in vivo* tissue biocompatibility. a, A slice of heart chamber before and after tissue clearing. **b-c,** Brighfield image of a heart slice with an injected z-wire cardiac tissue in the myocardium. scale bar, 1mm. **d,** Fluorescent image of an injected z-wire cardiac tissue in the myocardium showing implanted GFP-endothelial cells around the z-wire scaffold. The heart muscle has a green fluorescent background. Scale bar, 1mm. **e**, Image of z-wire tissue immediately after implantation. **f-h**, Histological section of subcutaneously implanted z-wire tissue stained for (f) H&E and (g-h) Masson's Trichrome after 1 month. In H&E staining, cell bodies are labeled in pink and cell nucleus are labeled in purple. Masson's Trichrome staining, collagens and extracellular matrices are labeled in green and blood vessels are labeled in dark red color. The implanted scaffold has no color and is shown in white color. Scale bar, 100μm.

In addition, green fluorescent HUVEC can also be incorporated into the skeletal muscle tissue to generate a vascular network (**Figure 19c**). The tension generated by the scaffold helps to form better vascular networks in comparison to no scaffold tissues (**Figure 19c**). Even though no active contraction has been observed yet, we envision to optimize the tissue fabrication protocol, stimulate the tissues with acetylcholine and perform video analysis to determine force of contraction. In addition, confocal imaging is also required to confirm myocyte fusion and maturation.

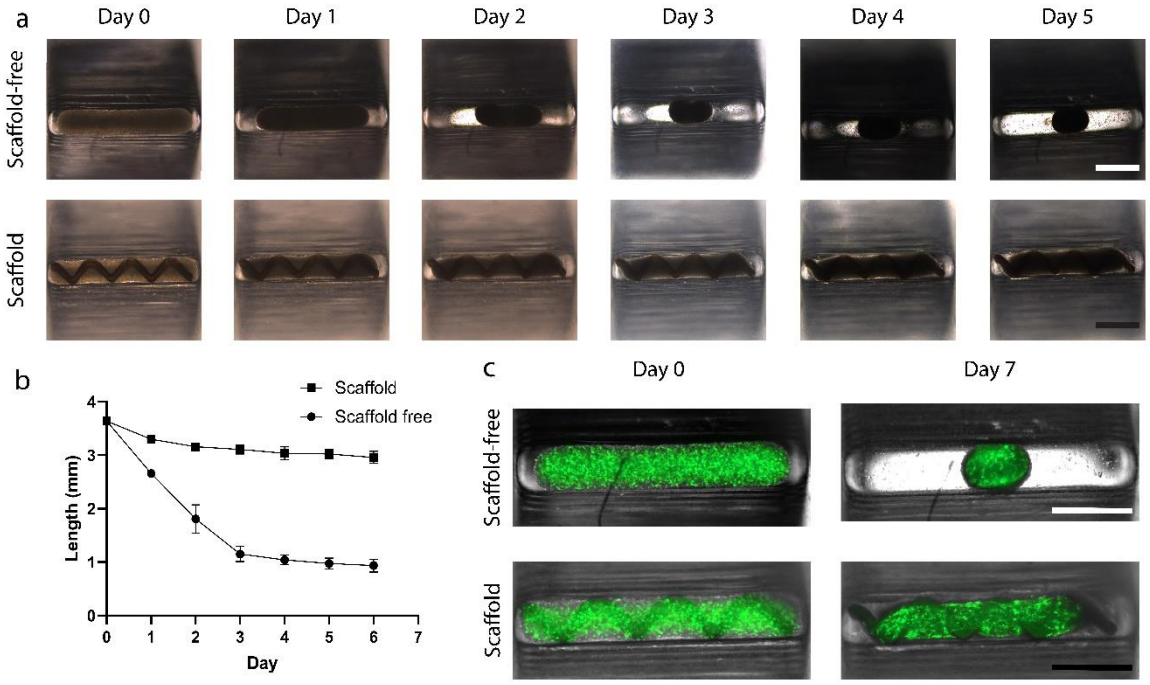

Figure 19: Production of skeletal muscle z-wire tissues. a, Brightfield image of micro-tissues assembled with or without micro-scaffolds. Scale bar, 1mm. **b**, Quantification of the tissue length of micro-tissues assembled with (n=5) or without scaffolds (n=5) over time. * $p<0.05$. **c**, brightfield image overlaid with fluorescent images of a z-wire tissue assembled with 15% GFP-endothelial cells (green), 80% C2C12 mice skeletal muscle cells, and 5% rat fibroblasts over time. Scale bar, 1mm.

4.8 Discussion

We have demonstrated for the first time the scalable tissue production of elongated cardiac tissues in the format of 384-well plate. Produced tissues can be easily extracted and

remain mechanically stable for manipulation during implantation. Although the current prototype contains PDMS materials, an entire customized 384-well plate could be manufactured with cell culture plastic (e.g. polystyrene) using an injection molding technique for large scale production[216]. When magnetic particles were integrated into the scaffold structure, the z-wire scaffolds presented self-assembly capability controlled by remote magnetic guidance. Imparting magnetic particles into z-wire scaffolds is a less invasive strategy than incorporating magnetic particles inside cells[217]. Since we grow the tissue around the z-wire scaffolds, only cells will directly interface with the host micro-environment, further minimizing undesired host response. When multiple z-wire tissues cluster together, tissues physically contact and naturally integrate with one another. In less than 3 days of culture, integrated tissues do not fall apart, even in the absence of the magnetic field. In the case of cardiac tissue engineering, such a design would avoid any conduction blocks generated by the presence of physical scaffolds in between the tissues. Furthermore, tissue contraction will not be constrained by the scaffold, as each scaffold are physically separated from one another. To help further mature the cardiac tissue *in vitro*, the mechanical properties of the z-wire scaffold could be fine-toned in future studies. Electrical stimulation could also be incorporated to accelerate tissue maturation. In this study, the generated magnetic field from the use of one external magnet can cover a large area which is beneficial for aligning a large quantity of tissues. If various local alignments are need in the tissue construct, an array of micro-magnets could be used to generate different magnetic fields locally. However, due to the potential interference between different magnetic fields, tissue patterning using magnetic field will inherently have relatively low resolution.

To fill an entire 384-well plate requires 115 million cells at the seeding density presented here. When considering scale up for future clinical studies where it has been suggested that close to one billion cells are required for transplantation[20], a total of nine plates would be needed. This is a small number of plates for an application of this scale, especially if multi-channel pipettes up to 384 channels (VIAFLO 96/384) are used to facilitate efficient and even aliquoting. Currently, it is possible to create thousands of tissue spheroids with a stirring bioreactor, but here we present the first feasible approach to assemble elongated functional tissues at a large scale. Moreover, unique from a bioreactor-based tissue production process, in this multi-well plate format each tissue could be routinely imaged with a high-content imaging system to track and monitor the culture condition of every single tissue over time. This capability of monitoring force of contraction and heart rate parameters allows us to identify and eliminate low-quality tissues that do not meet the functional standards or lack of proper tissue formation. In our experiments, we noticed that tissues could compress or bend the z-wire scaffolds to various extents (**Figure 8d**). This indicates that the optimization of scaffold mechanical property and quality control of the tissues selected for implantation could be essential to achieve consistent therapeutic results. A comparison of contraction force between z-wire tissues and other engineered cardiac tissues (**ECT**) was made to confirm that mechanical simulation results were in the right range of force (**Table 2**). Even though other ECT show higher peak active force of contraction, it is important to mention that calcium stimulation[111], electrical stimulation[218,219], or more mature tissues[218,219] were used in these experiments. To increase contraction force on z-wire tissues electrical stimulation or more mature cardiac cells could be used in the future.

Table 2: Contraction force comparison of engineered cardiac tissues.

Cell type	Number of CMS	Biomaterial scaffold	Shape	Force measurement	Peak Active Force (μN)	Reference
hESC-CMS /iPSC-CMS	99,000	Collagen	Circular loop	Deflection (PoMAC)	6	[218]
iPSC-CM	63,000	Collagen	Elongated wire	Deflection (PDMS)	50	[219]
NRCMS	1,750,000	Collagen	Circular loop	Isometric force transducer	340	[111]
NRCMS	480,000	PGSA	Elongated wire	Deflection (PGSA)	1.2	own work

High-throughput monitoring becomes relevant specially for drug testing applications where variation on tissue health parameters could help determine adverse effects at early drug development stages. This could help diminishing the costs of research and development of pharmaceutical companies. As a proof of concept, we showed that z-wire tissues are physiologically responsive to commonly used cardiac drugs such as isoprotenerol and epinephrine. Amplitude of contraction was increased when both epinephrine and isoprotenerol were administered. These results match the physiological effects found on human hearts when these drugs are applied. However, the video recording was made in six well plates instead of the 384 z-wire well plate. This affected the quality of the recording as background brightness and free-tissue movement generates noise when MuscleMotion software is used for analysis. In order to atone the noise, certain sections of the tissues were used for analysis instead of analyzing the whole tissue, which could generate different results. In consequence, there are some key limitations that need to be addressed to successfully confirm that the platform can indeed be used as a drug testing research tool. Current cardiac micro-tissues lack proper maturation as neonatal CMS and short culture times were used. Therefore, electrical and calcium stimulation, longer culture times and more adult cell

sources can be implemented to achieve higher forces of contraction and more matured tissues. A functional characterization through immunostaining and contraction analysis is also required to demonstrate a higher level of maturation in comparison to current cardiac-micro tissues. In addition, larger baseline and drug sample sizes and a wider range of drugs need to be tested inside the 384 z-wire well-plate. This would help determine if the observed variations are due to drug effects or changes in z-wire elastic properties across at different wells. . Also, a system similar to other studies that is capable of performing automated and scalable video analysis is required for drug screening purposes.[219]

When injected using a customized injection tool, a cluster of z-wire tissues can be delivered, and their positioning and orientation can be controlled inside the myocardium of a heart with one or multiple injections. For clinical applications, the z-wire tissue can be engineered simply by using clinically approved PGSA polymer and cells. There is no presence of hydrogel derived from animals, magnetic particles, or other potentially toxic or non-degradable materials, which significantly reduce the barrier of translation. In future work, we aim to demonstrate long-term cardiac functional improvement with minimally invasive intramyocardial delivery of z-wire tissues *in vivo*. Functional tissue integration in vivo will also be examined in future studies. Given that injection is a simple delivery method that requires minimal surgical manipulation in vivo, the delivery process could be guided by ultrasound imaging in both animal studies and human clinical trials. The same strategy could be applied to repair skeletal muscles or neuronal tissue where intra-tissue delivery is required, and tissue structural organization is important. The degradation rate of PGSA could be further modulated to support the specific duration of different tissue healing processes[205]. The combination of minimally invasive delivery of modular functional tissues and the use of

smart scaffolds with self-assembly capabilities can potentially change the way we surgically apply a variety of tissue engineered products.

The z-wire platform can be potentially used to fabricate other type of engineered tissues that require certain structure and support such as solid organs. Since skeletal muscle tissues are force generating and contractile units, they need a support to maintain an elongated shape similar to native muscle fibers. Due to the similarities with cardiac muscle, our z-wire platform is a good candidate for skeletal muscle tissue fabrication. As a proof of concept, we showed that engineered vascularized skeletal muscle tissues can be cultured using the z-wire platform. However, skeletal muscle cells need fuse in order to contract and mature properly.[220] Therefore more tissue characterization such as confocal imaging and force of contraction analysis are required to further evaluate this alternative of z-wire approach.

CHAPTER 5. CONCLUSIONS

The use of z-wire scaffolds provides a way to manipulate engineered micro-tissues both in vitro and in vivo. To date, the field has been rooted in enhancing the precision of scaffold fabrication, especially with the emergence of 3D printing technology, where the scaffolds are often viewed as static structural supports and lack dynamic functionalities. Appreciating the complex and dynamic nature of human tissues, we offer an innovative tissue assembly strategy that imparts scaffolds dynamic functionalities to guide tissue assembly over time in both in vitro culture and in surgical delivery. Recognizing this fourth dimension in bio-fabrication could fundamentally transform the way we approach tissue and organ engineering.

5.1 Future work

Future work posterior to this thesis project can be classified into three main aims: cardiac drug testing and screening, cardiac regenerative therapy, and alternative z-wire tissue fabrication. For drug testing we envision to establish a reliable high-throughput screening platform that helps monitoring our z-wire cardiac model which could help detecting adverse effects on novel pharmaceuticals. To achieve this, a wide range of drugs will be tested on a much wider sample of z-wire tissues to achieve a large biological data set that is representative and meaningful. For cardiac regenerative therapy we aim to repeat subcutaneous tissue delivery by substituting PGSA with poly(glycerol) sebacate (PGS), which we believe will have a better biodegradability and biocompatibility. Further experiments will involve intramyocardial injection of the cardiac z-wire tissues into rat heart MI models to assess the therapeutic effects of our approach. For alternative z-wire tissue fabrication, we plan to continue optimizing and characterizing the skeletal muscle tissues

here presented as well as exploring the fabrication of liver engineered tissues. Lastly, there is a need to more extensive characterization of mechanical properties and swelling properties of PGS at different temperature exposures.

CHAPTER 6. REFERENCES

1 Roth, G. A. *et al.* Global, regional, and national age-sex-specific mortality for 282 causes of death in 195 countries and territories, 1980–2017: a systematic analysis for the Global Burden of Disease Study 2017. *The Lancet* **392**, 1736-1788, doi:https://doi.org/10.1016/S0140-6736(18)32203-7 (2018).

2 Benjamin, E. J. *et al.* Heart Disease and Stroke Statistics—2017 Update: A Report From the American Heart Association. *Circulation* **135**, e146-e603, doi:10.1161/CIR.0000000000000485 (2017).

3 Tousoulis, D. *et al.* Pathophysiology of Atherosclerosis: The Role of Inflammation. *Current Pharmaceutical Design* **17**, 4089-4110, doi:10.2174/138161211798764843 (2011).

4 Seidman, M. A., Mitchell, R. N. & Stone, J. R. in *Cellular and Molecular Pathobiology of Cardiovascular Disease* (eds Monte S. Willis, Jonathon W. Homeister, & James R. Stone) 221-237 (Academic Press, 2014).

5 Whelan, R. S., Kaplinskiy, V. & Kitsis, R. N. Cell death in the pathogenesis of heart disease: mechanisms and significance. *Annual review of physiology* **72**, 19-44, doi:10.1146/annurev.physiol.010908.163111 (2010).

6 Burke, A. P. & Virmani, R. Pathophysiology of Acute Myocardial Infarction. *Medical Clinics of North America* **91**, 553-572, doi:https://doi.org/10.1016/j.mcna.2007.03.005 (2007).

7 Laflamme, M. A. & Murry, C. E. Heart regeneration. *Nature* **473**, 326-335, doi:10.1038/nature10147 (2011).

8 Kajstura, J. *et al.* Apoptotic and necrotic myocyte cell deaths are independent contributing variables of infarct size in rats. *Laboratory investigation; a journal of technical methods and pathology* **74**, 86-107 (1996).

9 Sam, F. *et al.* Progressive left ventricular remodeling and apoptosis late after myocardial infarction in mouse heart. *American journal of physiology. Heart and circulatory physiology* **279**, H422-428, doi:10.1152/ajpheart.2000.279.1.H422 (2000).

10 GENG, Y.-J. Molecular Mechanisms for Cardiovascular Stem Cell Apoptosis and Growth in the Hearts with Atherosclerotic Coronary Disease and Ischemic Heart Failure. *Annals of the New York Academy of Sciences* **1010**, 687-697, doi:10.1196/annals.1299.126 (2003).

11 Jugdutt, B. I. Ischemia/Infarction. *Heart Failure Clinics* **8**, 43-51, doi:https://doi.org/10.1016/j.hfc.2011.08.006 (2012).

12 Merkus, D. *et al.* Coronary vasoconstrictor influence of angiotensin II is reduced in remodeled myocardium after myocardial infarction. *American Journal of Physiology-Heart and Circulatory Physiology* **291**, H2082-H2089, doi:10.1152/ajpheart.00861.2005 (2006).

13 Eng, G. *et al.* Assembly of complex cell microenvironments using geometrically docked hydrogel shapes. *Proceedings of the National Academy of Sciences of the United States of America* **110**, 4551-4556, doi:10.1073/pnas.1300569110 (2013).

14 McGuigan, A. P. & Sefton, M. V. Vascularized organoid engineered by modular assembly enables blood perfusion. *Proceedings of the National Academy of Sciences* **103**, 11461-11466, doi:10.1073/pnas.0602740103 (2006).

15 Zhang, B., Montgomery, M., Davenport-Huyer, L., Korolj, A. & Radisic, M. Platform technology for scalable assembly of instantaneously functional mosaic tissues. *Sci Adv* **1**, e1500423-e1500423, doi:10.1126/sciadv.1500423 (2015).

16 Zeng, L. *et al.* Bioenergetic and functional consequences of bone marrow-derived multipotent progenitor cell transplantation in hearts with postinfarction left ventricular remodeling. *Circulation* **115**, 1866-1875, doi:10.1161/circulationaha.106.659730 (2007).

17 Iso, Y. *et al.* Multipotent human stromal cells improve cardiac function after myocardial infarction in mice without long-term engraftment. *Biochem Biophys Res Commun* **354**, 700-706, doi:10.1016/j.bbrc.2007.01.045 (2007).

18 Noiseux, N. *et al.* Mesenchymal stem cells overexpressing Akt dramatically repair infarcted myocardium and improve cardiac function despite infrequent cellular fusion or differentiation. *Molecular therapy : the journal of the American Society of Gene Therapy* **14**, 840-850, doi:10.1016/j.ymthe.2006.05.016 (2006).

19 Leor, J. *et al.* Bioengineered cardiac grafts: A new approach to repair the infarcted myocardium? *Circulation* **102**, Iii56-61, doi:10.1161/01.cir.102.suppl_3.iii-56 (2000).

20 Reinecke, H. & Murry, C. E. Taking the Death Toll After Cardiomyocyte Grafting: A Reminder of the Importance of Quantitative Biology. *Journal of Molecular and Cellular Cardiology* **34**, 251-253, doi:https://doi.org/10.1006/jmcc.2001.1494 (2002).

21 Müller-Ehmsen, J. *et al.* Survival and Development of Neonatal Rat Cardiomyocytes Transplanted into Adult Myocardium. *Journal of Molecular and Cellular Cardiology* **34**, 107-116, doi:https://doi.org/10.1006/jmcc.2001.1491 (2002).

22 Laflamme, M. A. *et al.* Cardiomyocytes derived from human embryonic stem cells in pro-survival factors enhance function of infarcted rat hearts. *Nature biotechnology* **25**, 1015-1024, doi:10.1038/nbt1327 (2007).

23 Montgomery, M. *et al.* Flexible shape-memory scaffold for minimally invasive delivery of functional tissues. *Nature Materials* **16**, 1038, doi:10.1038/nmat4956

https://www.nature.com/articles/nmat4956#supplementary-information (2017).

24 Riegler, J. *et al.* Human engineered heart muscles engraft and survive long term in a rodent myocardial infarction model. *Circulation research* **117**, 720-730 (2015).

25 Mason, C. & Dunnill, P. A brief definition of regenerative medicine. *Regenerative Medicine* **3**, 1-5, doi:10.2217/17460751.3.1.1 (2008).

26 Lancaster, M. A. *et al.* Cerebral organoids model human brain development and microcephaly. *Nature* **501**, 373-379, doi:10.1038/nature12517 (2013).

27 Kurobe, H., Maxfield, M. W., Breuer, C. K. & Shinoka, T. Concise review: tissue-engineered vascular grafts for cardiac surgery: past, present, and future. *Stem Cells Transl Med* **1**, 566-571, doi:10.5966/sctm.2012-0044 (2012).

28 Moreira-Teixeira, L. S., Georgi, N., Leijten, J., Wu, L. & Karperien, M. Cartilage tissue engineering. *Endocrine development* **21**, 102-115, doi:10.1159/000328140 (2011).

29 Oryan, A., Alidadi, S., Moshiri, A. & Maffulli, N. Bone regenerative medicine: classic options, novel strategies, and future directions. *Journal of orthopaedic surgery and research* **9**, 18, doi:10.1186/1749-799x-9-18 (2014).

30 Song, J. J. *et al.* Regeneration and experimental orthotopic transplantation of a bioengineered kidney. *Nature Medicine* **19**, 646, doi:10.1038/nm.3154

https://www.nature.com/articles/nm.3154#supplementary-information (2013).

31 Nicolas, C. T. *et al.* Concise Review: Liver Regenerative Medicine: From Hepatocyte Transplantation to Bioartificial Livers and Bioengineered Grafts. *STEM CELLS* **35**, 42-50, doi:10.1002/stem.2500 (2017).

32 Griffith, M. *et al.* Artificial corneas: a regenerative medicine approach. *Eye* **23**, 1985-1989, doi:10.1038/eye.2008.409 (2009).

33 Christman, K. L. & Lee, R. J. Biomaterials for the treatment of myocardial infarction. *J Am Coll Cardiol* **48**, 907-913, doi:10.1016/j.jacc.2006.06.005 (2006).

34 Rebouças, J. d. S., Santos-Magalhães, N. S. & Formiga, F. R. Cardiac Regeneration using Growth Factors: Advances and Challenges. *Arq Bras Cardiol* **107**, 271-275, doi:10.5935/abc.20160097 (2016).

35 Ylä-Herttuala, S. & Martin, J. F. Cardiovascular gene therapy. *The Lancet* **355**, 213-222, doi:https://doi.org/10.1016/S0140-6736(99)04180-X (2000).

36 Singla, D. K. Stem cells and exosomes in cardiac repair. *Current Opinion in Pharmacology* **27**, 19-23, doi:https://doi.org/10.1016/j.coph.2016.01.003 (2016).

37 Ong, S.-G. & Wu, J. C. Exosomes as Potential Alternatives to Stem Cell Therapy in Mediating Cardiac Regeneration. *Circulation Research* **117**, 7-9, doi:doi:10.1161/CIRCRESAHA.115.306593 (2015).

38 Keshtkar, S., Azarpira, N. & Ghahremani, M. H. Mesenchymal stem cell-derived extracellular vesicles: novel frontiers in regenerative medicine. *Stem Cell Research & Therapy* **9**, 63, doi:10.1186/s13287-018-0791-7 (2018).

39 Barad, L., Schick, R., Zeevi-Levin, N., Itskovitz-Eldor, J. & Binah, O. Human Embryonic Stem Cells vs Human Induced Pluripotent Stem Cells for Cardiac Repair. *Canadian Journal of Cardiology* **30**, 1279-1287, doi:https://doi.org/10.1016/j.cjca.2014.06.023 (2014).

40 Lalit, P. A., Hei, D. J., Raval, A. N. & Kamp, T. J. Induced pluripotent stem cells for post-myocardial infarction repair: remarkable opportunities and challenges. *Circ Res* **114**, 1328-1345, doi:10.1161/circresaha.114.300556 (2014).

41 Durrani, S., Konoplyannikov, M., Ashraf, M. & Haider, K. H. Skeletal myoblasts for cardiac repair. *Regenerative medicine* **5**, 919-932, doi:10.2217/rme.10.65 (2010).

42 Ye, L., Zimmermann, W.-H., Garry, D. J. & Zhang, J. Patching the heart: cardiac repair from within and outside. *Circulation research* **113**, 922-932 (2013).

43 Zhang, J. Engineered Tissue Patch for Cardiac Cell Therapy. *Curr Treat Options Cardiovasc Med* **17**, 399-399, doi:10.1007/s11936-015-0399-5 (2015).

44 Müller-Ehmsen, J., Kedes, L. H., Schwinger, R. H. G. & Kloner, R. A. Cellular Cardiomyoplasty—A Novel Approach to Treat Heart Disease. *Congestive Heart Failure* **8**, 220-227, doi:10.1111/j.1527-5299.2002.00292.x (2002).

45 Müller-Ehmsen, J. *et al.* Rebuilding a Damaged Heart. *Circulation* **105**, 1720-1726, doi:doi:10.1161/01.CIR.0000013782.76324.92 (2002).

46 Zhang, M. *et al.* Cardiomyocyte Grafting for Cardiac Repair: Graft Cell Death and Anti-Death Strategies. *Journal of Molecular and Cellular Cardiology* **33**, 907-921, doi:https://doi.org/10.1006/jmcc.2001.1367 (2001).

47 SUZUKI, K. *et al.* Dynamics and mediators of acute graft attrition after myoblast transplantation to the heart. *The FASEB Journal* **18**, 1153-1155, doi:10.1096/fj.03-1308fje (2004).

48 Gepstein, L. *et al.* In Vivo Assessment of the Electrophysiological Integration and Arrhythmogenic Risk of Myocardial Cell Transplantation Strategies. *STEM CELLS* **28**, 2151-2161, doi:10.1002/stem.545 (2010).

49 Chong, J. J. *et al.* Human embryonic-stem-cell-derived cardiomyocytes regenerate non-human primate hearts. *Nature* **510**, 273-277, doi:10.1038/nature13233 (2014).

50 Shiba, Y. *et al.* Allogeneic transplantation of iPS cell-derived cardiomyocytes regenerates primate hearts. *Nature* **538**, 388-391, doi:10.1038/nature19815 (2016).

51 Yu, J. *et al.* The use of human mesenchymal stem cells encapsulated in RGD modified alginate microspheres in the repair of myocardial infarction in the rat. *Biomaterials* **31**, 7012-7020, doi:https://doi.org/10.1016/j.biomaterials.2010.05.078 (2010).

52 Ryu, J. H. *et al.* Implantation of bone marrow mononuclear cells using injectable fibrin matrix enhances neovascularization in infarcted myocardium. *Biomaterials* **26**, 319-326, doi:https://doi.org/10.1016/j.biomaterials.2004.02.058 (2005).

53 Khan, M. *et al.* Skeletal myoblasts transplanted in the ischemic myocardium enhance in situ oxygenation and recovery of contractile function. *American journal of physiology. Heart and circulatory physiology* **293**, H2129-2139, doi:10.1152/ajpheart.00677.2007 (2007).

54 He, K. L. *et al.* Autologous skeletal myoblast transplantation improved hemodynamics and left ventricular function in chronic heart failure dogs. *The Journal of heart and lung transplantation : the official publication of the International Society for Heart Transplantation* **24**, 1940-1949, doi:10.1016/j.healun.2005.02.024 (2005).

55 Lerman, D. A., Alotti, N., Ume, K. L. & Péault, B. Cardiac Repair and Regeneration: The Value of Cell Therapies. *Eur Cardiol* **11**, 43-48, doi:10.15420/ecr.2016:8:1 (2016).

56 Tse, H.-F. *et al.* Paracrine effects of direct intramyocardial implantation of bone marrow derived cells to enhance neovascularization in chronic ischaemic myocardium. *European Journal of Heart Failure* **9**, 747-753, doi:10.1016/j.ejheart.2007.03.008 (2007).

57 Suzuki, K. *et al.* Cell transplantation for the treatment of acute myocardial infarction using vascular endothelial growth factor-expressing skeletal myoblasts. *Circulation* **104**, I207-212, doi:10.1161/hc37t1.094524 (2001).

58 Murtuza, B. *et al.* Transplantation of skeletal myoblasts secreting an IL-1 inhibitor modulates adverse remodeling in infarcted murine myocardium. *Proc Natl Acad Sci U S A* **101**, 4216-4221, doi:10.1073/pnas.0306205101 (2004).

59 Menasché, P. *et al.* Myoblast transplantation for heart failure. *The Lancet* **357**, 279-280, doi:https://doi.org/10.1016/S0140-6736(00)03617-5 (2001).

60 Menasché, P. *et al.* Autologous skeletal myoblast transplantation for severe postinfarction left ventricular dysfunction. *Journal of the American College of Cardiology* **41**, 1078-1083, doi:https://doi.org/10.1016/S0735-1097(03)00092-5 (2003).

61 Dib, N. *et al.* Feasibility and safety of autologous myoblast transplantation in patients with ischemic cardiomyopathy. *Cell transplantation* **14**, 11-19, doi:10.3727/000000005783983296 (2005).

62 Menasche, P. *et al.* The Myoblast Autologous Grafting in Ischemic Cardiomyopathy (MAGIC) trial: first randomized placebo-controlled study of myoblast transplantation. *Circulation* **117**, 1189-1200, doi:10.1161/circulationaha.107.734103 (2008).

63 Ghostine, S. *et al.* Long-term efficacy of myoblast transplantation on regional structure and function after myocardial infarction. *Circulation* **106**, I131-136 (2002).

64 Gavira, J. J. *et al.* A comparison between percutaneous and surgical transplantation of autologous skeletal myoblasts in a swine model of chronic myocardial infarction. *Cardiovascular research* **71**, 744-753, doi:10.1016/j.cardiores.2006.06.018 (2006).

65 Ullah, I., Subbarao, R. B. & Rho, G. J. Human mesenchymal stem cells - current trends and future prospective. *Biosci Rep* **35**, e00191, doi:10.1042/BSR20150025 (2015).

66 Mahla, R. S. Stem Cells Applications in Regenerative Medicine and Disease Therapeutics. *Int J Cell Biol* **2016**, 6940283-6940283, doi:10.1155/2016/6940283 (2016).

67 Choi, Y. S. *et al.* Differentiation of human adipose-derived stem cells into beating cardiomyocytes. *J Cell Mol Med* **14**, 878-889, doi:10.1111/j.1582-4934.2010.01009.x (2010).

68 Xu, W. *et al.* Mesenchymal stem cells from adult human bone marrow differentiate into a cardiomyocyte phenotype in vitro. *Experimental biology and medicine (Maywood, N.J.)* **229**, 623-631, doi:10.1177/153537020422900706 (2004).

69 Shake, J. G. *et al.* Mesenchymal stem cell implantation in a swine myocardial infarct model: engraftment and functional effects. *Ann Thorac Surg* **73**, 1919-1925; discussion 1926, doi:10.1016/s0003-4975(02)03517-8 (2002).

70 Nagaya, N. *et al.* Transplantation of mesenchymal stem cells improves cardiac function in a rat model of dilated cardiomyopathy. *Circulation* **112**, 1128-1135, doi:10.1161/circulationaha.104.500447 (2005).

71 Williams, A. R. *et al.* Enhanced effect of combining human cardiac stem cells and bone marrow mesenchymal stem cells to reduce infarct size and to restore cardiac function after myocardial infarction. *Circulation* **127**, 213-223, doi:10.1161/circulationaha.112.131110 (2013).

72 Katritsis, D. G. *et al.* Transcoronary transplantation of autologous mesenchymal stem cells and endothelial progenitors into infarcted human myocardium. *Catheterization and cardiovascular interventions : official journal of the Society for Cardiac Angiography & Interventions* **65**, 321-329, doi:10.1002/ccd.20406 (2005).

73 van Berlo, J. H. *et al.* c-kit+ cells minimally contribute cardiomyocytes to the heart. *Nature* **509**, 337-341, doi:10.1038/nature13309 (2014).

74 Andersen, D. C., Andersen, P., Schneider, M., Jensen, H. B. & Sheikh, S. P. Murine "Cardiospheres" Are Not a Source of Stem Cells with Cardiomyogenic Potential. *STEM CELLS* **27**, 1571-1581, doi:10.1002/stem.72 (2009).

75 Penicka, M. *et al.* One-day kinetics of myocardial engraftment after intracoronary injection of bone marrow mononuclear cells in patients with acute and chronic myocardial infarction. *Heart (British Cardiac Society)* **93**, 837-841, doi:10.1136/hrt.2006.091934 (2007).

76 Freyman, T. *et al.* A quantitative, randomized study evaluating three methods of mesenchymal stem cell delivery following myocardial infarction. *Eur Heart J* **27**, 1114-1122, doi:10.1093/eurheartj/ehi818 (2006).

77 Thomson, J. A. *et al.* Embryonic Stem Cell Lines Derived from Human Blastocysts. *Science* **282**, 1145-1147, doi:10.1126/science.282.5391.1145 (1998).

78 He, J. Q., Ma, Y., Lee, Y., Thomson, J. A. & Kamp, T. J. Human embryonic stem cells develop into multiple types of cardiac myocytes: action potential characterization. *Circ Res* **93**, 32-39, doi:10.1161/01.Res.0000080317.92718.99 (2003).

79 Caspi, O. *et al.* Transplantation of Human Embryonic Stem Cell-Derived Cardiomyocytes Improves Myocardial Performance in Infarcted Rat Hearts. *Journal of the American College of Cardiology* **50**, 1884-1893, doi:https://doi.org/10.1016/j.jacc.2007.07.054 (2007).

80 Leor, J. *et al.* Human embryonic stem cell transplantation to repair the infarcted myocardium. *Heart (British Cardiac Society)* **93**, 1278-1284, doi:10.1136/hrt.2006.093161 (2007).

81 Moon, S.-H. *et al.* The use of aggregates of purified cardiomyocytes derived from human ESCs for functional engraftment after myocardial infarction. *Biomaterials* **34**, 4013-4026, doi:https://doi.org/10.1016/j.biomaterials.2013.02.022 (2013).

82 van Laake, L. W., Passier, R., Doevendans, P. A. & Mummery, C. L. Human embryonic stem cell-derived cardiomyocytes and cardiac repair in rodents. *Circ Res* **102**, 1008-1010, doi:10.1161/circresaha.108.175505 (2008).

83 Shiba, Y. *et al.* Human ES-cell-derived cardiomyocytes electrically couple and suppress arrhythmias in injured hearts. *Nature* **489**, 322-325, doi:10.1038/nature11317 (2012).

84 Romagnuolo, R. *et al.* Human Embryonic Stem Cell-Derived Cardiomyocytes Regenerate the Infarcted Pig Heart but Induce Ventricular Tachyarrhythmias. *Stem Cell Reports* **12**, 967-981, doi:10.1016/j.stemcr.2019.04.005 (2019).

85 Liu, Y.-W. *et al.* Human embryonic stem cell–derived cardiomyocytes restore function in infarcted hearts of non-human primates. *Nature biotechnology* **36**, 597-605, doi:10.1038/nbt.4162 (2018).

86 Takahashi, K. & Yamanaka, S. Induction of pluripotent stem cells from mouse embryonic and adult fibroblast cultures by defined factors. *Cell* **126**, 663-676, doi:10.1016/j.cell.2006.07.024 (2006).

87 Nelson, T. J. *et al.* Repair of acute myocardial infarction by human stemness factors induced pluripotent stem cells. *Circulation* **120**, 408-416, doi:10.1161/circulationaha.109.865154 (2009).

88 Singla, D. K., Long, X., Glass, C., Singla, R. D. & Yan, B. Induced pluripotent stem (iPS) cells repair and regenerate infarcted myocardium. *Molecular pharmaceutics* **8**, 1573-1581, doi:10.1021/mp2001704 (2011).

89 Templin, C. *et al.* Transplantation and tracking of human-induced pluripotent stem cells in a pig model of myocardial infarction: assessment of cell survival, engraftment, and distribution by hybrid single photon emission computed tomography/computed tomography of sodium iodide symporter transgene expression. *Circulation* **126**, 430-439, doi:10.1161/circulationaha.111.087684 (2012).

90 Ahmed, R. P., Ashraf, M., Buccini, S., Shujia, J. & Haider, H. Cardiac tumorigenic potential of induced pluripotent stem cells in an immunocompetent host with myocardial infarction. *Regen Med* **6**, 171-178, doi:10.2217/rme.10.103 (2011).

91 Zhang, Y. *et al.* Intramyocardial transplantation of undifferentiated rat induced pluripotent stem cells causes tumorigenesis in the heart. *PloS one* **6**, e19012, doi:10.1371/journal.pone.0019012 (2011).

92 Carvajal-Vergara, X. *et al.* Patient-specific induced pluripotent stem-cell-derived models of LEOPARD syndrome. *Nature* **465**, 808-812, doi:10.1038/nature09005 (2010).

93 Ieda, M. *et al.* Direct reprogramming of fibroblasts into functional cardiomyocytes by defined factors. *Cell* **142**, 375-386, doi:10.1016/j.cell.2010.07.002 (2010).

94 Frisch, S. M. & Screaton, R. A. Anoikis mechanisms. *Current Opinion in Cell Biology* **13**, 555-562, doi:https://doi.org/10.1016/S0955-0674(00)00251-9 (2001).

95 Lee, K. Y. & Mooney, D. J. Alginate: properties and biomedical applications. *Progress in polymer science* **37**, 106-126, doi:10.1016/j.progpolymsci.2011.06.003 (2012).

96 Roche, E. T. *et al.* Comparison of biomaterial delivery vehicles for improving acute retention of stem cells in the infarcted heart. *Biomaterials* **35**, 6850-6858, doi:https://doi.org/10.1016/j.biomaterials.2014.04.114 (2014).

97 Janmey, P. A., Winer, J. P. & Weisel, J. W. Fibrin gels and their clinical and bioengineering applications. *J R Soc Interface* **6**, 1-10, doi:10.1098/rsif.2008.0327 (2009).

98 Christman, K. L. *et al.* Injectable Fibrin Scaffold Improves Cell Transplant Survival, Reduces Infarct Expansion, and Induces Neovasculature Formation in Ischemic Myocardium. *Journal of the American College of Cardiology* **44**, 654-660, doi:https://doi.org/10.1016/j.jacc.2004.04.040 (2004).

99 Dikovsky, D., Bianco-Peled, H. & Seliktar, D. The effect of structural alterations of PEG-fibrinogen hydrogel scaffolds on 3-D cellular morphology and cellular migration. *Biomaterials* **27**, 1496-1506, doi:10.1016/j.biomaterials.2005.09.038 (2006).

100 Habib, M. *et al.* A combined cell therapy and in-situ tissue-engineering approach for myocardial repair. *Biomaterials* **32**, 7514-7523, doi:10.1016/j.biomaterials.2011.06.049 (2011).

101 Kraehenbuehl, T. P. *et al.* Human embryonic stem cell-derived microvascular grafts for cardiac tissue preservation after myocardial infarction. *Biomaterials* **32**, 1102-1109, doi:https://doi.org/10.1016/j.biomaterials.2010.10.005 (2011).

102 Kraehenbuehl, T. P., Ferreira, L. S., Zammaretti, P., Hubbell, J. A. & Langer, R. Cell-responsive hydrogel for encapsulation of vascular cells. *Biomaterials* **30**, 4318-4324, doi:10.1016/j.biomaterials.2009.04.057 (2009).

103 Tang, J. *et al.* Heart Repair Using Nanogel-Encapsulated Human Cardiac Stem Cells in Mice and Pigs with Myocardial Infarction. *ACS nano* **11**, 9738-9749, doi:10.1021/acsnano.7b01008 (2017).

104 Smit, N. W. *et al.* Human Cardiomyocyte Progenitor Cells in Co-culture with Rat Cardiomyocytes Form a Pro-arrhythmic Substrate: Evidence for Two Different Arrhythmogenic Mechanisms. *Front Physiol* **8**, doi:10.3389/fphys.2017.00797 (2017).

105 Hirt, M. N., Hansen, A. & Eschenhagen, T. Cardiac Tissue Engineering State of the Art. *Circulation Research* **114**, 354-367, doi:https://doi.org/10.1161/CIRCRESAHA.114.300522 (2014).

106 Wnorowski, A. & Wu, J. C. 3-Dimensionally Printed, Native-Like Scaffolds for Myocardial Tissue Engineering. *Circulation Research* **120**, 1224-1226, doi:https://doi.org/10.1161/CIRCRESAHA.117.310862 (2017).
107 Miyahara, Y. *et al.* Monolayered mesenchymal stem cells repair scarred myocardium after myocardial infarction. *Nature Medicine* **12**, 459-465, doi:10.1038/nm1391 (2006).
108 Shimizu, T. *et al.* Fabrication of pulsatile cardiac tissue grafts using a novel 3-dimensional cell sheet manipulation technique and temperature-responsive cell culture surfaces. *Circ Res* **90**, e40, doi:10.1161/hh0302.105722 (2002).
109 Eschenhagen, T. *et al.* Three-dimensional reconstitution of embryonic cardiomyocytes in a collagen matrix: a new heart muscle model system. *FASEB journal : official publication of the Federation of American Societies for Experimental Biology* **11**, 683-694, doi:10.1096/fasebj.11.8.9240969 (1997).
110 Zimmermann, W. H. *et al.* Engineered heart tissue for replacement therapy. *The Journal of Heart and Lung Transplantation* **21**, 162, doi:10.1016/S1053-2498(01)00732-X (2002).
111 Zimmermann, W. H. *et al.* Three-dimensional engineered heart tissue from neonatal rat cardiac myocytes. *Biotechnology and bioengineering* **68**, 106-114 (2000).
112 Zimmermann, W. H. *et al.* Tissue engineering of a differentiated cardiac muscle construct. *Circ Res* **90**, 223-230, doi:10.1161/hh0202.103644 (2002).
113 Zimmermann, W. H. *et al.* Cardiac grafting of engineered heart tissue in syngenic rats. *Circulation* **106**, I151-157 (2002).
114 Zimmermann, W.-H. *et al.* Engineered heart tissue grafts improve systolic and diastolic function in infarcted rat hearts. *Nature Medicine* **12**, 452, doi:10.1038/nm1394

https://www.nature.com/articles/nm1394#supplementary-information (2006).
115 Yildirim, Y. *et al.* Development of a biological ventricular assist device: preliminary data from a small animal model. *Circulation* **116**, I16-23, doi:10.1161/circulationaha.106.679688 (2007).
116 Tiburcy, M. *et al.* Defined Engineered Human Myocardium With Advanced Maturation for Applications in Heart Failure Modeling and Repair. *Circulation* **135**, 1832-1847, doi:10.1161/CIRCULATIONAHA.116.024145 (2017).
117 Hashizume, R. *et al.* Biodegradable elastic patch plasty ameliorates left ventricular adverse remodeling after ischemia–reperfusion injury: A preclinical study of a porous polyurethane material in a porcine model. *The Journal of Thoracic and Cardiovascular Surgery* **146**, 391-399.e391, doi:https://doi.org/10.1016/j.jtcvs.2012.11.013 (2013).
118 Stevens, K. R. *et al.* Physiological function and transplantation of scaffold-free and vascularized human cardiac muscle tissue. *Proceedings of the National Academy of Sciences of the United States of America* **106**, 16568-16573, doi:10.1073/pnas.0908381106 (2009).
119 Miyagi, Y. *et al.* Biodegradable collagen patch with covalently immobilized VEGF for myocardial repair. *Biomaterials* **32**, 1280-1290, doi:https://doi.org/10.1016/j.biomaterials.2010.10.007 (2011).

120 Dvir, T. *et al.* Prevascularization of cardiac patch on the omentum improves its therapeutic outcome. *Proceedings of the National Academy of Sciences* **106**, 14990-14995, doi:10.1073/pnas.0812242106 (2009).
121 Bursac, N., Loo, Y., Leong, K. & Tung, L. Novel anisotropic engineered cardiac tissues: studies of electrical propagation. *Biochem Biophys Res Commun* **361**, 847-853, doi:10.1016/j.bbrc.2007.07.138 (2007).
122 Dvir, T. *et al.* Nanowired three-dimensional cardiac patches. *Nature Nanotechnology* **6**, 720-725, doi:10.1038/nnano.2011.160 (2011).
123 Liu, J. *et al.* Autologous stem cell transplantation for myocardial repair. *American Journal of Physiology-Heart and Circulatory Physiology* **287**, H501-H511, doi:10.1152/ajpheart.00019.2004 (2004).
124 Xiong, Q. *et al.* Functional consequences of human induced pluripotent stem cell therapy: myocardial ATP turnover rate in the in vivo swine heart with postinfarction remodeling. *Circulation* **127**, 997-1008, doi:10.1161/circulationaha.112.000641 (2013).
125 Chi, N.-H. *et al.* Cardiac repair achieved by bone marrow mesenchymal stem cells/silk fibroin/hyaluronic acid patches in a rat of myocardial infarction model. *Biomaterials* **33**, 5541-5551, doi:https://doi.org/10.1016/j.biomaterials.2012.04.030 (2012).
126 Chi, N.-H., Yang, M.-C., Chung, T.-W., Chou, N.-K. & Wang, S.-S. Cardiac repair using chitosan-hyaluronan/silk fibroin patches in a rat heart model with myocardial infarction. *Carbohydrate Polymers* **92**, 591-597, doi:https://doi.org/10.1016/j.carbpol.2012.09.012 (2013).
127 Li, R. K. *et al.* Survival and function of bioengineered cardiac grafts. *Circulation* **100**, Ii63-69, doi:10.1161/01.cir.100.suppl_2.ii-63 (1999).
128 Wang, Q. *et al.* Functional engineered human cardiac patches prepared from nature's platform improve heart function after acute myocardial infarction. *Biomaterials* **105**, 52-65, doi:https://doi.org/10.1016/j.biomaterials.2016.07.035 (2016).
129 Frederick, J. R. *et al.* Stromal cell-derived factor-1alpha activation of tissue-engineered endothelial progenitor cell matrix enhances ventricular function after myocardial infarction by inducing neovasculogenesis. *Circulation* **122**, S107-S117, doi:10.1161/CIRCULATIONAHA.109.930404 (2010).
130 Fleischer, S., Shapira, A., Feiner, R. & Dvir, T. Modular assembly of thick multifunctional cardiac patches. *Proceedings of the National Academy of Sciences* **114**, 1898-1903, doi:10.1073/pnas.1615728114 (2017).
131 Ott, H. C. *et al.* Perfusion-decellularized matrix: using nature's platform to engineer a bioartificial heart. *Nature Medicine* **14**, 213-221, doi:10.1038/nm1684 (2008).
132 Wolfe, P. S., Sell, S. A. & Bowlin, G. L. in *Tissue Engineering: From Lab to Clinic* (eds Norbert Pallua & Christoph V. Suscheck) 41-67 (Springer Berlin Heidelberg, 2011).
133 Sackett, S. D. *et al.* Extracellular matrix scaffold and hydrogel derived from decellularized and delipidized human pancreas. *Scientific Reports* **8**, 10452, doi:10.1038/s41598-018-28857-1 (2018).
134 Gilbert, T. W., Freund, J. M. & Badylak, S. F. Quantification of DNA in biologic scaffold materials. *J Surg Res* **152**, 135-139, doi:10.1016/j.jss.2008.02.013 (2009).
135 Reis, L., Chiu, L. L. Y., Feric, N., Fu, L. & Radisic, M. in *Cardiac Regeneration and Repair* (eds Ren-Ke Li & Richard D. Weisel) 49-81 (Woodhead Publishing, 2014).

136 Estrada, V., Tekinay, A. & Müller, H. W. in *Progress in Brain Research* Vol. 214 (eds Alexander Dityatev, Bernhard Wehrle-Haller, & Asla Pitkänen) 391-413 (Elsevier, 2014).

137 Matsubayashi, K. *et al.* Improved left ventricular aneurysm repair with bioengineered vascular smooth muscle grafts. *Circulation* **108 Suppl 1**, Ii219-225, doi:10.1161/01.cir.0000087450.34497.9a (2003).

138 Kai, D. *et al.* Stem cell-loaded nanofibrous patch promotes the regeneration of infarcted myocardium with functional improvement in rat model. *Acta biomaterialia* **10**, 2727-2738, doi:https://doi.org/10.1016/j.actbio.2014.02.030 (2014).

139 Srisuwan, Y., Baimark, Y. & Suttiruengwong, S. Toughening of Poly(L-lactide) with Blends of Poly(ε-caprolactone-co-L-lactide) in the Presence of Chain Extender. *Int J Biomater* **2018**, 1294397-1294397, doi:10.1155/2018/1294397 (2018).

140 Katsumata, K., Saito, T., Yu, F., Nakamura, N. & Inoue, Y. The toughening effect of a small amount of poly(ε-caprolactone) on the mechanical properties of the poly(3-hydroxybutyrate-co-3-hydroxyhexanoate)/PCL blend. *Polymer Journal* **43**, 484-492, doi:10.1038/pj.2011.12 (2011).

141 Salazar, B. H., Cashion, A. T., Dennis, R. G. & Birla, R. K. Development of a Cyclic Strain Bioreactor for Mechanical Enhancement and Assessment of Bioengineered Myocardial Constructs. *Cardiovasc Eng Technol* **6**, 533-545, doi:10.1007/s13239-015-0236-8 (2015).

142 Kim, B.-S., Nikolovski, J., Bonadio, J. & Mooney, D. J. Cyclic mechanical strain regulates the development of engineered smooth muscle tissue. *Nature biotechnology* **17**, 979-983, doi:10.1038/13671 (1999).

143 Piao, H. *et al.* Effects of cardiac patches engineered with bone marrow-derived mononuclear cells and PGCL scaffolds in a rat myocardial infarction model. *Biomaterials* **28**, 641-649, doi:https://doi.org/10.1016/j.biomaterials.2006.09.009 (2007).

144 Fujimoto, K. L. *et al.* An elastic, biodegradable cardiac patch induces contractile smooth muscle and improves cardiac remodeling and function in subacute myocardial infarction. *J Am Coll Cardiol* **49**, 2292-2300, doi:10.1016/j.jacc.2007.02.050 (2007).

145 Fujimoto, K. L. *et al.* Placement of an elastic biodegradable cardiac patch on a subacute infarcted heart leads to cellularization with early developmental cardiomyocyte characteristics. *Journal of cardiac failure* **18**, 585-595, doi:10.1016/j.cardfail.2012.05.006 (2012).

146 Wang, Y., Ameer, G., Sheppard, B. & Langer, R. A tough biodegradable elastomer. *Nature biotechnology* **20**, 602-606, doi:10.1038/nbt0602-602 (2002).

147 Marsano, A. *et al.* The effect of controlled expression of VEGF by transduced myoblasts in a cardiac patch on vascularization in a mouse model of myocardial infarction. *Biomaterials* **34**, 393-401, doi:https://doi.org/10.1016/j.biomaterials.2012.09.038 (2013).

148 Marsano, A. *et al.* Scaffold stiffness affects the contractile function of three-dimensional engineered cardiac constructs. *Biotechnology progress* **26**, 1382-1390, doi:10.1002/btpr.435 (2010).

149 Tran, R. T. *et al.* Synthesis and characterization of a biodegradable elastomer featuring a dual crosslinking mechanism. *Soft matter* **6**, 2449-2461, doi:10.1039/C001605E (2010).

150 Huyer, L. D. *et al.* Biomaterial based cardiac tissue engineering and its applications. *Biomedical materials (Bristol, England)* **10**, 034004, doi:10.1088/1748-6041/10/3/034004 (2015).
151 Okano, T., Yamada, N., Sakai, H. & Sakurai, Y. A novel recovery system for cultured cells using plasma-treated polystyrene dishes grafted with poly(N-isopropylacrylamide). *J Biomed Mater Res* **27**, 1243-1251, doi:10.1002/jbm.820271005 (1993).
152 Zhang, L. *et al.* Derivation and high engraftment of patient-specific cardiomyocyte sheet using induced pluripotent stem cells generated from adult cardiac fibroblast. *Circulation. Heart failure* **8**, 156-166, doi:10.1161/circheartfailure.114.001317 (2015).
153 Kim, K. *et al.* Donor cell type can influence the epigenome and differentiation potential of human induced pluripotent stem cells. *Nature biotechnology* **29**, 1117-1119, doi:10.1038/nbt.2052 (2011).
154 Bar-Nur, O., Russ, H. A., Efrat, S. & Benvenisty, N. Epigenetic memory and preferential lineage-specific differentiation in induced pluripotent stem cells derived from human pancreatic islet beta cells. *Cell stem cell* **9**, 17-23, doi:10.1016/j.stem.2011.06.007 (2011).
155 Freed, L. E., Engelmayr, G. C., Jr., Borenstein, J. T., Moutos, F. T. & Guilak, F. Advanced material strategies for tissue engineering scaffolds. *Advanced materials (Deerfield Beach, Fla.)* **21**, 3410-3418, doi:10.1002/adma.200900303 (2009).
156 Nelson, D. M., Ma, Z., Fujimoto, K. L., Hashizume, R. & Wagner, W. R. Intra-myocardial biomaterial injection therapy in the treatment of heart failure: Materials, outcomes and challenges. *Acta biomaterialia* **7**, 1-15, doi:10.1016/j.actbio.2010.06.039 (2011).
157 Han, S.-K. in *Innovations and Advances in Wound Healing* 201-213 (Springer Berlin Heidelberg, 2016).
158 Leor, J. *et al.* Intracoronary Injection of In Situ Forming Alginate Hydrogel Reverses Left Ventricular Remodeling After Myocardial Infarction in Swine. *Journal of the American College of Cardiology* **54**, 1014-1023, doi:https://doi.org/10.1016/j.jacc.2009.06.010 (2009).
159 Landa, N. *et al.* Effect of injectable alginate implant on cardiac remodeling and function after recent and old infarcts in rat. *Circulation* **117**, 1388-1396, doi:10.1161/circulationaha.107.727420 (2008).
160 Mihardja, S. S., Sievers, R. E. & Lee, R. J. The effect of polypyrrole on arteriogenesis in an acute rat infarct model. *Biomaterials* **29**, 4205-4210, doi:10.1016/j.biomaterials.2008.07.021 (2008).
161 Yu, J. *et al.* The effect of injected RGD modified alginate on angiogenesis and left ventricular function in a chronic rat infarct model. *Biomaterials* **30**, 751-756, doi:10.1016/j.biomaterials.2008.09.059 (2009).
162 Ruvinov, E., Leor, J. & Cohen, S. The promotion of myocardial repair by the sequential delivery of IGF-1 and HGF from an injectable alginate biomaterial in a model of acute myocardial infarction. *Biomaterials* **32**, 565-578, doi:10.1016/j.biomaterials.2010.08.097 (2011).
163 Lai, R. C. *et al.* Exosome secreted by MSC reduces myocardial ischemia/reperfusion injury. *Stem Cell Research* **4**, 214-222, doi:https://doi.org/10.1016/j.scr.2009.12.003 (2010).

164 Teng, X. *et al.* Mesenchymal Stem Cell-Derived Exosomes Improve the Microenvironment of Infarcted Myocardium Contributing to Angiogenesis and Anti-Inflammation. *Cellular Physiology and Biochemistry* **37**, 2415-2424, doi:10.1159/000438594 (2015).

165 Ibrahim, Ahmed G.-E., Cheng, K. & Marbán, E. Exosomes as Critical Agents of Cardiac Regeneration Triggered by Cell Therapy. *Stem Cell Reports* **2**, 606-619, doi:https://doi.org/10.1016/j.stemcr.2014.04.006 (2014).

166 Tang, J. *et al.* Therapeutic microparticles functionalized with biomimetic cardiac stem cell membranes and secretome. *Nature communications* **8**, 13724, doi:10.1038/ncomms13724 (2017).

167 Luo, L. *et al.* Fabrication of Synthetic Mesenchymal Stem Cells for the Treatment of Acute Myocardial Infarction in Mice. *Circ Res* **120**, 1768-1775, doi:10.1161/circresaha.116.310374 (2017).

168 Hao, X. *et al.* Angiogenic effects of sequential release of VEGF-A165 and PDGF-BB with alginate hydrogels after myocardial infarction. *Cardiovascular research* **75**, 178-185, doi:10.1016/j.cardiores.2007.03.028 (2007).

169 Christman, K. L., Fok, H. H., Sievers, R. E., Fang, Q. & Lee, R. J. Fibrin glue alone and skeletal myoblasts in a fibrin scaffold preserve cardiac function after myocardial infarction. *Tissue Eng* **10**, 403-409, doi:10.1089/107632704323061762 (2004).

170 Yu, J. *et al.* Restoration of left ventricular geometry and improvement of left ventricular function in a rodent model of chronic ischemic cardiomyopathy. *The Journal of Thoracic and Cardiovascular Surgery* **137**, 180-187, doi:https://doi.org/10.1016/j.jtcvs.2008.08.036 (2009).

171 Huang, N. F., Yu, J., Sievers, R., Li, S. & Lee, R. J. Injectable biopolymers enhance angiogenesis after myocardial infarction. *Tissue Eng* **11**, 1860-1866, doi:10.1089/ten.2005.11.1860 (2005).

172 Mukherjee, R. *et al.* Targeted myocardial microinjections of a biocomposite material reduces infarct expansion in pigs. *Ann Thorac Surg* **86**, 1268-1276, doi:10.1016/j.athoracsur.2008.04.107 (2008).

173 Dorsey, S. M. *et al.* MRI evaluation of injectable hyaluronic acid-based hydrogel therapy to limit ventricular remodeling after myocardial infarction. *Biomaterials* **69**, 65-75, doi:https://doi.org/10.1016/j.biomaterials.2015.08.011 (2015).

174 Wu, J. *et al.* Infarct stabilization and cardiac repair with a VEGF-conjugated, injectable hydrogel. *Biomaterials* **32**, 579-586, doi:https://doi.org/10.1016/j.biomaterials.2010.08.098 (2011).

175 Arslan, F. *et al.* Mesenchymal stem cell-derived exosomes increase ATP levels, decrease oxidative stress and activate PI3K/Akt pathway to enhance myocardial viability and prevent adverse remodeling after myocardial ischemia/reperfusion injury. *Stem Cell Research* **10**, 301-312, doi:https://doi.org/10.1016/j.scr.2013.01.002 (2013).

176 Bian, S. *et al.* Extracellular vesicles derived from human bone marrow mesenchymal stem cells promote angiogenesis in a rat myocardial infarction model. *Journal of Molecular Medicine* **92**, 387-397, doi:10.1007/s00109-013-1110-5 (2014).

177 Ma, J. *et al.* Exosomes Derived from Akt-Modified Human Umbilical Cord Mesenchymal Stem Cells Improve Cardiac Regeneration and Promote Angiogenesis via Activating Platelet-Derived Growth Factor D. *STEM CELLS Translational Medicine* **6**, 51-59, doi:10.5966/sctm.2016-0038 (2017).

178 Feng, Y., Huang, W., Wani, M., Yu, X. & Ashraf, M. Ischemic preconditioning potentiates the protective effect of stem cells through secretion of exosomes by targeting Mecp2 via miR-22. *PloS one* **9**, e88685, doi:10.1371/journal.pone.0088685 (2014).

179 Yu, B. *et al.* Cardiomyocyte protection by GATA-4 gene engineered mesenchymal stem cells is partially mediated by translocation of miR-221 in microvesicles. *PloS one* **8**, e73304, doi:10.1371/journal.pone.0073304 (2013).

180 Yu, B. *et al.* Exosomes secreted from GATA-4 overexpressing mesenchymal stem cells serve as a reservoir of anti-apoptotic microRNAs for cardioprotection. *International Journal of Cardiology* **182**, 349-360, doi:https://doi.org/10.1016/j.ijcard.2014.12.043 (2015).

181 Wang, K. *et al.* Enhanced Cardioprotection by Human Endometrium Mesenchymal Stem Cells Driven by Exosomal MicroRNA-21. *STEM CELLS Translational Medicine* **6**, 209-222, doi:10.5966/sctm.2015-0386 (2017).

182 Wang, N. *et al.* Mesenchymal stem cells-derived extracellular vesicles, via miR-210, improve infarcted cardiac function by promotion of angiogenesis. *Biochimica et Biophysica Acta (BBA) - Molecular Basis of Disease* **1863**, 2085-2092, doi:https://doi.org/10.1016/j.bbadis.2017.02.023 (2017).

183 White, A. J. *et al.* Intrinsic cardiac origin of human cardiosphere-derived cells. *European Heart Journal* **34**, 68-75, doi:10.1093/eurheartj/ehr172 (2011).

184 Davis, D. R. *et al.* Validation of the Cardiosphere Method to Culture Cardiac Progenitor Cells from Myocardial Tissue. *PloS one* **4**, e7195, doi:10.1371/journal.pone.0007195 (2009).

185 Makkar, R. R. *et al.* Intracoronary cardiosphere-derived cells for heart regeneration after myocardial infarction (CADUCEUS): a prospective, randomised phase 1 trial. *The Lancet* **379**, 895-904, doi:https://doi.org/10.1016/S0140-6736(12)60195-0 (2012).

186 Vandergriff, A. *et al.* Targeting regenerative exosomes to myocardial infarction using cardiac homing peptide. *Theranostics* **8**, 1869-1878, doi:10.7150/thno.20524 (2018).

187 Vrijsen, K. R. *et al.* Cardiomyocyte progenitor cell-derived exosomes stimulate migration of endothelial cells. *J Cell Mol Med* **14**, 1064-1070, doi:10.1111/j.1582-4934.2010.01081.x (2010).

188 Khan, M. *et al.* Embryonic stem cell-derived exosomes promote endogenous repair mechanisms and enhance cardiac function following myocardial infarction. *Circulation research* **117**, 52-64, doi:10.1161/CIRCRESAHA.117.305990 (2015).

189 Liu, B. *et al.* Cardiac recovery via extended cell-free delivery of extracellular vesicles secreted by cardiomyocytes derived from induced pluripotent stem cells. *Nature Biomedical Engineering* **2**, 293-303, doi:10.1038/s41551-018-0229-7 (2018).

190 Huang, K. *et al.* An off-the-shelf artificial cardiac patch improves cardiac repair after myocardial infarction in rats and pigs. *Science Translational Medicine* **12**, eaat9683, doi:10.1126/scitranslmed.aat9683 (2020).

191 Li, Q. *et al.* Overexpression of insulin-like growth factor-1 in mice protects from myocyte death after infarction, attenuating ventricular dilation, wall stress, and cardiac hypertrophy. *The Journal of Clinical Investigation* **100**, 1991-1999, doi:10.1172/JCI119730 (1997).

192 Macarthur, J. W., Jr. *et al.* Preclinical evaluation of the engineered stem cell chemokine stromal cell-derived factor 1alpha analog in a translational ovine

myocardial infarction model. *Circ Res* **114**, 650-659, doi:10.1161/circresaha.114.302884 (2014).

193 Hwang, H. & Kloner, R. A. The combined administration of multiple soluble factors in the repair of chronically infarcted rat myocardium. *Journal of cardiovascular pharmacology* **57**, 282-286, doi:10.1097/FJC.0b013e3182058717 (2011).

194 Takahashi, Y. *et al.* Visualization and in vivo tracking of the exosomes of murine melanoma B16-BL6 cells in mice after intravenous injection. *Journal of biotechnology* **165**, 77-84, doi:10.1016/j.jbiotec.2013.03.013 (2013).

195 Engelmayr, G. C. *et al.* Accordion-like honeycombs for tissue engineering of cardiac anisotropy. *Nature Materials* **7**, 1003-1010, doi:10.1038/nmat2316 (2008).

196 Holmes, J. W., Borg, T. K. & Covell, J. W. Structure and mechanics of healing myocardial infarcts. *Annu Rev Biomed Eng* **7**, 223-253, doi:10.1146/annurev.bioeng.7.060804.100453 (2005).

197 Chuong, C. J., Sacks, M. S., Templeton, G., Schwiep, F. & Johnson, R. L., Jr. Regional deformation and contractile function in canine right ventricular free wall. *The American journal of physiology* **260**, H1224-1235, doi:10.1152/ajpheart.1991.260.4.H1224 (1991).

198 Rappaport, D., Adam, D., Lysyansky, P. & Riesner, S. Assessment of myocardial regional strain and strain rate by tissue tracking in B-mode echocardiograms. *Ultrasound in Medicine & Biology* **32**, 1181-1192, doi:http://dx.doi.org/10.1016/j.ultrasmedbio.2006.05.005 (2006).

199 Demer, L. L. & Yin, F. C. Passive biaxial mechanical properties of isolated canine myocardium. *The Journal of physiology* **339**, 615-630, doi:10.1113/jphysiol.1983.sp014738 (1983).

200 Ifkovits, J. L., Padera, R. F. & Burdick, J. A. Biodegradable and radically polymerized elastomers with enhanced processing capabilities. *Biomedical materials* **3**, 034104 (2008).

201 Liang, W., Cho, H. C. & Marban, E. Wnt signalling suppresses voltage-dependent Na(+) channel expression in postnatal rat cardiomyocytes. *J Physiol* **593**, 1147-1157 (2015).

202 Burridge, P. W. *et al.* Chemically defined generation of human cardiomyocytes. *Nat Methods* **11**, 855-860, doi:10.1038/nmeth.2999 (2014).

203 Zhang, B. *et al.* Biodegradable scaffold with built-in vasculature for organ-on-a-chip engineering and direct surgical anastomosis. *Nat Mater* **15**, 669-678 (2016).

204 Lang, N. *et al.* A blood-resistant surgical glue for minimally invasive repair of vessels and heart defects. *Science translational medicine* **6**, 218ra216-218ra216 (2014).

205 Nijst, C. L. E. *et al.* Synthesis and Characterization of Photocurable Elastomers from Poly(glycerol-co-sebacate). *Biomacromolecules* **8**, 3067-3073, doi:10.1021/bm070423u (2007).

206 Liu, Q., Jiang, L., Shi, R. & Zhang, L. Synthesis, preparation, in vitro degradation, and application of novel degradable bioelastomers—A review. *Progress in Polymer Science* **37**, 715-765 (2012).

207 Wu, W., Allen, R. A. & Wang, Y. Fast-degrading elastomer enables rapid remodeling of a cell-free synthetic graft into a neoartery. *Nature medicine* **18**, 1148-1153, doi:10.1038/nm.2821 (2012).

208 Anderson, J. R. *et al.* Fabrication of topologically complex three-dimensional microfluidic systems in PDMS by rapid prototyping. *Analytical chemistry* **72**, 3158-3164 (2000).

209 McBain, S. C., Yiu, H. H. & Dobson, J. Magnetic nanoparticles for gene and drug delivery. *International journal of nanomedicine* **3**, 169 (2008).

210 Frey, N. A., Peng, S., Cheng, K. & Sun, S. Magnetic nanoparticles: synthesis, functionalization, and applications in bioimaging and magnetic energy storage. *Chemical Society reviews* **38**, 2532-2542, doi:10.1039/b815548h (2009).

211 Pankhurst, Q. A., Connolly, J., Jones, J. K. & Dobson, J. Applications of magnetic nanoparticles in biomedicine. *Journal of Physics D: Applied Physics* **36**, 167-181 (2003).

212 Morrison, B. M. Neuromuscular Diseases. *Seminars in neurology* **36**, 409-418, doi:10.1055/s-0036-1586263 (2016).

213 Mase, V. J. *et al.* Clinical application of an acellular biologic scaffold for surgical repair of a large, traumatic quadriceps femoris muscle defect. *Orthopedics* **33** (2010).

214 Grogan, B. F., Hsu, J. R. & Consortium, S. T. R. Volumetric muscle loss. *JAAOS-Journal of the American Academy of Orthopaedic Surgeons* **19**, S35-S37 (2011).

215 Bach, A. D., Beier, J. P., Stern-Staeter, J. & Horch, R. E. Skeletal muscle tissue engineering. *J Cell Mol Med* **8**, 413-422, doi:10.1111/j.1582-4934.2004.tb00466.x (2004).

216 Shirure, V. & George, S. Design considerations to minimize the impact of drug absorption in polymer-based organ-on-a-chip platforms. *Lab on a Chip* **17**, 681-690 (2017).

217 Ottersbach, A. *et al.* Improved heart repair upon myocardial infarction: Combination of magnetic nanoparticles and tailored magnets strongly increases engraftment of myocytes. *Biomaterials* **155**, 176-190, doi:https://doi.org/10.1016/j.biomaterials.2017.11.012 (2018).

218 Zhao, Y. *et al.* A Platform for Generation of Chamber-Specific Cardiac Tissues and Disease Modeling. *Cell* **176**, 913-927.e918, doi:10.1016/j.cell.2018.11.042 (2019).

219 Thavandiran, N. *et al.* Functional arrays of human pluripotent stem cell-derived cardiac microtissues. *Scientific Reports* **10**, 6919, doi:10.1038/s41598-020-62955-3 (2020).

220 Kim, J. H., Jin, P., Duan, R. & Chen, E. H. Mechanisms of myoblast fusion during muscle development. *Curr Opin Genet Dev* **32**, 162-170, doi:10.1016/j.gde.2015.03.006 (2015).